T.C
SÜLEYMAN DEMİREL UNIVERSITY
GRADUATE SCHOOL OF NATURAL AND APPLIED SCIENCES

DETERMINATION OF QUALITY PARAMETERS OF GAMMA SPECTROMETER SYSTEM

Faez Qahtan Waheed WAHEED

Supervisor
Prof. Dr. İskender AKKURT

Ph.D. THESIS
DEPARTMENT OF PHYSICS
ISPARTA - 2020

COMMITMENT

I hereby declare that all information in this document has been obtained and presented in accordance with academic rules and ethical conduct. I also declare that, as required by these rules and conduct, I have fully cited and referenced all materials and results that are not original to this work.

Faez Qahtan Waheed WAHEED

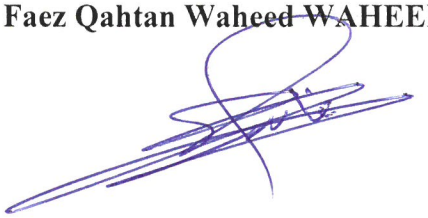

TABLE OF CONTENTS

ABSTRACT

Ph.D. Thesis

DETERMINATION OF QUALITY PARAMETERS OF GAMMA SPECTROMETER SYSTEM

Faez Qahtan Waheed WAHEED

Süleyman Demirel University
Graduate School of Natural and Applied Sciences
Department of Physics

Supervisor: Prof. Dr. İskender AKKURT

Radiations started to be used in a variety of different fields with the development of technology. As the high value of radiation is hazardous for human health, the quality parameters of gamma spectrometer become vital, and they should be measured carefully. The scintillation detectors are usually preferred among other types of detection systems because of their higher detection efficiencies, cheap availability, low-level measurements of gamma-emitters, resistant to thermal effects and weather conditions.

FLUKA is one of the most preferred simulation codes. It uses the Monte Carlo technique to simulate transportation and interaction with the matter of about 60 particles over a wide energy range with high accuracy.

In this study, important quality parameters of the gamma spectrometer system have been determined and also, the impact of the source-detector distance has been determined for each value of these parameters. Thus, fundamental data for further works have been obtained. FLUKA code has been used to support the experimentally results. The detector has been modeled with FLUKA code and the results of the simulations have been compared with measurements. A good agreement has been found between simulation and experimentally results. This study demonstrates that FLUKA can be apply to determin of quality parameters for various energies and source-detector distances when it is difficult in practice.

Keywords: Gamma-ray measurement, FLUKA, Quality parameters, NaI(Tl) detector, Geometry.

2020, 119 pages

ÖZET

Doktora Tezi

GAMA IŞINI ÖLÇÜMLERİ İÇİN GEOMETRİK YAPI ÇARPANININ ARAŞTIRILMASI

Faez Qahtan Waheed WAHEED

Süleyman Demirel Üniversitesi
Fen Bilimleri Enstitüsü
Fizik Anabilim Dalı

Danışman: Prof. Dr. İskender AKKURT

Teknolojinin gelişmesiyle birlikte çok çeşitli alanlarda radyasyonlar kullanılmaya başlanmıştır. Yüksek radyasyon değeri insan sağlığı için tehlikeli olduğundan, gama spektrometresinin kalite parametreleri hayati hale gelir ve dikkatle ölçülmeleri gerekmektedir. Sintilasyondetektörleri, daha yüksek algılama verimlilikleri, ucuz bulunabilirlikleri, düşük seviyeli gama yayıcı ölçümleri, termal etkilere ve hava koşullarına dirençli olmaları nedeniyle genellikle diğer detektör sistemleri arasında tercih edilirler.

FLUKA, en çok tercih edilen simülasyon kodlarından biridir. Yüksek doğrulukta ve geniş bir enerji aralığında yaklaşık 60 parçacığın taşınmasını ve etkileşimini simüle etmek için Monte Carlo tekniğini kullanmaktadır.

Bu çalışmada, gama spektrometresinin önemli kalite parametreleri belirlenmiş ve ayrıca bu parametrelerin her bir değeri için kaynak-detektör mesafesinin etkisi belirlenmiştir. Böylelikle daha ileri çalışmalar için temel veriler elde edilmiştir. FLUKA kodu, ölçüm sonuçlarını test etmek amacıyla kullanılmıştır. Detektör, FLUKA kodu ile modellenmiş ve simülasyonların sonuçları ölçümlerle karşılaştırılmıştır. Simülasyon ve ölçülen sonuçlar arasında iyi bir uyum bulunmuştur. Bu çalışma, FLUKA'nınçeşitli enerjiler ve kaynak-detektör mesafeleri için kalite parametrelerini belirlemenin pratikte zor olduğu durumlarda kullanılabilir olduğunu göstermektedir.

Anahtar Kelimeler: Gama ışını ölçümü, FLUKA, kalite parametreleri, NaI(Tl) dedektör, geometri.

2020, 119 sayfa

ACKNOWLEDGMENTS

I praise thee, ALLAH, for whatever thou have taught me and whatever thou have inspired me with throughout this work.

I want to put this page into lively moments of the conclusion of this study, and I am proud of them and seize the opportunity to thank those people whom were necessary for doing this work.

I would like to express my sincere appreciation and gratitude to my supervisor, Prof. Dr. İskender AKKURT, who sparked my interest in applied Monte Carlo simulation, for his supportive guidance and help throughout the thesis, which were invaluable on the chapters of the thesis enrich the whole work and for his words that always encourage me to work hard. This thesis is a successful result of the joint work with my supervisor Prof. Dr. İskender AKKURT my sincere gratitude and appreciation to him again. I would like to express my great thanks to Dr. Gaber FAISEL, Prof. Dr. Aslı KARAKAŞ, Dr. Feride KULALI, and to the head of the department of physics and all the physics department staff during my study. Also deeply thank to Dr. Hakan AKYILDIRIM and Dr. Kadir Günoğlu for their in valuable support in gamma spectrometer laboratory throughout my study time.

I dedicate this work to my father (Qahtan Waheed), who was the reason to succeed for all the family and after that, I am greatly indebted to my family, especially my mother who kept encouraging me to do my best to get my (Ph.D.) degree. I would like to thank all my brothers, my sisters; Bushra, special thanks to my wife Rana and my daughters: Danyah, Tasnim, and my son Abdul Azeez. Thanks to all my friends who have supported and advised me throughout my study time.

Faez Qahtan Waheed WAHEED
ISPARTA, 2020

LIST OF FIGURES

LIST OF TABLES

Page

1. INTRODUCTION

1.1. Radiation Basics

Radiation and radioactivity were discovered more than 100 years ago and radioactivity phenomenon occurs when energy is released from an atom spontaneously. After this discovery, the science of radioactivity has been extensively studied. Radiation can defines as energy in the form of electromagnetic waves or particles that pass through heavy dense materials, for the purpose of this study, radiation has enough energy for ionization or excitation matter that interacts with, and causes bad effected in human beings because of the damage in living cells (Akkurt, I., & Tekin, H. O. 2020).

Radioactivity is a continuously decreasing quantity which is a function of the half-life of the responsible radionuclides (UNEP, 2016; Ivanova, D., et al., 2016)**.** Today the radioactivity uni□in the System International of unit (SI) are Curie (Ci) and Becquerel (Bq). A Bq equal to one disintegration per second (dis/s), while 1 Curie (Ci) is equal to 3.7 x 10^{10} Bq (L'Annunziata, M. F., 2012).

Ionizing radiation is radiation with enough energy so that during an interaction with an atom, it can remove tightly bound electrons from the orbit of an atom, causing the atom to become charged or ionized, ionizing radiation is a part of nature and of human activities in medicine, research, industry, energy production and some especially military application (Waheed, F. Q. W., & Akkurt, İ., 2017).

1.2. Source of Radioactivity

The main origin of radioactivity belongs to two categorizations; natural sources and man-made sources. Natural source of radiation comes from terrestrial radionuclides, terrestrial radionuclides are distributing widely in the earth's crust and sources arising from the cosmic ray. Other sources arise from human activities concerned with the use of radiation and radioactive materia□ from which releases of radionuclides into the environment may occur (A□array, E., 2016; Akkurt, İ., et al., 2020).

One source of radiation is the nuclei of unstable atoms where the nuclides disintegrate in a process where in general, one element is transforming into another, the excess energy of the nuclide being dissipated as electromagnetic radiation or particles. As

a result, radiation is transporting as energy. There are four forms of ionizing radiation (Akyildirim, H. et al., 2020).

Radiation risks to people and the environment that may arise from the use of radiation and radioactive materials, the radiation must be controlled through the application of standards safety (Daniel, G., 2008; Justice, H., 2016).

1.2.1. Natural sources

Natural radiation sources comprise extraterrestrial and terrestrial radiation sources (UN, 2000). The extraterrestrial radiation sources include two types of radiation sources which are cosmic rays and cosmogonic radionuclides. Cosmic rays incident on the top of the atmosphere consis□ of a nucleonic component which in aggregate accoun□ for 98% of the total, and 2% electrons. The nucleonic component is primarily protons (88%) and alpha particles (11%), with the remainder heavier nuclei. When they enter the upper layer atmosphere, they undergo interactions that may produce charged particles, gamma rays, and neutrons (Beer, J., et al., 2012).

The cosmogenic radionuclides are produced by the collision of the highly energetic cosmic-ray particles with stable elemen□ in the atmosphere and the ground. Many different cosmogenic radionuclides are produced, such as ^{14}C. It is the most important, and other less significant cosmogenic radionuclides such as ^{3}H, ^{7}Be, and ^{22}Na. The cosmic radiation intensity depends upon the degree of shielding provided by the atmosphere, altitude and barometric pressure (Huffert, A. M. et al., 1994).

The other natural sources are primordial radionuclides. these sources have very long half-lives, as comparable to the age of the earth, they are classified into:-

- Series radionuclides groups of radionuclides that are headed by parent radionuclides which decay in sequence to other radionuclides with different half-lives and decay modes, and finally end up as stable isotopes. There are three natural series headed by ^{238}U, ^{235}U, and ^{232}Th, as shown in Figures 1.1, 1.2, and 1.3 respectively (Friedberg, W., et al., 1999; RCT 1.05-SG, 2013).
- Non-series radionuclides; they decay directly to stable nuclide. The most important of non-series radionuclides are the isotopes ^{40}K, ^{87}Rb, ^{113}Cd and ^{115}In. In terms of population radiation dose, ^{40}K and ^{87}Rb are the most significant radionuclides. The

radioactive isotope of ^{40}K can decay by beta followed by the emission of a 1460.8 keV gamma-ray whereas ^{87}Rb is a pure beta emitter (Mostafa, G., et al., 2002; RCT 1.06-SG, 2013; Cottingham, W. N., et al., 2001).

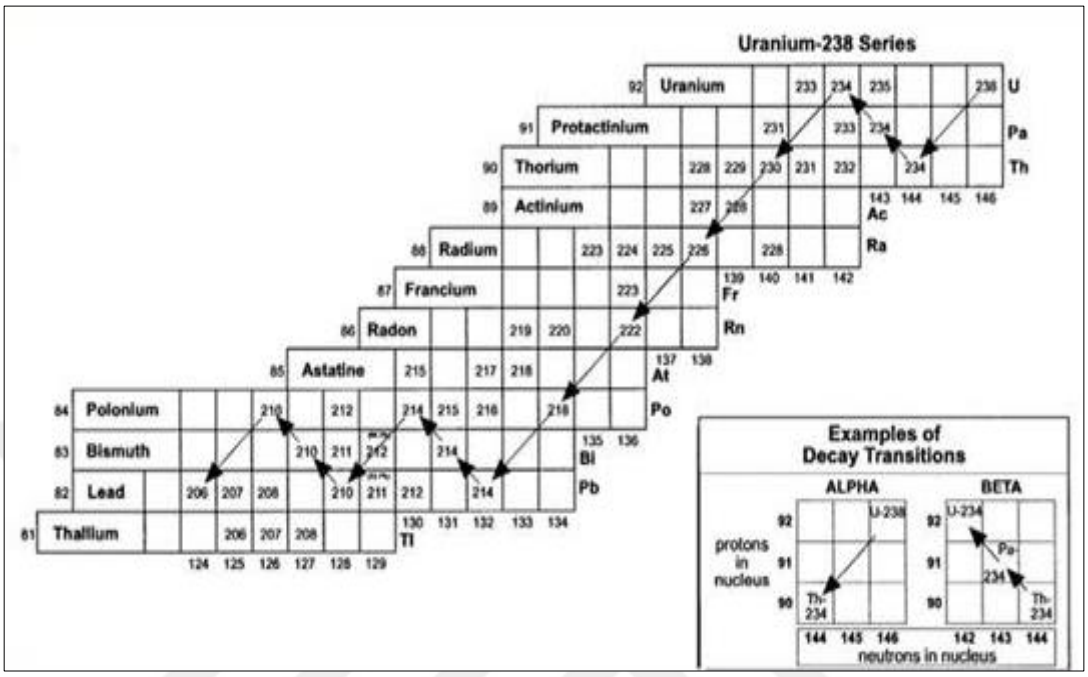

Figure 1.1. ^{238}U decay series (Harb, S. R. M., 2004)

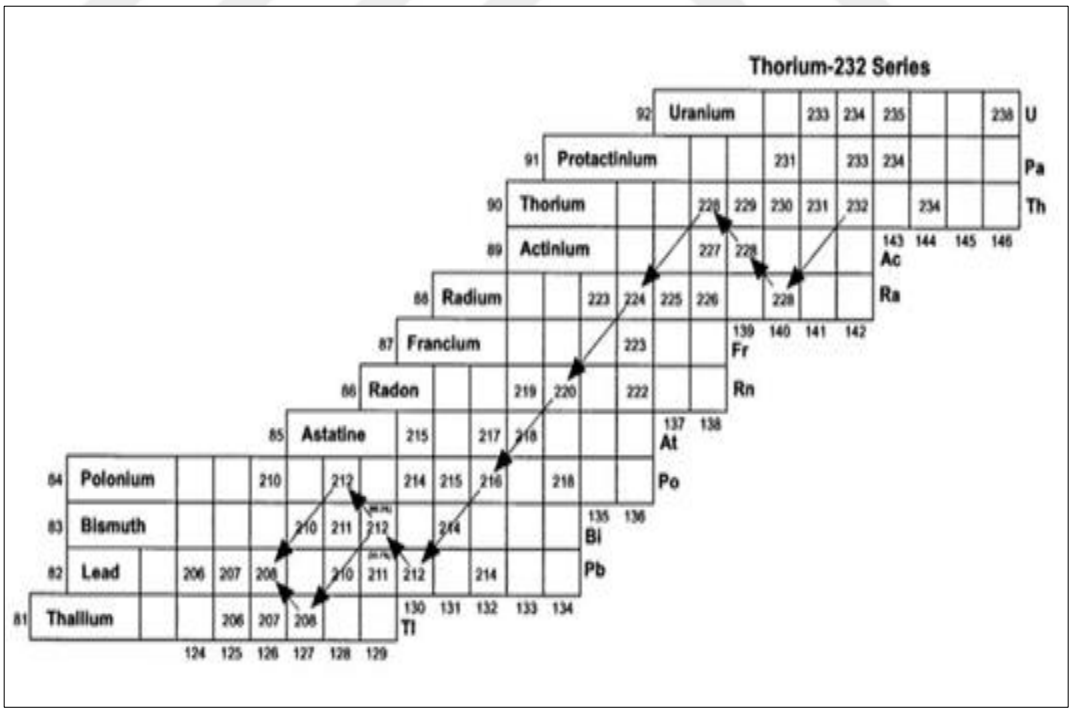

Figure 1.2. ^{232} Th decay series (Harb, S. R. M., 2004).

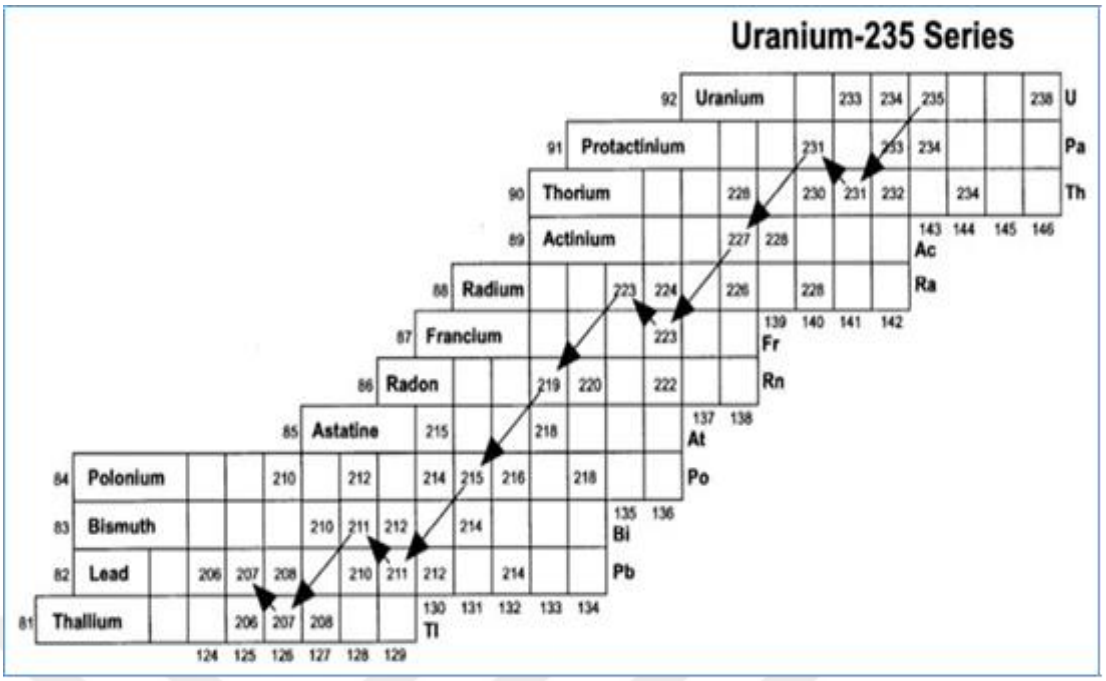

Figure 1.3. ^{235}U decay series (Harb, S. R. M., 2004).

1.2.2. Man-made sources

Some radionuclides have been released into the environment by a human for various purposes. The man-made sources of radiation may result from physical processes involving nuclear fission and fusion, nuclear explosions, neutron activation, and nuclear accelerators. In the middle of the 20th century, linear accelerators were developed for producing artificial radionuclides. The application of nuclear fission in 1940, presented the ability of humans to produce large quantities of artificial radionuclides by neutron-induced nuclear reactors which are the most important sources of artificially created radionuclides (Masson, O., et al., 2011; RCT 1.07-SG, 2013).

The fission process causes a high neutron flux density that produced in nuclear weapons explosions or fission reactors, it led to the production of large quantities of fission and activation produc. Fission produc are the isotopes with a mass number in the range of 70-170, formed by ^{235}U thermal fission and other heavy fissile nuclei (e.g., ^{239}Pu). High-yield fission produc includes "^{89}Sr, ^{90}Sr, ^{91}Y, ^{95}Zr, ^{95}Nb, ^{99}Mo, ^{103}Ru, ^{131}I, ^{133}Xe, ^{137}Cs, ^{140}Ba, ^{140}La, ^{141}Ce, ^{144}Ce, ^{143}Pr, and ^{147}Nd" (Wania, F., et al, 1998).

However, in most situations, the most radiologically important fission produc are ^{89}Sr, ^{90}Sr, ^{131}I, and ^{137}Cs because of their high yields, long half-lives and chemical properties (Kalilainen, J., 2015).

1.3. The types of Radiation

1.3.1. Ionization radiation

One source of radiation is the nuclei of unstable atoms where the nuclides disintegrate in a process wshere, in general, one element is transforming into another, the excess energy of the nuclide being dissipated as electromagnetic radiation or particles. As a result, radiation is transporting as energy (Karkosh, H. L. et al., 2016).

1.3.1.1. Alpha radiation (α)

This is a particulate radiation of helium nuclei comprises of two protons, two neutrons, no electrons, and almost relatively large mass, highly energetic, short-range with regular slow velocity through the air (1.4 – 2.2 x 10^4 cm/sec), as shown in Figure 1.4.

Alpha particles have low penetration and higher ionization. Depending on their energy, it is stopping completely in a few centimeters of air, a normal paper, or the dead tissue of the outer layer of human skin. Commonly, sources of alpha radiation are Uranium and Plutonium and element with atomic number > 82, except Samarium which has an atomin number of 62 (Smith, B. T., 2010; Vahlbruch, H., et al., 2016).

The standard notation for alpha decay is:-

$$\begin{matrix} A \\ Z \end{matrix} X_n \rightarrow \begin{matrix} A-4 \\ Z-2 \end{matrix} Y_{n-2} + \begin{matrix} 4 \\ 2 \end{matrix} He_2^{2+} \qquad (1\text{-}1)$$

The external exposure to alpha particles are not considered hazard because they just impact on the outer human soft tissue, this impact is of far less concern than internal exposure, internal exposure through inhalation, ingestion, or absorption into the bloodstream could be very harmful when a sensitive tissue is exposing to alpha particles (Cember, H., 1996).

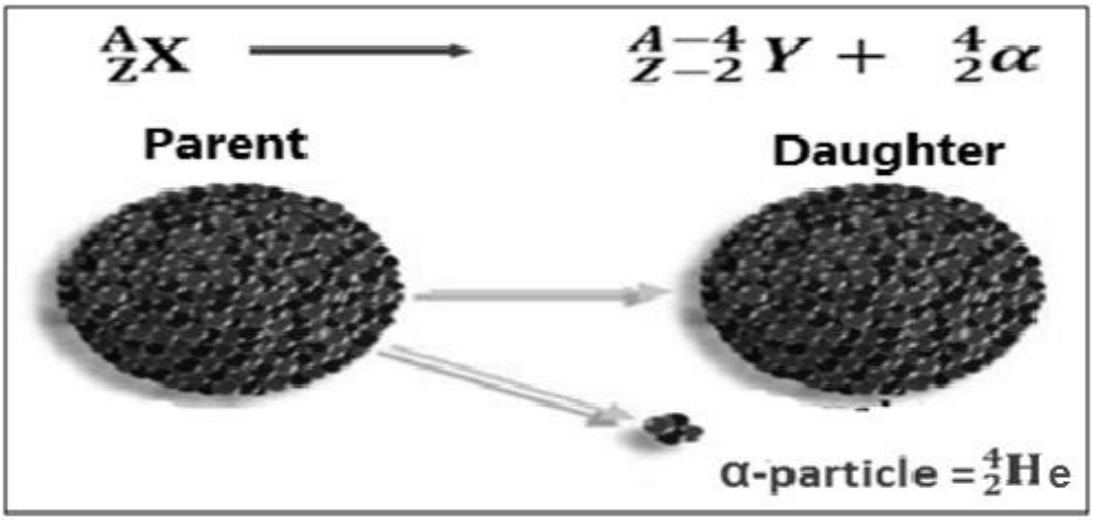

Figure 1.4. Alpha particle decay mode (RCT 1.05-SG, 2013).

1.3.1.2. Beta radiation (β)

This is an electron (β^-) or a positron (β^+) emitted by an atomic nucleus. This process is shown in Figure 1.5 and Figure 1.6. Beta particles are of very low mass and have more penetration ability when compared with alpha particles. Beta particles disappear in a thin layer of plastic, some millimeters of glass, or low Z number element. It can be absorbed in the dead layer of human skin and the living tissue, causing ionization which can be harmful. All unstable elements may not emit positive or negative electron, and in this situation, a proton inside nuclei can capture the electron from the closest shell and changed as a neutron ($p+e^- \rightarrow n$), this phenomenon name is electron captivating (Al-Sarray, E., & AKKURT, İ., 2016).

The standard notation for beta minus (when N>Z):-

$$^A_ZX \rightarrow {}_{Z+1}{}^AY + \beta^- + \nu^- \quad (1\text{-}2)$$

The standard notation for beta plus (when N<Z):-

$$^A_ZX \rightarrow {}_{Z-1}{}^AY + \beta^+ + \nu \quad (1\text{-}3)$$

The standard notation for electron capture (when N<Z):-

$$^A_ZX + e^- \rightarrow {}_{Z-1}{}^AY + \nu \quad (1\text{-}4)$$

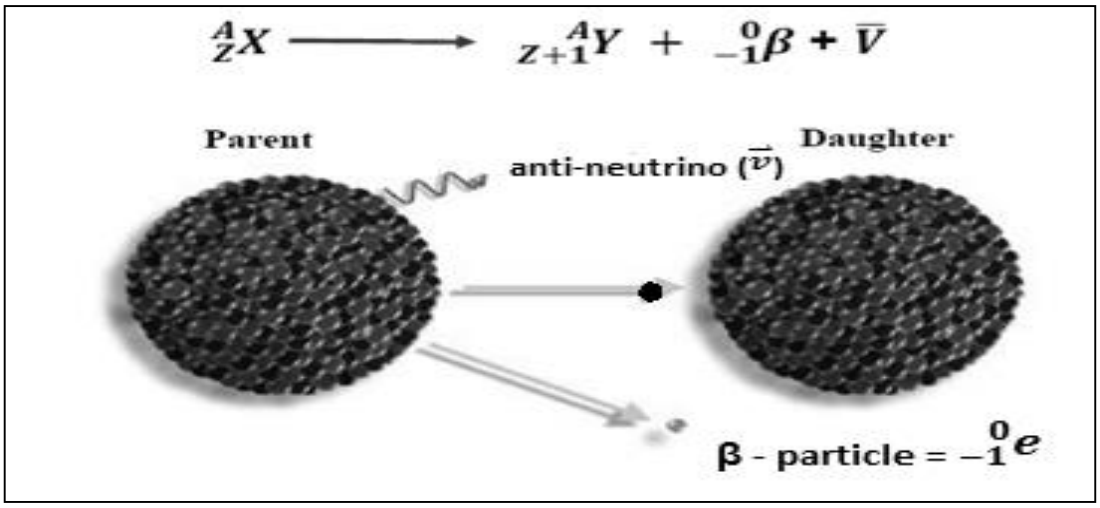

Figure 1.5. The beta particle mines emission (Waheed, F., Q., & Akkurt, I., 2017).

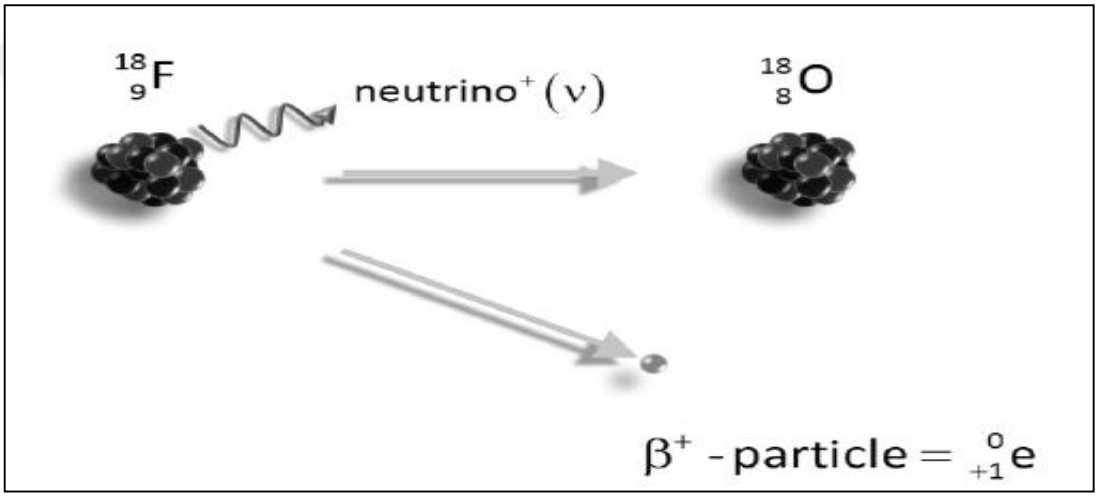

Figure 1.6. The positron particle emission (RCT 1.06-SG, 2013).

1.3.1.3. Gamma-rays radiation (γ)

This is a high energy of gamma-ray that emergences at the light speed emit from an excited atomic nucleus. Gamma-ray are more penetrating than alpha and beta particles, they move as small bundles or packe□of energy (Figure 1.7). They are often accompanying the emission of alpha or beta particles from a nucleus. Gamma-rays interact during its path with the electrons of the potential barrier into which it is absorbing some or all the gamma-ray energy, causing ionization which can be harmful to the outer or internal living tissue. Typically, very dense attenuators, such as lead, steel, or layers of cement wall with a made of dense structure, may be used for shielding (CNSC, 2017; IAEA-TECHDOC-1191).

The standard notation for gamma-ray is:-

$$^{A}_{Z}X^{*} \rightarrow {}^{A}_{Z}X + \gamma \quad (1\text{-}5)$$

$$E\gamma = \hbar \frac{c}{\lambda} \quad (1\text{-}6)$$

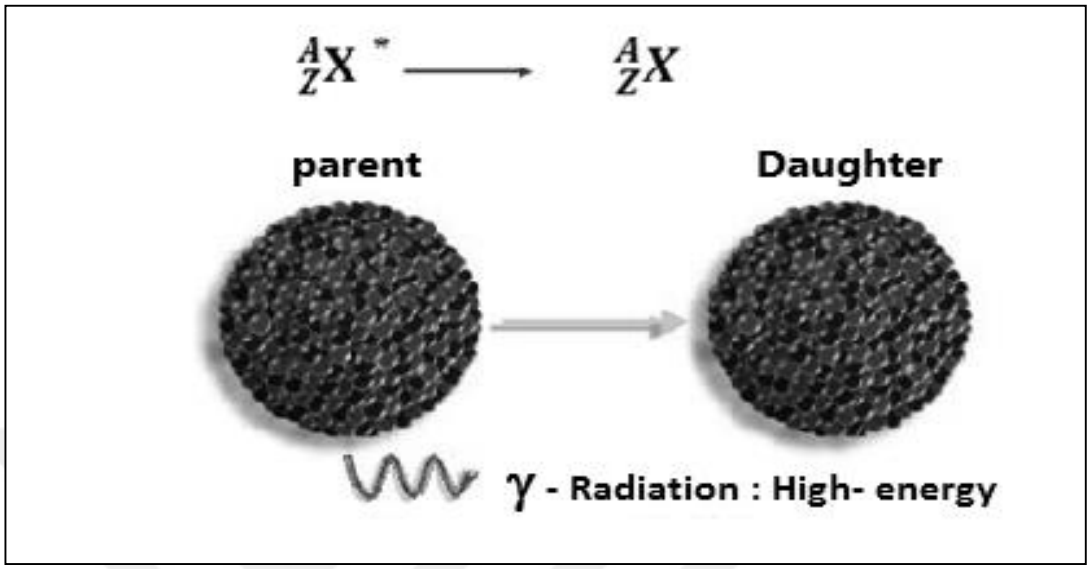

Figure 1.7. The processes of gamma-ray emission (Abdlhamed, A.F., & Akkurt, I., 2018)

1.3.1.4. Neutron

Neutron is a particle releases from natural fission element such as californium isotropic source. The mass of neutron is approaching to the mass of the proton, it is relatively small and light in atomic terms, neutral charge, high energy, therefore, it has high penetration because of neutral electricity, it passes through the air in hundred meters, because neutrons are electrically neutral, they do not promptly interact with orbital electrons and ionize the barrier that passes through, however, when they interact with the nuclei of atoms in the barrier they can damage them and transfer barrier to unstable atom, which means that they can be very damaging to the human tissue. Neutron penetration through the material relatively easily, and can shielded by Hydrogen-rich element and compound (Price, B., et al., 1957; Dickstein, P., & Vanunu, S., 2016). The neutron emission processes are shown in Figure 1.8.

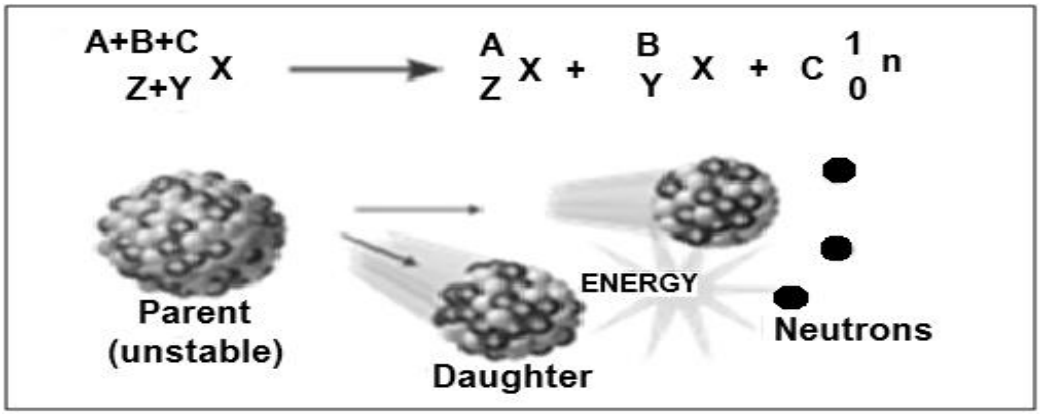

Figure 1.8. Neutrons radiation (RCT 1.13-SG, 2013)

Table 1.1. The radiation properties (RCT 1.07-SG, 2013).

Radiation	Symbol	Form	Origin	Essential Parts	Mass (amu)	Charge	Energy Spectrum	Miscellaneous information
Alpha	α	Charge particle	nucleus	2p, 2n	4	+2	MeV	Mono-energetic; from heavy radionuclides
Beta (-minus) (Negatron)	β^-	Charge particle	nucleus	1 e^-	<< 1	-1	0 to max	Fission products
Gamma	γ	Electro magnetic Radiation	nucleus	Photon	None	None	MeV	Usually follows particle emission
X-ray	X	Electro magnetic Radiation	Electron orbital	Photon	None	None	keV	Cascade following EC; Bremsstrahlung
Positron Beta plus	B^+	Charged particle	nucleus	Antimatter equivalent of 1e^-	<<1	+1	0 to max	Will annihilate with e^-
Neutron	η	Un charged particle	nucleus	1 η	1	0	eV to MeV	Born "fast"
Proton	P	Charged particle	nucleus	1P	1	+1	eV to MeV	Scattered in neutron interactions
Ion/ Fission fragment	FF	Charged particle	nucleus	Light and heavy nuclei	varies	>>1	MeV	Results from fission
Neutreno	v	Un charged particle	nucleus	--	0	0	MeV	From B^+ decay
Antineutrino	□	Un charged particle	nucleus	--	0	0	MeV	From B^- decay

1.3.2. Non-Ionizing radiation

Non-ionization radiation can travel at a speed of light, but it doesn't have the amount of sufficient energy needed to ionize an atom which interacts with. There are many examples of non-ionizing radiation such as; the radar wave, the radio wave that comes from a radio station, the microwave, and the visible light that comes from a lamp.

Although the word "radiation" can be used to mean ionizing or non-ionizing radiation, it is most often used to mean ionizing radiation (IARC, 2020).

Figure 1.9 shows full electromagnetic spectrum includes ionizing radiation and non-ionizing radiation. It can conclude from the spectrum shape that the gamma-ray and X-ray are ionizing and all other are electromagnetic waves are non-ionizing radiation.

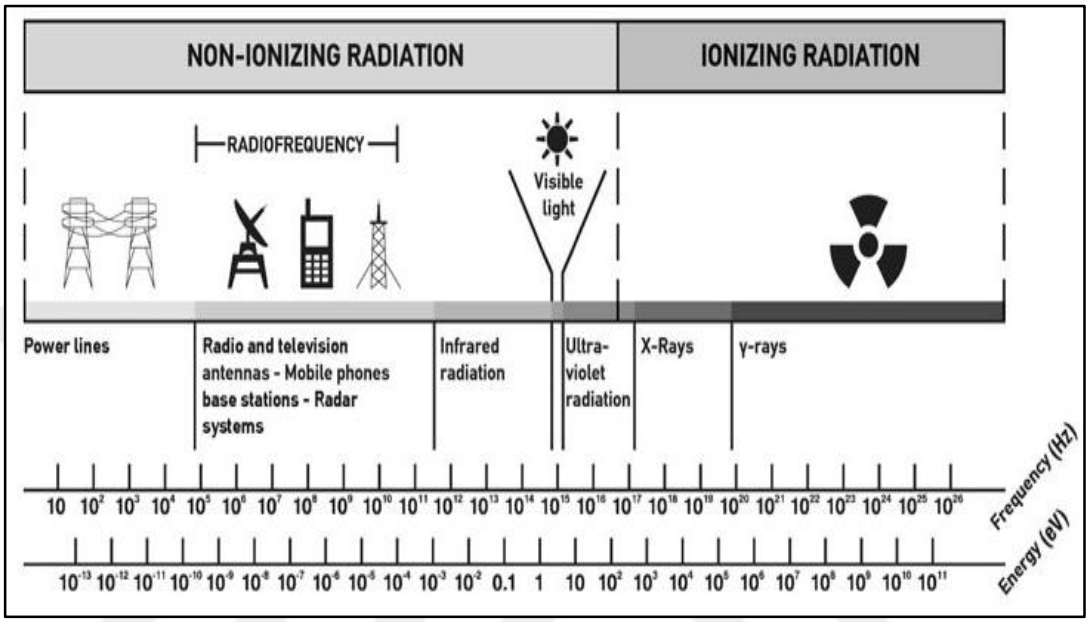

Figure 1.9. The electromagnetic radiations (Al-Sarray, E., & Akkurt, İ., 2016).

1.4. Physics of Interactions of Gamma-ray

A gamma-ray penetrating through a medium will interact with the atoms and nuclei in that medium through various mechanisms and usually transfers energy in this process. The types and likelihoods of these interactions are functions of gamma-ray energy, gamma-ray polarization, the atomic number, and physical properties of the medium (Martine, A., 2012; Jubair, S. I., 2011).

The gamma-ray interaction with matter includes several processes depending on some parameters, the most important for gamma-rays with energies up to several MeV being (Martine, J. E., 2006).

In the Photoelectric interaction, the gamma-ray losses all the kinetic energy to the atomic electron; elastic (coherent) scattering (scattering with saving energy); Compton (incoherent) scattering (the gamma-ray is changing the direction, losses a part of i□

kinetic energy to an atomic electron, behaves as though it were free); Pair production in general, a gamma-ray of sufficient energy generates an electron-positron pair in the electromagnetic field of the atomic nucleus (Tsoulfanidis, N., 1995).

The gamma-ray interaction with matter is consistently statistical in nature, and therefore must be described in probability conditions. The interaction probability per unit path length is fundamental in describing how gamma-ray matter interact is habitually referring to as the linear attenuation coefficient (μ) (Chilton, A. B., 1984).

That (μ) is constant for a given material and type of interaction implies that the probability of interaction per unit path length is independent of the path length prior traveled befor the interaction. The linear interaction coefficient is a function of the energy of the particle (Akyıldırım, H., 2018).

Depending on the nature of the interaction, it may a□o be a function of the energy of the particle after scattering, the energy of the recoil atom or electron, the angles of deflection of the scattered radiation and recoil atom or electron and angles of emission of secondary particles, all measured from the initial direction of the incident particle (Cherry, S. R., 2012).

Gamma-ray energy is customarily designated as hv, (usually expressed in uni□ of electron vol□, "eV"), where h is Planck's constant (6.63×10^{-34} J.s) and v is the frequency of gamma-ray or the electromagnetic wave, Figure 1.10 illustrates the relative importance of predominant interactions based on the incident gamma-ray energy and the atomic number (Z) of the attenuator (Knoll, G. F., 2000; Evans, R. D., 1955).

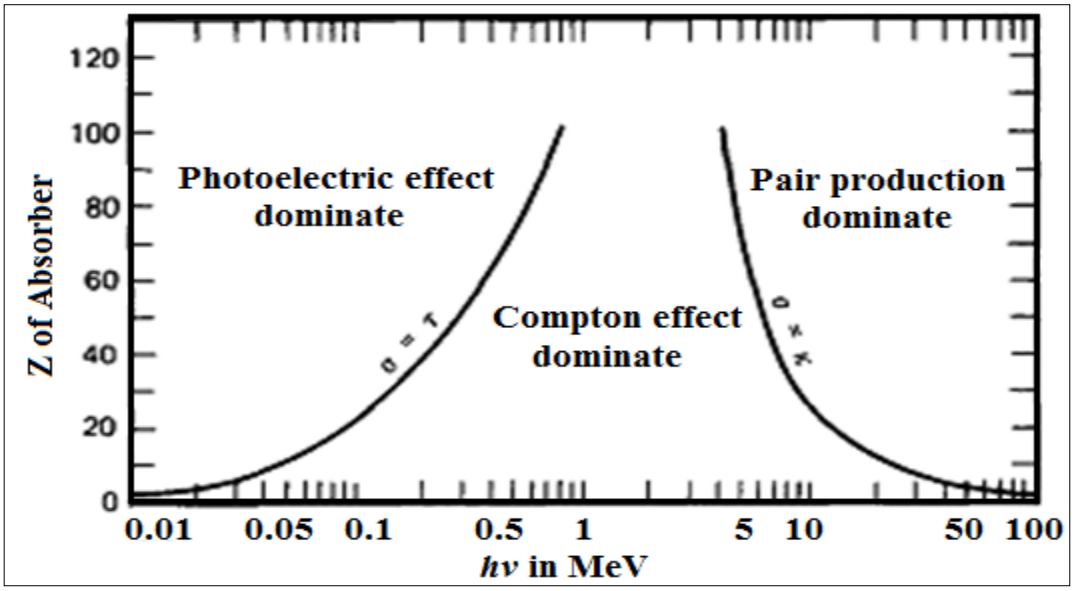

Figure 1.10. Relative importance of the three major types of gamma interactions (Krane, K. S., & Halliday, D., 1987).

The concluded from Figure 1.10 clearly shows that Compton scattering is dominant at the intermediate energy range for all Z values. Therefore, appropriate selection of the source radiation energy can ensure that Compton scattering is the predominant interaction at the Z value of the target material.

For example; the energy peak for ^{137}Cs at 0.662 MeV, referring to the Figure 1.10, at this energy Compton scattering phenomena is the dominant interaction for any material with an atomic number below 90 (atomic numbers for some typical meta□ are; lead Z = 82, steel Z=27, aluminium Z=13). Therefore with a ^{137}Cs radiation source, Compton scattering becomes the dominant interaction for most engineering materia□ of interest. The same can be said for a ^{60}Co source with energy peaks at 1.173 MeV and 1.332 MeV.

The reduction in the intensity of an incident beam as it travels through matter follows an exponential relationship, which is a function of the distance travelling and the interaction (attenuation) coefficient. The attenuation coefficient is, in turn, a function of the incident gamma-ray energy and the material type (Evans, R. D., 1955). Accordingly, the transmitted intensity *'I'* of the beam with initial intensity *'I_o'* after traveled a distance *x* in a homogeneous absorber is given by (Tsoulfanidis, N., 1995; Knoll, G., 2010).

$$I = I_o e^{-(\tau+\sigma+\kappa)x} = I_o e^{-\mu x} \qquad (1\text{-}7)$$

$$\mu\,(E) = \mu_\tau + \mu_\sigma + \mu_\kappa = \rho \frac{N_A}{A} \sigma_a \qquad (1\text{-}8)$$

where $\mu = \tau + \sigma + \kappa$ is known as the "total linear attenuation coefficient", which is a measure of primary gamma-rays which will be involved in photoelectric (τ), Compton (σ), and pair production (κ) interactions and ρ: mass density, A: atomic, N_A: Avagadro's number, σ_a: total atomic cross-section.

As mentioned, photoelectric and pair production interactions absorb the entire energy of the incident gamma-ray and result in the emission of secondary particles. In both cases the resultant particles (photoelectrons and electron/positron pairs, respectively) exhibit distinctive particle energies that can be easily identified, allowing their influence on Compton scattering measuremen□to be corrected (Evans, R. D., 1955).

1.4.1. The Photoelectric effect

The first physical phenomenon of gamma-ray interaction with matter results is the photoelectric effect (a first mechanism), it is an all-or-none energy loss. The energy of the incident gamma-ray should be equal to or more than the energy of the orbital electron. The physical phenomena effect is only significant for initial gamma-rays energies less than 1 MeV. Liberated electron as a result with high velocity is called photoelectron, as illustrated in Figure 1.11.

The energy is given by:-

$$E_{pe} = hf - \varphi \qquad (1\text{-}9)$$

The high velocity electron, which is called a photoelectron, is a directly ionizing particle and typically has adequate energy to repel other electrons from the orbits of other atoms, and it continues its path producing secondary ion-pairs until all of its energy is exhausted. The probability of photoelectric effect is maximum when the energy of the gamma-ray is of an equal value to the binding energy of the electron. The tighter an electron is bound to the nucleus, the higher the probability of photoelectric effect so most majority of photoelectrons are inner-shell electrons. The photoelectric effect seem primarily as an effect of low energy gamma-rays with energies near the electron binding energies of materials and high Z materials whose inner-shell electrons have high binding energies (Mahdi, K., 2017).

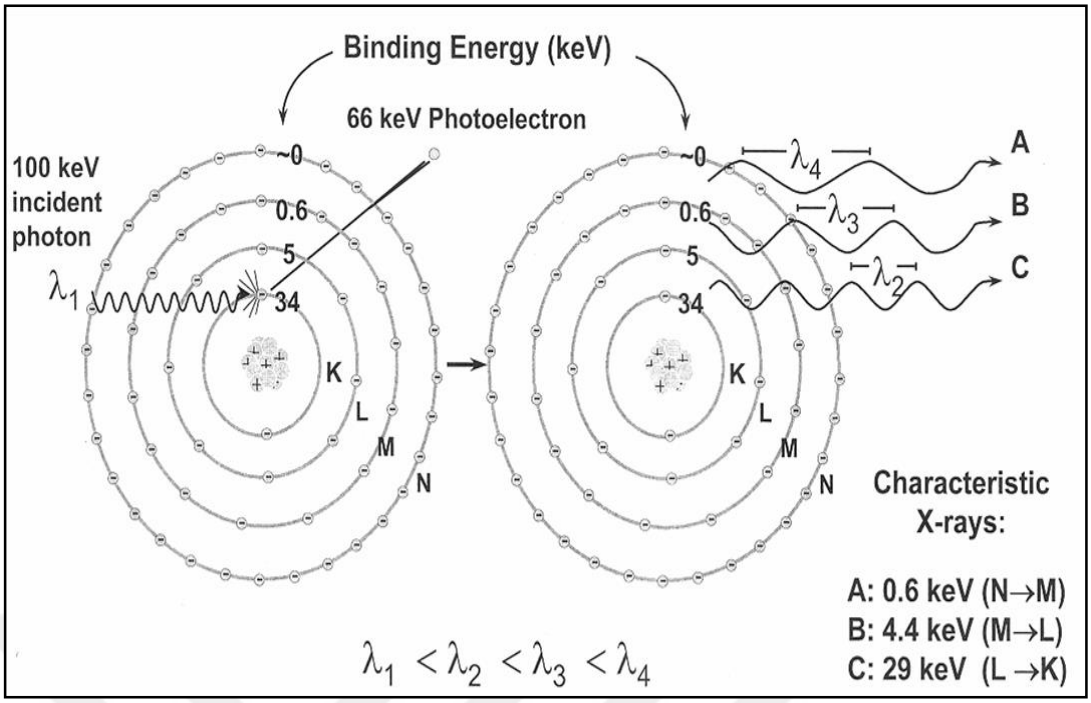

Figure 1.11. The mechanism of photoelectric effect phenomena (Shleien, B., 1992).

1.4.2. Compton Scattering

Compton (incoherent) interaction (the second mechanism) refers to the interaction of a gamma-ray with an individual electron, in Copmton scattering relatively small part of the energy could be transferred to the electron, there is a partial energy loss for the incoming gamma-ray, in Compton scattering, a gamma-ray of energy *hv* interac□with an atomic electron in the direction Ω = (θ, φ), see Figure 1.12.

Compton scattering is the dominant interaction phenomenon for most absorbers when the incident gamma-ray energy (0.2 - 5 MeV), the gamma-ray is changing the directions with lost energy during the collision, to conserve the momentum, an electron will take different energy.

By Compton scattering phenomena, scattered gamma-rays are appearing in different direction and energy, so that Compton gamma-ray are appearing around and behind absorber, these scattered gamma-rays are differ from the direct one emitted from the gamma-ray emitter. The Compton interaction probability increases in leve□for loosely bound electrons, therefore, most Compton electrons are valence electrons (Lipps, F. W., & Tolhoek, H. A., 1954).

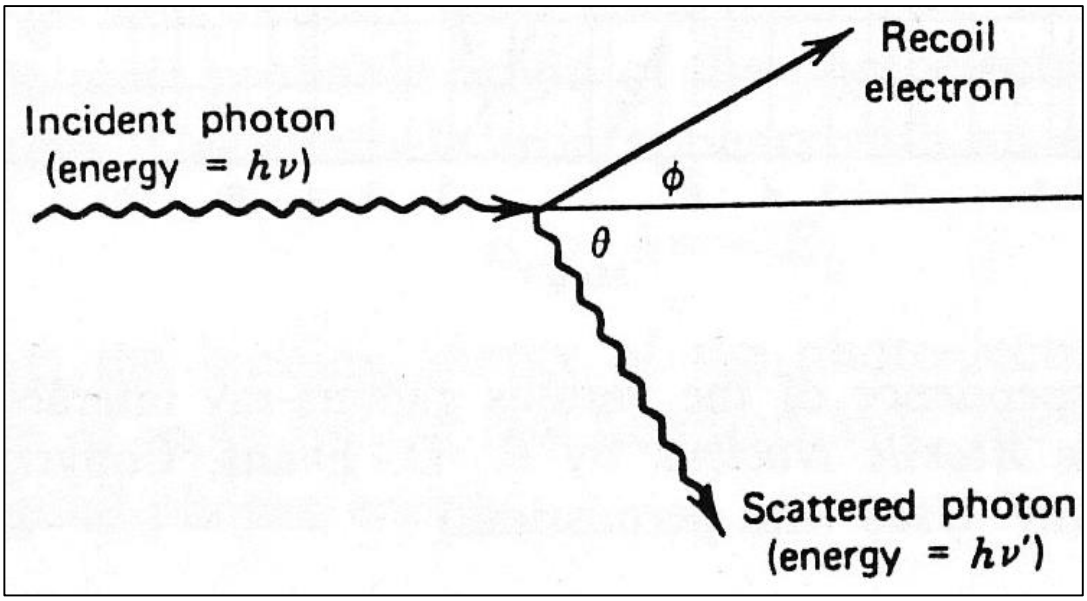

Figure 1.12. Compton Scattering (Tsoulfanidis, N., 1984).

There are two cases to illustrate incoherent (Compton) scattering. The first, a case of scattering by free (unbound) electrons at rest .This involves a collision between an incident gamma-ray with energy $h\nu_o$ and an atomic electron with a rest mass equivalent to m_oc^2 (0.511 MeV). The incident gamma-ray survives the collision by scattering with reduced energy, $h\nu'$, depending on the initial energy and the angle of scattering θ. The values of scattered energy and scattering angle are governed by the rules of conservation of energy and momentum. The electron recoi□as a result of the collision with an angle Φ, with respect to the path of the incident gamma-ray, a momentum p and kinetic energy T (Tsoulfanidis, N., 1984).

A detailed understanding of Compton scattering requires consideration of the kinematics and probability of the Compton scattering interaction within the target material.

Conservation of energy and momentum leads to the 'energy-angle relationship' (Knoll, G. F., 2000; Evans, R., 1955).

$$h\nu' = \frac{h\nu_o}{\left[1+\left(\frac{h\nu_o}{m_oc^2}\right)(1-\cos\theta)\right]} \qquad (1\text{-}10)$$

This expression relates the energy of the scattered gamma-ray to the incident energy and the angle of scattering. The "energy-angle relationship" can be exploited in practical applications. By measuring the energy, one can directly obtain the angle of scattering and consequently determine the direction from which the scattered gamma-

ray has emerged. The mathematical expression for the relationship described the angular differential Cross-section for unpolarized gamma-ray incoherently (Compton) scattered with a free electron is as follows (Knoll, G. F., 2000; Evans, R. D., 1955; Heitler, W., 1954).

$$\frac{d\sigma_{KN}(h\nu,\theta)}{d\Omega} = \frac{r_o^2}{2}(1-\cos^2\theta)\left[\frac{1}{1+\alpha(1-\cos\theta)}\right]^2\left\{1\frac{\alpha^2(1-\cos\theta)^2}{(1+\cos^2\theta)[1+\alpha(1-\cos\theta)]}\right\} \quad (1\text{-}11)$$

This has also been expressed as (Sood, A., & White, M., C., 2004).

$$\frac{d\sigma_{KN}}{d\Omega} = \frac{r_o^2}{2}\left(\frac{h\nu'}{h\nu}\right)^2\left[\frac{h\nu}{h\nu'} + \frac{h\nu'}{h\nu} - sin^2\theta\right] \quad (1\text{-}12)$$

Where r_o is 'the classical electron radius' given by:-

$r_o = e^2/4\pi\epsilon_o\, m_o c^2 = 2.818 \times 10^{-13} cm$, and $\alpha = h\nu_o/m_o c^2$ is the relativistic factor of the gamma-ray, for radioactive source ^{137}Cs is 1.2947. The Klein-Nishina formula is represented graphically in Figure 1.13 (Knoll, G. F., 2000). Based on this approximation source energies and scattering angles can be appropriately selected to optimize system performance. Given the incident gamma-ray energy, *hv*, Equation (1-15) is sampled for the exiting angle. Equation (1-13) is used to determine the scattered gamma-ray's energy.

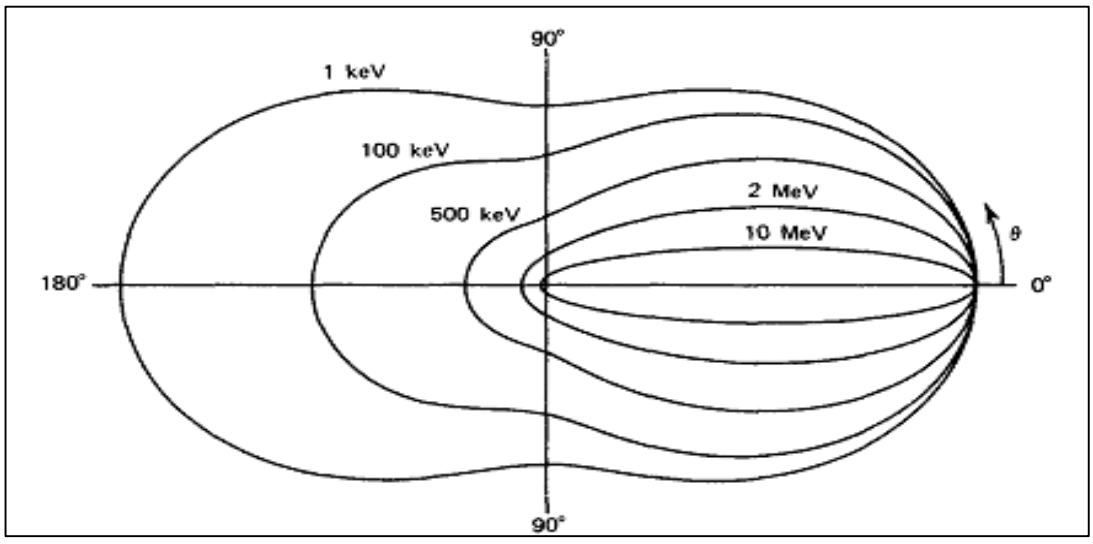

Figure 1.13. A polar plot of the number of gamma-rays Compton-scattered into a unit solid angle at the scattering angle θ (Knoll, G. F., 2000).

In the real world, the second case, the electrons are neither stationary nor free. The electron rotation may introduce a low-level deviation in Compton gamma-ray energy shift that gives rise to Compton broadening or the so-called Doppler broadening of the

Compton line. The binding energy of electrons in an atom resul□ in an incoherent atomic-cross section minimal than that measured by straightway multiply the electron Compton scattering cross-section with the Z value. This effect becomes significant for heavy elements and at low gamma-rays energies. In the theoretical simulation of incoherent scattering cross-sections, the binding energy phenomena are almost taken into calculation during an incoherent scattering function (Sood, A., & White, M., 2004) Since:-

$$\frac{d\sigma_{inc}^{atom}}{d\Omega}(E,\theta,Z) = S(X,Z)\cdot\frac{d\sigma_{KN}^{e}}{d\Omega}(E,\theta) \qquad (1\text{-}13)$$

Where *S* (*X*, *Z*) is the incoherent scattering function. Values of this function for various elemen□ are published in tabular form by (Hubbell, J. H., et al., 1975), as a function of *X*, the inverse length and *Z*. This function represen□ the probability that the atom is raised to an excited or ionized state as a result of accepting a recoil momentum of *2hX*. Here *h* is the Planck's constant and the parameter *X* is the inverse length, given by:-

$$X = \frac{1}{\lambda}\sin\frac{\theta}{2}(\lambda\ in\ units\ of\ Angstroms) \qquad (1\text{-}14)$$

$$= \kappa\alpha\sqrt{1-\mu}$$

Where $\kappa = 10^{-8}\,mc/\left(h\sqrt{2}\right) = 29.1445\ cm^{-1}$ and α is the initial gamma-ray energy in uni□ of rest mass energy of an electron.

S (X, Z) increases rapidly, especially for low-*Z* elemen□, at small values of *X*, and approaches a maximum value of *Z*, the atomic number, at large *X* (Hussein, E., & Whynot, T., 1989). As a result, the incoherent scattering function modifies the Klein-Nishina cross section prominently under conditions where the electron binding effect is strong.

1.4.3. Pair Production.

Pair production (the third mechanism) occurs when all of energy of the gamma-ray is converted to mass. This conversion of energy to mass only occurs in the presence of a strong electric field, which can be viewed as a catalyst. Such strong electric fields are seen near the nucleus of atoms and are stronger for high Z materials. Figure1.14, following, schematically shows pair production and the fate of the positron when it

combines with an electron (its anti-particle) at the end of its path. In pair production, a gamma gamma-ray simply vanishes in the vicinity of a nucleus, and in return a pair of electrons is replacing instead: one negatively charged and one positively charged. These anti-particles are also called an electron and a positron, respectively. The mass of these electrons has been created from the pure energy of the gamma-ray, according to the familiar Einstein equation E = mc2, where (E) is energy in joules, (m) is mass in kilograms, and (c) is the velocity of light in m/sec (Smathes, K. L., & Karp, A. H., 2008).

In pair production, the antimatter, do not exist freely in nature and cannot exist near matter, they will interact with the first electron, An electron and the positron destroy each other as a result of this interaction (Davis, J., R., 2000).

The value of the gamma-ray energy greater than the 1.022 MeV wants to create the mass that equal to the mass of two electrons, this excess energy is completely divided through the two-electrons as the kinetic energy of movement, and they desert out of the atom with magnificent speed. Considered known as the annihilation reaction, This converts matter back into energy, Both the positron and electron disappear, two gamma gamma-rays are released with an energy of 0.511 MeV (Wright, S. A., et al., 2011).

The total kinetic energy of the electron-positron is given by the following:-

$$E_{e^-} + E_{e^+} = h\nu - 2m_o c^2 \qquad (1\text{-}15)$$

The likelihood of pair production phenomenon less than photoelectric effect and Compton scattering interactions because the gamma-ray must approaching the nucleus. The likelihood increases for high atomic Z number of barriers and high energies of the incident particles (Cember, H., et al., 2008).

The main benefit use of the positron emission as a result of the Pair production phenomena in many medical diagnosis and treatment application such as; tomography, a nuclear medicine, imaging procedure, It is also used in radiation therapy treatment (Schoenung, S., 2011).

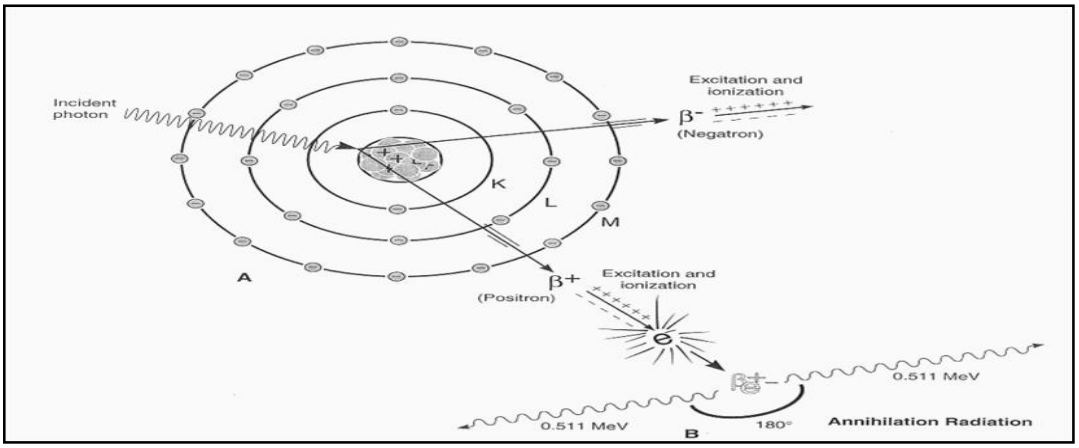

Figure 1.14. Pair Production (Tait, W. H., 1980).

Table 1.2. Photo-matter interaction Chart (Moe, H. J., & Vallario, E. J., 1988).

Name	Energy level	Description	Secondary or Scatter	Where important	Interaction
Classical, Thompson, Coherent	Under 10 keV	Photon of low energy interacts with total atom. Atom absorbs photon and becomes excited. Atom gives off photon with same wavelength and energy	Scatter	Not important	$E_i = E_s$
Compton	Through diagnostic range	Photon interacts with outer-shell electron. Electron is ejected. Photon continues on with less energy. Usually in different direction. Significant as major source of fog on film, patient dose, and technologist dose	Scatter	diagnostic range	$E_i = (E_b+E_{ke})+E_s$
Photoelectric	Through diagnostic range; must be about equal to or above binding energy	Photon interacts with inner-shell electron (usually K-shell). Ejects electron from K or L-shell. Resultant cascading emits characteristic radiation. Significant because bone has more interaction then soft tissue, resulting in different absorption.	Secondary	diagnostic range	$E_i = (E_b + E_{ke})$
Pair Production	1.02 MeV; not significant below 10 MeV	Photon interacts with nuclear field and converts energy into one electron and one positron. Positron quickly interacts with available electron with mutual inhalation resulting, giving off 1.02 MeV of energy in multiples photons	Secondary	Radiation therapy	$E_i = E_{e-} + E_{e+}$ $= + E_s + E_s$
Photo disintegration	Over 10 MeV	Photon interacts with nucleus of atom. Nuclear field is disrupted by photon energy and nucleus is disassembled. Nuclear fragments are created and move away	Secondary	Radiation therapy	$E_i = E_b + E_b + ...$ $+ E_s + E_s + \ldots$ $+ E_{ke} + E_{ke} + \ldots$

1.5. Gamma-Ray Detection Method

The technique of the radiation measurement system to detect gamma-ray depends on the gamma-ray properties which interacts with the active area of the detector crystal. Therefore, the gamma-ray spectrometer involves generating electrical signa as a result of gamma-ray matter interaction (DOE-HDBK-1019/1-93, 1993).

The quality of the gamma-ray detection technique is based on the process of excitation or ionization of active area in the detector medium by the penetration of an incident gamma-ray inside the active area. Electromagnetic waves that have high energy such as; gamma-ray or X-ray give rise to energetic electrons by one of the three major forms of gamma-ray matter interaction, namely the photoelectric effect, Compton scattering, and Pair production (Knol , Atomic, 2003).

There are many kinds of radiation detectors such as passive and active detectors, the active detector contains many kinds of medium materia such as gas, liquid, and solid (which contain scintillation or semiconductor) detectors. All gamma-ray spectrometers compose of a detector and some sort of a readout circuitry, may provide information about radiation properties, such as i energy, intensity, and/or the type of radiation, the effect caused by incident gamma-ray on the active area of the detector is not remaining, the counting is concerned only with the detector. Note that, however, the quality of the gamma-ray detection system is only a factor in overall instrument response to gamma-ray. The location of the gamma-ray spectrometer relative to the isotropic gamma emitter, geometry buildup factor, and self-absorption of the gamma by the capsule of the source are some of the parameters participatory (Holdsworth, A., et al., 2019).

1.5.1. Scintillation detectors

The older measurement system for detection the ionizing radiation is a scintillation detector technique, the detection, and the spectroscopy by using the scintillation process remains one of the most useful methods. The properties of the scintillation crystal possess the following (Jehouani, A., et al., 2000; Akkurt, I., et al., 2005).

a. It should transform the kinetic energy of an incident gamma-ray into detectable visible light with high scintillation efficiency.

b. This transformation should be as possible linear proportional visible light absorbed to incident gamma-ray energy over a wide range .

c. The absorption material should be transparent to the wavelength of i□ own emission for good light collection .

d. The decay time of the induced 1uminescence phenomena should be short so that fast signal pu□es be generated .

e. The absorption medium should be good visible light quality and subject to production in sizes large enough to be interested as a measuring system .

f. The refraction index should be near that of glass (~1.5) to permit efficient coup1ing of the scintillation 1ight to the photomultiplier tube.

For such, NaI(Tl) detectors are preferring usually when compared with other kinds of detection systems, because of their higher readout counting compared with the number of incident particles, cheap availability, and low-level measuremen□ of gamma-emitter, NaI (Tl) scintillation system techniques have been used widely for radiation spectroscopy and radioisotope based applications including medical, industrial areas, and other research investigation (Akkurt, I., et al., 2010).

Furthermore, the scintillation detection technique has other suitable features that lead to reliable resul□ for low-level radioactive source measuremen□ because of excellent intrinsic efficiency, measuring at room condition (no refrigeration). However, the quality of the detection result depends strongly on some parameters such as; absolute efficiency, geometric configuration, counting time, the activity of the gamma-ray emitter, and the distance between the center of the detector and isotropic sealed source (Salgado, C., et al., 2012; Akkurt, I., et al., 2011).

Nowadays, The NaI(Tl) scintillation detectors have many characteristics to select in numerous sophisticated applications in open areas where the bad weather circumstance. Radiation measuremen□ based on scintillation detectors a□o have a high intrinsic detection against high radiation level due to the Z number of Iodine (Z = 53) and, due to the density of the active area of the scintillation detector. All in all, the scintillation detection system shows a high photopeak to the Compton ratio (Thilagam, L., et al., 2015; Akkurt, I., et al., 2014).

When the electromagnetic wave such as gamma-ray interacts with the active area of the crystal, it yields scintillation that is converting as signal, during a photomultiplier tube medium that is made up of a photocathode, this electric signal converts the energy of related to the number of the incident electromagnetic waves (gamma-ray or X-ray) in the visible light range, as a resul□of gamma-ray matter interaction within the active area, the energy converts to electrons that are completely concentrated and accelerated by the dynodes, resulting in secondary electrons (Orion, I., & Wielopolski, L., 2002; Casanovas, R., et al., 2012).

The electron were generating from multiplication practicability method creates a pu□e that approaches the anode, this pulse is collected with adequate intensity to be processed in a scintillation detection device. The electron intensity is related to the number of incoming gamma-ray and the energy (Baccouche, S., et al., 2012).

The output reading of the scintillation detector that used to plotting the spectrum is related to the absorption that happens in the internal active area of the detection system, in the fact the output reading does not refer completely the true gamma-ray intensity as a result to the variation of the detector's energy detection and other physical phenomena interaction (Salgado, C., et al., 2009).

Although the output reading can be measured experimentally with the use of different calibrated isotropic gamma-ray emitter with energies of emission covering the entire range of interest, the number of these isotropic gamma-ray emitters can be limited and time-exhaustion (Figure 1.15) (Kovaltchouk, V., & Marchrafi, R., 2011).

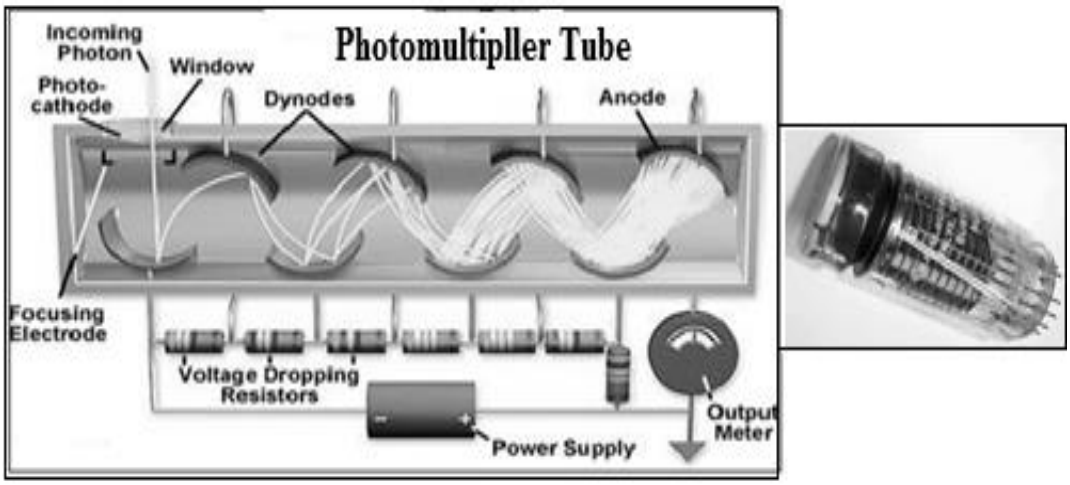

Figure 1.15. Photomultiplier tube of scintillation detectors (Akyildirim, H., et al., 2017).

1.5.2. Semiconductor detectors

The main scintillation detectors have been used for gamma-ray spectra analysis. Another type is a semiconductor detector, the main advantage of it is their high energetic resolution, which is about 10 to 20 times better than the scintillator detectors because the energy needed to produce a pair of charge carriers is very low (only about 2.96 eV) with the consequence that for a certain amount of absorbed energy (Knoll, G. F., 2000).

There are older Ge(Li)-semiconductor detectors and the increasingly used high-purity germanium detectors (HPGe). Germanium detector is a semiconductor diode having a *P-I-N* structure (**P**-type, **I**ntrinsic region**, N**-type**),** the Intrinsic region *(I)* is sensitive to ionizing radiation, especially gamma rays. Under reverse bias voltage, the electric field extends across the intrinsic (depleted) region. When gamma-rays enter the depleted region of a detector, holes, and electrons (charge carriers) are produced and are moved forward to the *P* and *N* electrodes by the electric field. These charges, which are in proportion to the energy deposited in the detector by the incoming gamma-rays, they are converted into voltage pu□es by an integral charge sensitive preamplifier (Reguigui, N., 2006).

The band gap in germanium is 0.7 eV, which means a small amount of energy is required to excite an electron into the conduction band whereas in the valance band a hole is created. The electrical conductivity of a semiconductor is therefore changed when a semiconductor is exposed to radiation. The HPGe detector is cooled to 77 K with liquid nitrogen, in order to reduce dark current and detector noise (Martin, A., 2012). A coaxial HPGe detector p-type geometry was using as shown in Figure 1.16.

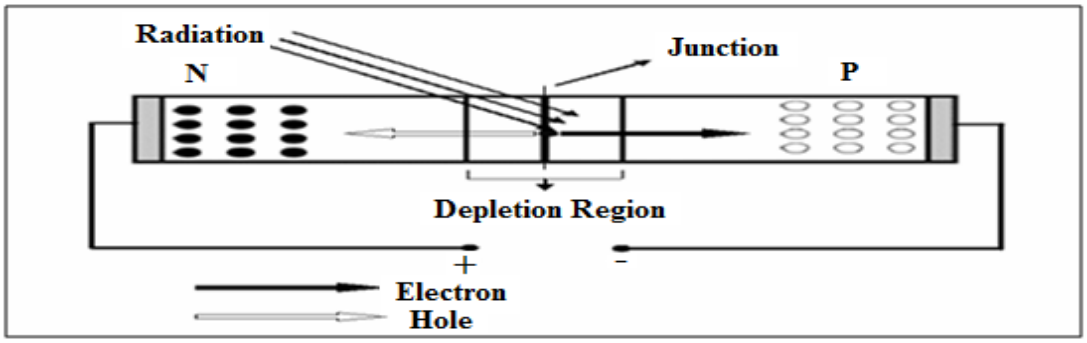

Figure 1.16. Schematic of a P-N semiconductor detector (IAEA, 1995).

1.5.3. Gas-filled detector

Any contained gas volume that has a pair of electrodes can serve as a gas filled detector. The cylindrical shapes are usually used as one electrode and an axial wire mounted in the center is used as the other electrode. Insulators support the axial electrode. The main quality parameters of the gas-filled detector for detection the number of the incoming particle are; the size of the air chamber, the shape of the air chamber, volume, and geometry configuration is a function of the desired detector properties, as shown in Figure 1.17. The gas consumed in the gas-filled detector most probably noble gases or any other gaseous compound that will interact with incoming particle and leads to ionize and crew ion-pair, all kinds of gasses are using in the gas-filled detector including normal air or noble gases or compound that ionize the air chamber are more readily to obtain the preferred gas-filled detector efficiency (Moe, H. J., & Vallario, E. J., 1988).

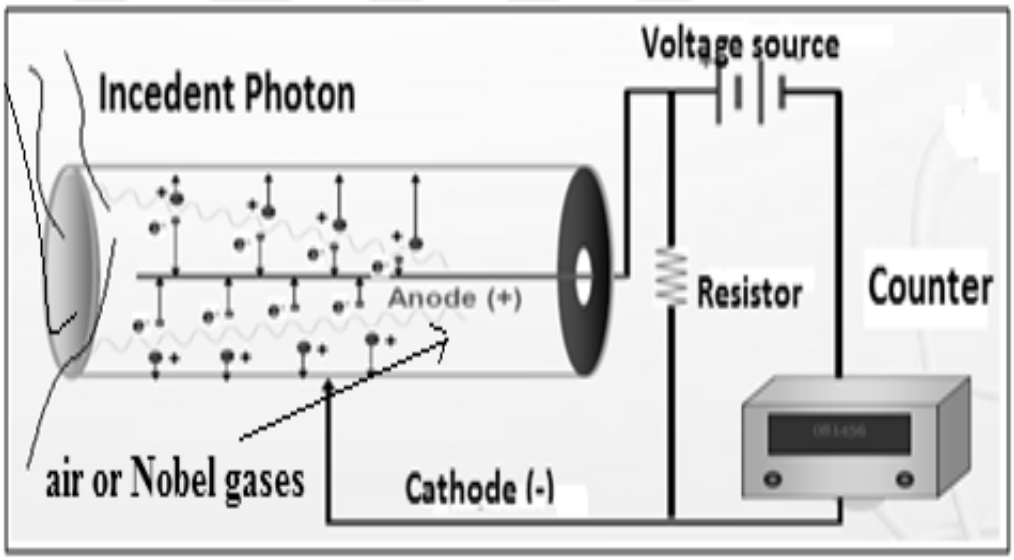

Figure 1.17. Configuration of the gas-filled detector (Bentayeb, K., 2013).

The most common kinds of gas-filled detectors are; Geiger-Mueller tubes, ion chamber, and proportional counter which depend on the regions of operation voltage. Figure 1.18 shows the different regions of operation of gas-filled detectors. The proportional tubes rely on the gas multiplication phenomenon to amplify the charge represented by the original ion pairs created within the gas. Therefore, the pulses are considerably larger than those forms in ion chambers that used under the same condition.

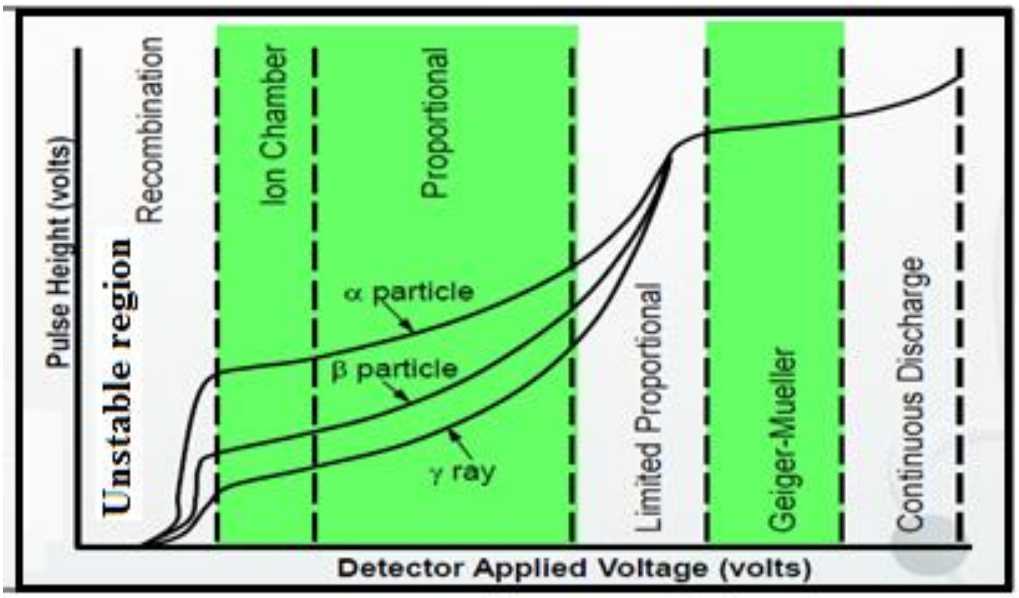

Figure 1.18. The most common region of the gas-filled detectors (Copenhaver, E. D., et al., 1986).

When incident particles are passing through an air chamber, it will interact with the used gas, the result of this interaction creates both excited and ionized atoms until lost all or a part of its energy along its path. The resulting positive ion and free-electron is calling an ion pair. Ions can be formed directly as a result of interaction when incoming particle is charged particles such as alpha or beta, but when incoming particle is electromagnetic wave such gamma or neutral particle such as neutron, the readout by will happen through a secondary process in which some of the particle energy is first converted to an energetic electron or "delta ray" (Shazly, A., et al., 2011).

The practical quantity of interest is the total number of ion pairs created along the track of the radiation. A minimum amount of particle energy is equal to the ionization energy of the gas molecules and must be transferred to permit the ionization process to occur (Moe, H., J., 1992; Shleien, B., 1992).

1.6. Quality Parameters on Gamma-Spectrometer System

Radiation applications started to be used in a variety of different fields with the development of technology such as medicine, military, agriculture, energy, etc. In all those fields radiation measurement is important especially gamma-ray as it is uncharging and difficult to detect. It is also necessary to build radiation protection principles and methods for human health (Waheed, F., 2019; Karkosh, H., et al., 2016).

The quality of radiation measurement is important for radiation protection, the radiation shielding design, and other proposes, the higher level of radiation is hazardous for human health, any error or any bad measurement lead to bad decisions, it will impact our lives that will be difficult to illuminate it (El-Khayatt, A. & Akkurt, A., 2013). In this case, radiation measurement against ionization radiation becomes necessary and it should be investigated accurately. This measurement requires many different parameters to be considered such as the energy calibration, the absolute efficiency, the intrinsic efficiency, full width at half of the maximum, resolution, and the energy buildup factor (Singh, B., et al., 2013; Mann, K, et al., 2013).

Bearing in mind the wide variety of radiation applications and investigating, the passage of gamma-ray is being necessitated to get plausible resul in many applications related to the use of the radiation (Kavaz, E., & Ekinci, N., 2016). Therefore, obtaining a perfect experimental configuration is being considered as one of the most fundamental issues in radiation application and its measurement (Androulakaki, E., et al., 2016). The comfortable structure should be prepared carefully and respected for this kind of measuremen. Furthermore, obtaining this comfortable structure is an important convenient of the gamma-ray detection system and can affect its quality (Shirani, A., & Alamatsaz, M., 2013; Akkurt, I., et al., 2009).

1.6.1. Detector Efficiency

The efficiency of gamma-ray spectrometer measurement is done by the analysis of the readout result, the readout result may count or spectrum produced by the incoming ionization radiation as it interac with an active area of the detector. In the detector, the incoming ionization radiation interac with an active area of the measurement system to produce an electrical signal (Waheed, F., et al., 2019).

As all kinds of detection systems to measure ionization radiation as a function of i deposed energy, a correlation must be made between the readout counting and the number of the incoming particles. For example, the efficiency of gamma-ray sprctrometer is approximately 25%, minimal than 100% yields caused by parameters such as; the position of the detector relative to the source, scatter, and self-absorption of the radiation by the source are some of the factors involved (Mann, K., et al., 2012), see Figure 1.19.

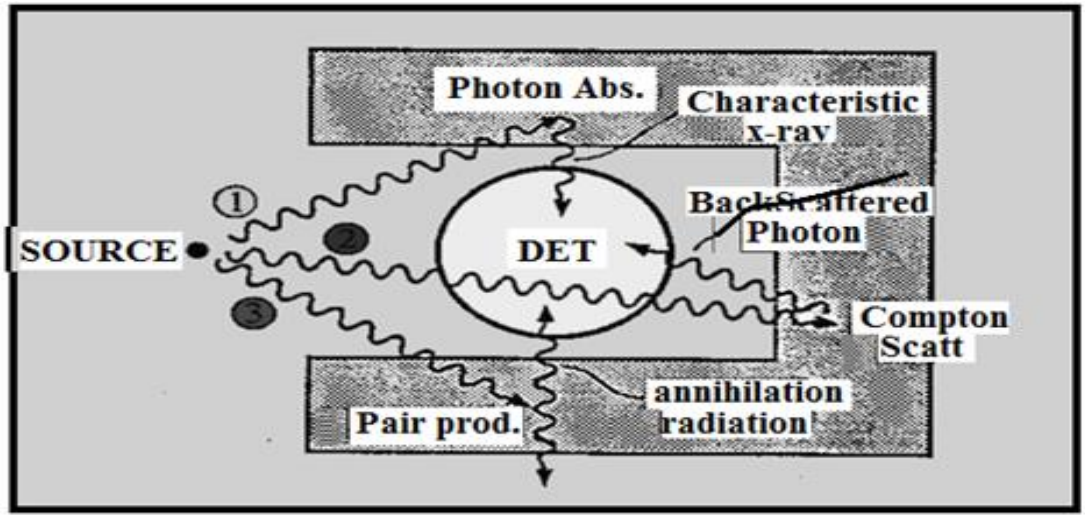

Figure 1.19. Different parameters effect on detection efficiency of a detection system (Tait, W. H., 1980).

The detection of the incoming ionizing radiation such as particle or electromagnetic waves is sometimes appeared as being the rate of coun□per unit time counted by the monitoring or scale of the detection system, of which coun□per minute (cpm) and coun□per second (cps) is commonly used. Count means a single detected event counted by a detection system. Count rate measuremen□are normally associated with the detection of incoming ionization radiation (Shah, K., et al., 2002).

Detection efficiency of a detector system depends on different parameters and thus various kinds of energy efficiency definitions are used to cover those parameters. Determination of the gamma spectroscopy efficiency can affect the measurement quality (Akkurt, I., et al, 2015; Sidhu, B., et al., 2012).

It is convent to subdivide counting efficiencies into two classes: absolute efficiency and intrinsic efficiency, the definition of the absolute efficiency is:-

Absolute efficiency: It is defined as the ratio of the number of coun□recorded by the detector (Nc) to the number of radiation (Ns) emitted by the source (in all directions) as represented in the following formula:-

$$\varepsilon_{abs} = \frac{number\ of\ pulses\ recorded}{number\ of\ radiation\ quanta\ emitted\ by\ source}\ x\ 100\ \% \qquad (1\text{-}16)$$

Especially in the radioactivity measurement, the absolute efficiency of the detector must be known:-

$$\boldsymbol{\varepsilon_{abs}} = \frac{\mathrm{Nc}}{\mathrm{Ns}}\ x\ 100\ \% \qquad (1\text{-}17)$$

Intrinsic efficiency: it is the ratio of the particle number recorded on the detector to the number of gamma rays hitting the detector.

$$\varepsilon_{int} = \frac{number\ of\ pulses\ recorded}{number\ of\ radiation\ quanta\ incident\ on\ detector}\ x\ 100\ \% \qquad (1\text{-}18)$$

Full-energy peak (or photo-peak) efficiency (FEPE):- it is the energy peak pu□es only, rather than a pu□e of any size, for the gamma-ray.

The photopeak efficiency suppose the interaction deposited the full energy of the incident particle are counted, these full energy photopeak even□appears at the highest end of the spectrum. On the other hand, even□that deposited a part of the incident particle energy then will appear farther to the spectrum. The number of full photopeak energy efficiency obtained by integrating the total area under the peak (Ashok, D., & Thomas, F., 2003).

The total and peak efficiency are related by the peak to total ratio r :-

$$r = \frac{\varepsilon\ peak}{\varepsilon\ total} \qquad (1\text{-}19)$$

The intrinsic & absolute efficiency are simply related to radiation source by:-

$$\varepsilon_{int} = \varepsilon_{abs} . (4\pi/\Omega) \qquad (1\text{-}20)$$

Where Ω is the solid angle of the detector seen from the actual source position.

The efficiency depends on detector properties and many other parameters such as; energy of the radiation, the geometry configuration, the detector diameter toward the incident particle. And source-detector distance, however, because the average path length of the radiation through the detector will change somewhat this spacing, Figure 1.20.

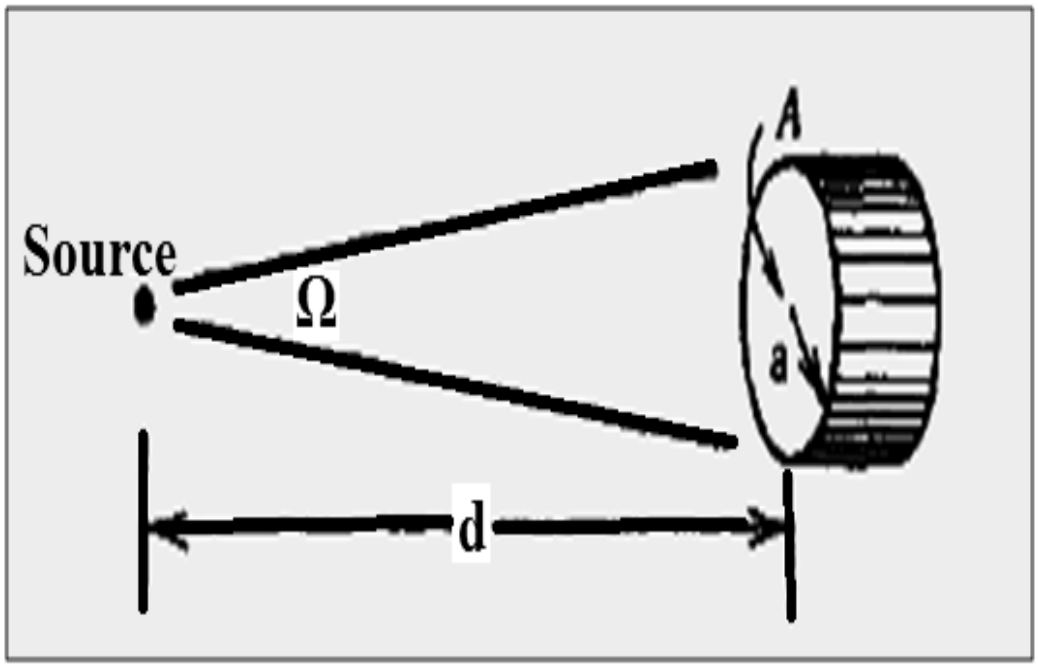

Figure 1.20. The solid angle effected of the detector efficiency (Tsoulfanidis, N., 1995).

Where d represen□ the source-detector distance, A & Ω is the angle between the normal to the surface element and the source direction. If was supposed the radiation emitter is a point source (negligible volume), then a second integration must be carried over all source volume. For the common case of a source of zero diameters located at a distance of detector in a cylindrical shape, Ω is given by:-

$$\Omega = 2\pi \left(1 - \frac{d}{\sqrt{d^2 + a^2}} \right) \quad (1\text{-}21)$$

Where d is the source-detector distance, a is a radius of the detector, when d >> a the solid reduces to the ratio of the detector plane frontal area A visible at the source to the square of the distance:-

$$\Omega \approx \frac{A}{d^2} = \frac{\pi a^2}{d^2} \quad (1\text{-}22)$$

1.6.2. Resolution and FWHM

The main purpose of the gamma spectrometry technique is to determine the gamma-emitters radionuclides and their activity during the research investigation. The energy resolution represents the ability of the detector to separate between peaks of gamm-ray. The energy resolution of the detection system is one of the significant quality parameters, the energy resolution is predestining the detection system to plot the

distinctly separate peaks of two close in gamma-ray energy spectrum as an alternative the detection system gives a single broad-spectrum peak of the gamma-ray energy. The energy resolution of the 3" x 3" NaI with thallium (Tl) activated in the normal spectrum plotting is approximately 7% when using ^{137}Cs isotropic real source that emittes gamma-ray energy at 0.662 MeV (Waheed, F., & Akkurt, L., 2018; ORTEC, E. N.).

The scintillation detector has excellent energy resolution for high gamma-ray energy, the more resolution a detector has, the more defined a gamma-ray spectrum becomes. Recall that the resolution of a detector is defined as the detector characteristic to be able to differentiate between two close radiation energies. The higher the energy resolution means that the detection system can discriminate between gamma-rays with similar energies, the closer the gamma-ray energies can be to each other and still be differentiated (Perez-Andujar, A., & Pibida, L., 2004; Waheed, F., & Akkurt, I., 2018).

At lower energies, the energy resolution is better and at higher energies it is worse, the energy resolution of the gamma-ray detection system is very necessary when identifying radionuclides (Gouda, M., M., et al., 2015). Furthermore, the non-proportional light response in the detection system makes it carry out the energy calibration method depended on spectrum width, which proves the agreement of the comparison between the spectrum peak width and to the peak channel corresponds (Milbrath, B. D., et al., 2005).

One important property of detector in radiation spectroscopy can be examined by noting the response to a monoenergetic source of that radiation. Figure 1.21 illustrates the differential pu□e height distribution that might be produced by e detector under these conditions and the response function refer to these distributions, the good resolution refers to the distribution around an average pu□e height, the bad resolution refers to the distribution with inferior performance (Wahee, F., & Akkurt, L., 2019).

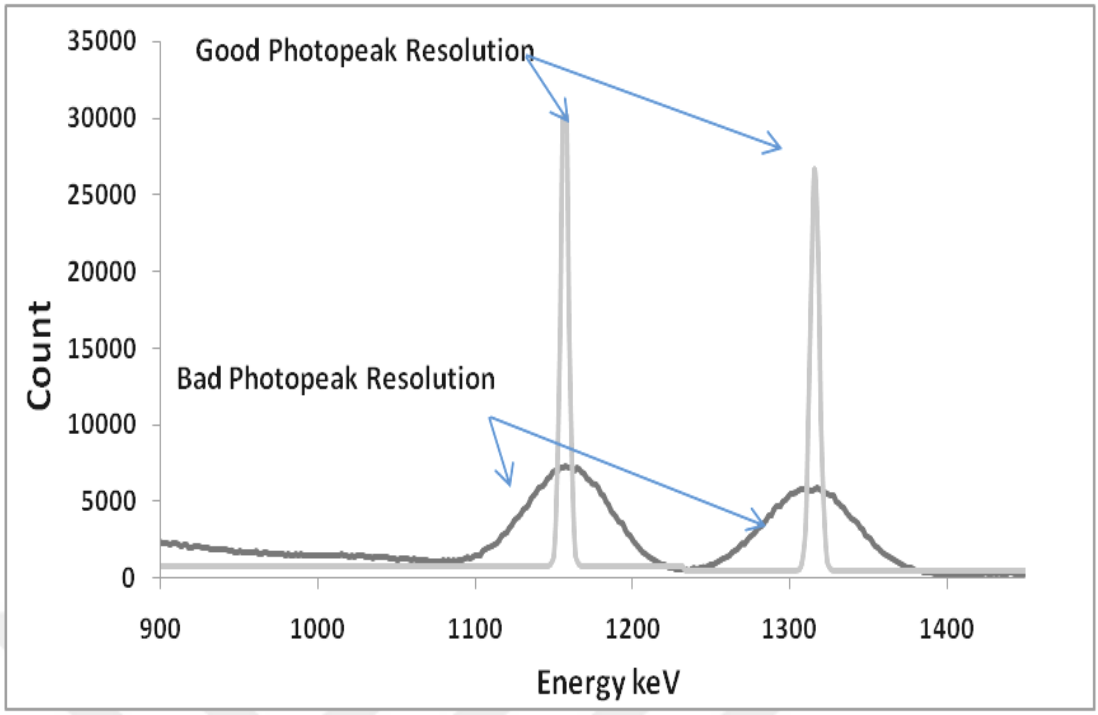

Figure 1.21. The differentiated between good and bad detector resolution.

1.6.3. Energy Buildup factor

As a result of gamma-ray matter interaction, a part or all of the incoming gamma-ray energy deposites in the barrier, experimentally, when the energy of the incoming gamma-ray less than 2 MeV, there are two probabilities of interactions can happen, absorbing or scattering and keep most of the initial energy during change the path (Kiran, K. U., et al., 2015).

The attenuation of the incoming gamma-ray is governed by the Beer-Lambert formula (Mayerhöfer, T. G., et al., 2020).

$$I = I_0 e^{-\mu x} \tag{1-23}$$

Where I representes the intensity of the shielded gamma-rays, I_o representes the incident gamma-rays intensity, μ gives the linear attenuation coefficient, and x represen□the barrier thickness (cm). However, experimentally, some gamma-rays are still arriving at the measuring point more than the number of gamma-rays described in Beer-Lambert formula, see Figure 1.22.

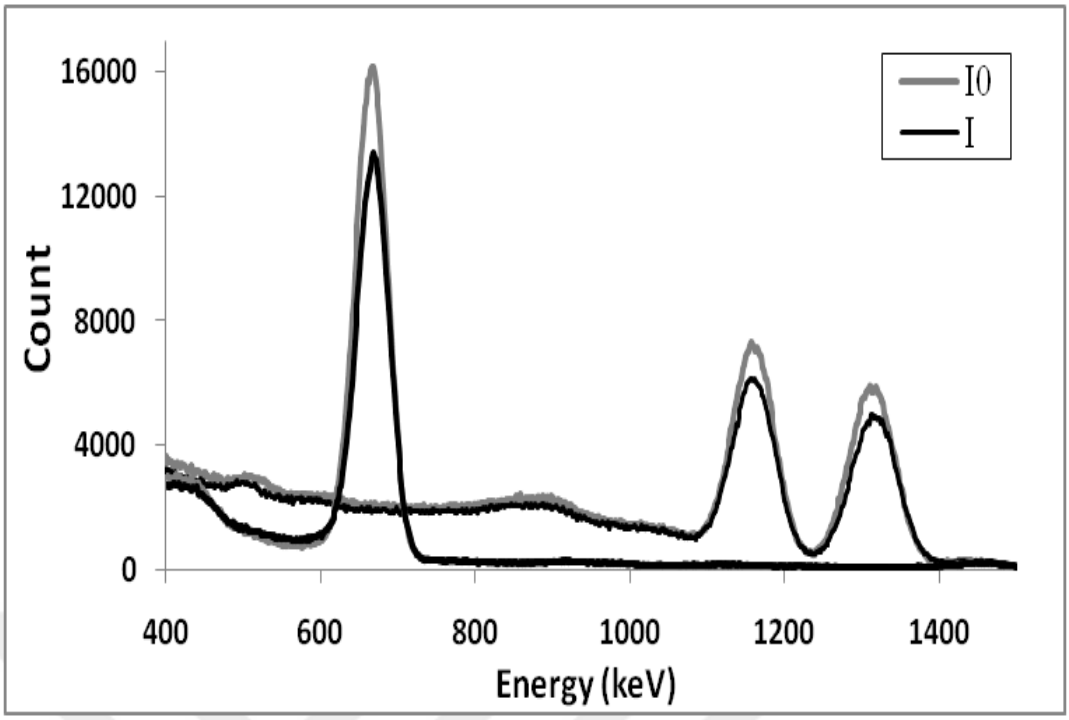

Figure 1.22. The spectrum with and without the barrier (Gunoglu, K., & Akkurt, İ. 2012).

The increased of gamma-rays intensity recorded at the detection system due to the buildup factor (Compton scattering phenomena) of the barrier (Jaeger, R., et al., 1968), and the simple mathematical form of the decay law is modified to a new form given in equation (1-24).

$$I = B.\ I_0 e^{-\mu x} \qquad (1\text{-}24)$$

Equation (1-23) is adequate just when both of the source and detection system are well collimated used lead collimators, it can be called the narrow beam geometry configuration. However, when both of the source and the detection system are not collimated using lead collimators (broad beam geometry configuration), it should take into consideration the buildup factor. Therefore, the formula (1-24) will show more ideality and precise value (Mann, K., et al., 2016; Guvendik, M., 1999).

Buildup factor definition; Buildup factors are the attenuator and geometry configuration-dependent parameters which correct the simple attenuation coefficient formula, so it contains the contribution of the collided part of the un collided incoming gamma-ray (Waheed, F. Q., et al., 2018; Hopkins, D., N., 2010).

There are many parameter that effect on the value of the energy buildup factor when both of the source and the detector are not collimated such as; the incoming gamma-

ray energy, the physical diameters of the gamma emitter, the density of the barrier, the atomic number of the barrier, the thickness of the barrier, the final geometry configuration of the detection system, and the source-detector distance (Shin, K., & Hirayama, H., 2001; ANSI/ANS-6.4.3-1991).

The knowledge of the buildup factor is significant in radiation applications and other research investigation measurements (Shirani, A., & Alama□az, M., H., 2013; Kavaz, E., & Ekinci, N., 2016; Dhillon, J., S., et al., 2012).

1.7. Detection Geometry

1.7.1. The attenuation of narrow beam geometry

The parameter illustrated the gamma-ray intensity calculation after the penetration in the thickness of the shielding material is the attenuation coefficient μ (Jaeger, R., G., et al., 1968). The linear attenuation coefficient depends on the incoming gamma E and on the medium properties when the geometry configuration is built well (Akkurt, I., et al., 2005), and may define as the eventuality per unit path length that the incoming gamma-ray will interact with the shielding material (Akyildirim, H., et al., 2017).

Taking into account like a typical geometry configuration, the attenuator is laying in the middle distance between a collimated beam and collimated detection system, The narrow beam geometry configuration prevents any incoming or secondary gamma-rays to be scattered and arriving in the detection system (Shimizu, A., & Hirayama, H., 2003), see Figure 1.23.

This typical configuration confirms the main linear attenuation coefficient formula to be applied. To arrive to the narrow beam geometry configuration, the incoming gamma-ray beam ought to be collimated by collimator that has a thin hole radius, a□o the gamma-ray emitter ought to be as a point diameter and far as possible from the detection system, the barrier ought to be midway between the gamma-ray emitter and the detection system, and it ought to be skinny enough to illuminate the scattering and second interaction from arriving the detection system. Additionally, there ought to be no scattering material beside the detector (Shirakawa, Y., 2000; Manohara, S., R., 2011; Singh, S., et al, 2010).

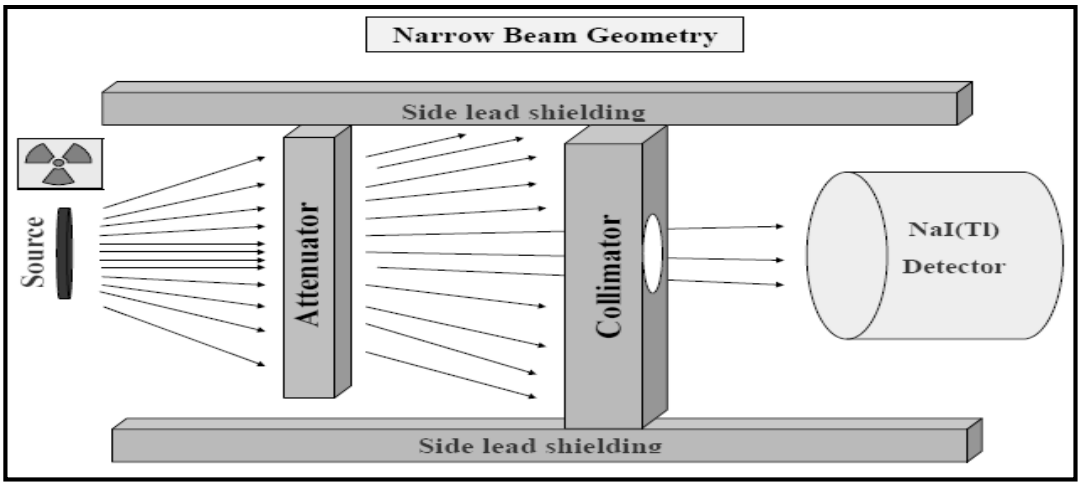

Figure 1.23. Attenuation characteristics of a narrow beam geometry.

1.7.2. The attenuation of broad beam geometry

In the broad beam geometry configuration, the detection system will measure the gamma-ray intensity greater than that described by Beer-Lambert law, because scattered gamma-rays and secondary interaction will be effected to the readout reading of the detection system, as shown in Figure 1.24. The additional number of incoming gamma-ray intensity arrived at the detection system more than described in the collimated beam geometry can be taken into account (Mann, K., S., et al., 2012; Sidhu, B., S., et al., 2000; Smathers, K. L., & Karp, A. H., 2008).

The main three different phenomena of gamma-ray matter interac□are; Photoelectric effect, Compton scattering, and Pair production. Experiment, in the incoming gamma-ray energy range from 0.511 MeV to 1.332 MeV, the photoelectric effect, and the pair production will cover the gamma-ray matter interaction, when just these two kinds of the interaction occur as a photon-matter interaction and when there are no collimators for both of the source and the detection system; then in the case, it called this geometry as the broad beam configuration (Waheed, F., 2018; Justice, H., 2016;; Karp, A., H., 2008; Sidhu, B., S., et al., 2012).

If the detection system is measuring all the incoming gamma-ras intensity including the collided gamma-ray and un collided gamma-ray, then the main linear attenuation coefficient that can be used for experimental or other investigation calculation as illustrated in below formula (Waheed, F., & Akkurt, I., 2017).

$$I = I_o \; B \; e^{-\mu x}$$

I = the intensity of the shielded gamma-rays.

I_o = the incident gamma-rays intensity.

μ = the linear attenuation coefficient in cm^{-1}

x = the thickness of the attenuator in cm

$$\mathbf{B} = \frac{\text{Qantity due to total number of particle at a piont}}{\text{Quantity due to only uncollided particle}}$$

$$= 1 + \left(\frac{\text{Number of scattering gamma-rays}}{\text{Number of uncollided gamma-rays}} \right) \quad (1\text{-}25)$$

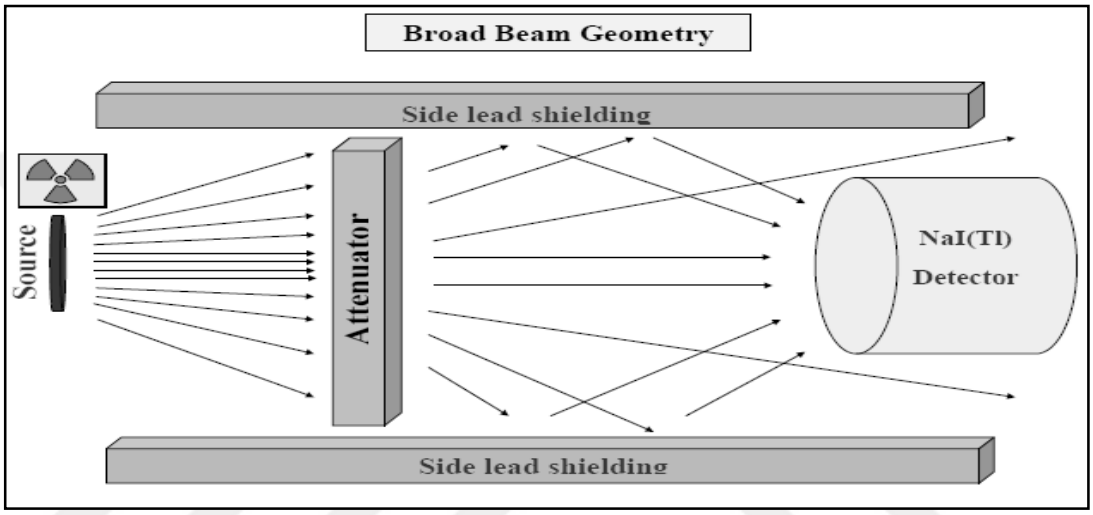

Figure 1.24. Un collimated geometry configuration

The energy buildup factor is a fundamental parameter that most taken into consideration when designing the final geometry of the detection system or other kinds of research investigation calculations. The value of the buildup factors that obtained from other investigation is forbidden to use in other calculation because it is dedicated to the geometry of the studied case. In addition, its value is available by cost from the American Nuclear Society. They are not available online anywhere that we could find (Hopkins, D., N., 2010).

In the situation of the broad beam geometry (not uses collimator), the detection system detects all un collided gamma-ray, gamma-rays that suffered from scattering, and secondary gamma-rays that occurs as a result of gamma-ray matter interactions. All in all, the detection system detects all gamma-rays arrived from all directions (Waheed, F., & Akkurt, I., 2017).

2. THE LITERATURE BACKGROUND

Calculation the quality parameters of gamma spectrometer system by using isotropic sealed sources, there are a different investigation have been done on this subject. In this section, some works related to the calculation and estimation the quality parameters in the gamma spectrometer are summarizing.

Akkurt and his team determined the absolute efficiency of the 3" x 3" scintillation detector experimentall and the detector was modeled by using the Monte Carlo code. The comparison had done between the results and with some published papers in the previous study. The NaI(Tl) scintillation detector efficiency depending on many parameters that affect the results such as source-detector distance, the result shows the variation of efficiency as a function of gamma-ray energy and source-detector distance. A good agreement had observed between experimental results and Monte Carlo simulation (Akkurt, I., et al., 2015).

Bagatelas and others investigated expermentally and with Monte Carlo code the efficiency of NaI(Tl) scintillation detector. It had proven that the Monte Carlo code provides accurate and suitable in some applications, especially where the practical measurement configuration for detector calibration cannot effectively for gamma-ray absorption. In addition, new efficiency and responsible function method had developed, in order to reduce the Compton scattering effect contribution under the interest region (Bagatelas, S., et al., 2010).

The absolute efficiency of scintillation detector as a function of energy had got using Monte Carlo code by Tekin, H. O. It had found that the results were moderately almost like available practical investigation data and confirming previous results on a NaI(Tl) crystal. It also showed that the simulation results aren't only almost like other experimental efficiency calculations, but also almost like other XCOM and Monte Carlo leads to other calculations. It often concluded that modelling geometry uses especially in radiation investigations such as nuclear reactors, high energy, and radiation therapy facilities (Tekin, H., O., 2016).

Salgado and his team presented a technical method for simulation of a NaI(Tl) scintillation detector by using Monte Carlo code, this procedure comprises measuring absolute efficiency curve practically and by simulation for two isotropic point sources

as a function of source-detector distance and the physical detector diameter. The simulation of the physical detector diameter is slightly differencing from the real detector diameter. The results of the efficiency curves comparison showed successful agreement with the physical diameters calculated by the method of the two-point source, It become clear it is necessary to consider the quality parameter of real gamma spectrometers such as efficiency, resolution, and FWHM when preparing the simulation input file to get a good agreement (Salgado, C, M., et al., 2012).

Hakimabad and others presented a way to simulate the mathematical response functions of 3" x 3" scintillation detector, according to the life spectrum of gamma spectroscopy from standard gamma-ray sources in a wide range of energy. A nonlinear mathematical response function of 3" x 3" NaI detector by using the Monte Carlo code program tested by comparing with the practical results. The energy spectrum comparison results have shown a good agreement with the measured one, less than ±3% relative deviation (Hakimabad, H. M., et al., 2007).

Waheed & Akkurt measured practically the buildup factors for a pure single layer material as a function of energy, thickness, and source-detector distance using 3" x 3" sodium iodide scintillation detector. The produced materials had tested against incoming gamma-rays to the energies 0.511, 0.662, and 1.275 MeV. The result has shown that the value of the buildup factor increases with increasing the atomic number, thickness, atomic mass, and density to the same energy and distance, and it decreases with increasing the energy and source-detector distance at the same attenuator thickness of different materials. The results also relevant, In narrow beam geometry, the buildup factor value was at a low level, but for a broad beam geometry the buildup factor decreases. This leads that the good geometry was getting in this study should use in future measuring to get more quality measurement (Waheed, F., & Akkurt, I., 2017).

Samad & Baydoun implemented a quality assurance parameters of the gamma spectroscopy. Standard methods were applying for the measurements and the analysis of important gamma spectrometers quality parameters such as the energy calibration, efficiency calibration, efficiency curves, resolution, and full energy peak for various compositions and densities were performing and corrected for attenuation and absorption at wide rage gamma-ray energy. The results had shown that quality

assurance is an essential tool to assure confidence and increase the reliability and accuracy of results (Samad, O. E., & Baydoun, R., 2018).

Kavas & Ekinci examined experimentally the buildup factor value for different cellulose nitrate (6 < Z and Z > 8). At the energy (1.5 MeV) where only Compton scattering is the dominant interaction process, the getting result shows that the number of the scattered gamma-ray increases with increasing the Z number of the attenuator. The energy buildup factor values affected by the attenuators's properties**.** All in all, the gamma's buildup factor is less when compared with other materials to the same chemical composition (Kavas, E., & Ekinci, N., 2016).

Harima and his team estimated the energy buildup factor values for different absorbers such as; water, air, and concrete for a gamma-ray isotropic point source, the results suggested parameters for the same chemical composition. The number of scattered gamma-rays for the compound is similar within the maximum deviation 50% of the previous study. As a result, the energy buildup value had converted to extensions level as a function of gamma-ray energy and source-detector distance (Harima, Y., et al., 2014).

Mann and others determined the buildup factor as a function of fixed energy of two-layered shield materials in such low-Z followed by high-Z, the results showed that the value of buildup factor increased when used high-Z single material. Thus, in radiation shielding designed of multi-layered materials is more effective than single-layer material (Mann, K., S., et al., 2016).

Abdul Haneefa and his team used a Monte Carlo code (FLUKA) to avoid the multi-leaf collimator in a simplified model, this procedure results shown the dose curves and beams distribution plots. Monte Carlo model with different collimator diameter shows perfect similarity for primary physical features in standard collimator diameter. Although percentage depth dose values in the buildup region show more subordination on the collimator diameter. The result recommended the use of FLUKA simulation for percentage depth dose curves and beam profiles for collimator diameter according to the previous parameter for gamma-ray beam models for better agree (<2%) in open area of beam profiles (Abdul Haneefa, K., et al., 2014).

Salgado and his team presented a simulation procedure for a scintillation detector with the Monte Carlo code. A mathematical response function was using for validation the

gamma efficiency calculation, the absolute efficiency was getting for both the practical and by MC code; the results compared and showed a successful agreement when using two isotropic gamma emitter (low and high energy). For this purpose, fitting dimension had found of the crystal to use in the detector's simulation of counting efficiency and obviously to calculate the activity (Salgado, C., et al., 2015).

Shi & Hirayama investigated the mathematical response functions of 3" x 3" NaI(Tl) crystal. The plotting of the spectrum curve shows that the Monte Carlo program simulation has some disagreements at low energies, because of the Sodium iodide efficiency calculation at low gamma energy. The result shows a simple procedure method for the investigation of response functions, but their data was getting with un-scattered gamma-ray situation. All in all, it is only applicable for the same geometry dimensions of the detector that used in their estimation and real NaI(Tl) crystal (Shi, H. X., & Hirayama, H., 2002).

Mouhti and his team performed a two different shapes of sodium iodide crystal using Monte Carlo simulations. The primary goal was to determine the mathematical response function and absolute efficiency of a cylindrical and spherical scintillation detector, the same procedure for calculating the absolute efficiency, and the response function had used to the gamma emitter range from 0.060–2.750 MeV. The results show successful agreement of the MC simulation, although scintillation detectors in different models (Mouhti, I., et al., 2017).

Mouhti and others used the Monte Carlo code for investigation a compact mathematical response function of the same diameter of NaI(Tl) scintillation detector and LaBr3(Ce) detectors. The gamma absolute efficiency and energy resolution curve were determining experimentally for the scintillation crystal in the range 0.060–1.408 MeV. An experimental efficiency determination and Monte Carlo simulation showed good agreement comparison of the results of the value, although the difference in the shapes. The present study confirmed that the reality input file simulation leads to a very useful for both of the absolute efficiency and the modeling detector calibration (Mouhti, I., et al., 2018).

Grujić and others prepared two procedures to calculate the surface activity of gamma emitter and develop mathematical response function practically and by using an MC Code program estimation. The absolute efficiency of the NaI(Tl) crystal, was first

examined fitting by the comparison of simulated and measured results for referent sources, the second validation of the function of energy that simulated with the Monte Carlo code. The results had compared with practically gamma-ray spectrum plotting; it shows a successful agreement between estimated and laboratory gamma-spectrum for the ^{137}Cs isotropic gamma emitter, this comparison affirms that the proposed structured model of NaI(Tl) crystal is positively for gamma-rays energies more than 0.1 MeV (Grujić, S., et al., 2013).

Moreira and his team confirmed the use of the Monte Carlo code as a successful procedure for investigation and determination of the absolute efficiency calibration and related geometries configuration. The procedure method applied for the dedication the ratio of the number of the gamma-rays emitted from the source to that number of gamma-rays reach the measuring point. Output data show complex situations to the prepare simulation input file to determine the activity of surface contamination for all gamma energy ranges. Therefore, many parameters of the contamination area should be known when prepare about measuring situations to get successful agreement between practical and simulation (Moreira, M., et al., 2010).

Young-Yong and his team calculated the individual dose rate from the converted energy spectrum using the G-factor, which had related to the use of mathematical response function. To make validations of the method , experimental verifications were using a 3″ x 3″ NaI(Tl) scintillation detector were conducting at the geometry of the isotropic gamma emitter such as ^{57}Co, ^{137}Cs, and ^{60}Co. Results confirmed that the method of validation in the energy, dose rate, activity, response function, and source-detector distance of isotropic gamma emitter in a good agreement between the simulation and experimental calculation for low-energy and the high energy of ^{60}Co (Young-Yong, J., et al., (2015).

Saraiva and others created a model for describing an ORTEC scintillation device covered by a thin beryllium window for determination parameters such as; calibration sources, activity diameters, absolute efficiency, and efficiency transfer factors for proposal configuration geometry prepared as matrix effects. The simulation preparation had done by using the Monte Carlo and supported experimentally by using a ^{60}Co isotropic real source. The comparison results show successful agreement between practically measuring and MC estimations. The results had fulfilled by two

parameters; source-detector distances and energy respectively, confirming that the model corresponds to the sensitive area of real detector diameters (Saraiva, A., et al., 2016).

Shirmardi & Alamatsaz selected three energies (0.662, 1.173, and 1.332 MeV) to study the shielding properties and relevant parameters based on three different methods; experimentally by using 3" x 3" NaI(Tl) scintillation detector, X-COM online program, and Monte Carlo code. By comparing the results, it had concluded that the probability of energy absorption increases with increasing the barite percentage addition to the shielding compound (concrete). The results showed that there is an accepted agreement between; Monte Carlo, online calculation program (XCOM), and the practical calculation. All MC results had showed that the relative error is less than 4 percentage (Shirmardi, A., & Alamatsaz, M., H,. 2013).

Vahabi and his team used Monte Carlo code to configure suitable geometry for such experimental measurements and supported with XCOM calculation. It had found that the Monte Carlo results were very close to XCOM values and experimental results. A similar investigation of other calculation has done using Monte Carlo with different geometry. It had noticed that the difference between comparison from low and high gamma energy, this differentiate from low gamma energy more than moderate energy. The results referred that the proposal modeling can apply as a comfortable procedure for the laboratory measurements. Besides, the practical configuration is more suitable for low gamma emitter. This kind of investigation can apply for many radiation detectors that used in radiation applications such as; radiological dosimetry, attenuator materials, and nuclear medicine application of diagnostic and treatments (Vahabi, S. M., et al., 2017).

Chandani and his team developed the calibration analysis method using a gamma-ray spectrometer supported with the Monte Carlo Code. In order to investigate the positive algorithm to fulfill the background level of radiation, the gamma-ray spectrum curve from ^{226}Ra isotropic sealed source had investigated and many calculation procedures had studied for the gamma spectroscopy curve. From simulation results, the spatial distribution of the absolute efficiency results and the efficiency calibration determined. The simulation procedure uses when a different container diameter is using in real experiments (Chandani, Z., et al., (2017).

The total efficiencies and spectrum curve had carried out using the MC code by Byun and his team. The NaI(Tl) detector diameter had modeled using a different simulation, the detector diameter had tested against mono-energy isotropic of gamma emitter. Code program has many options for detection incident particle (Gamma-ray), using different cards, for more reality; source diameter, kinds of distribution, and others should model to get successful agreements. The results show that the application of the gamma spectrometer analysis is in preparation (Byun, S. H., et al., 2004).

Kiran and his team used the 3" x 3" NaI(Tl) crystal scintillation and MC computer code to show the impact of collimator thickness and attenuator thickness to the quality of the results when using thick targets and collimator, there is a bad effect of the scattered gamma-ray. The gamma spectroscopy curve shows the contribution of collimator diameter on gamma-ray scattering. In order to increase the scattering fraction in Compton phenomena, the contribution of scattering background should minimize, which can achieve by using a narrow beam geometry. The number of scattering gamma-rays decreases with increasing energy, in order to minimize the number of gamma-ray reach to measuring point, a narrow beam geometry should apply for more reality. The practically results showed successful agreement with the literature background and supported with MC Code (Kiran, K. U., et al., 2015).

Androulakaki and his team developed a routine for the estimation of gamma-ray matter interaction using FLUKA code. FLUKA code had developed to estimate the resolution value of the spectral curve of a scintillation crystal, the present work had focused on the inappropriate situation of the main natural decay series. The comparison had done of two kinds of simulation codes (FLUKA & MCNP-CP), to the gamma-ray emitter on the range from (0.1 MeV - 3 MeV). The laboratory spectrum had supported the MC code, the comparison of absolute efficiency and curve shape for high activity showed a good agreement with low statistic error (Androulakaki, E. G., et al., 2016).

Hendrik**s** and his team made the time of measurement and energy calibrations of the natural radionuclide analysis an option. The MC code uses for many radiological applications such as energy calibration, geological investigation, experimental correction of the detector diameter and geometry. The results confirmed that the

reduction of the time of measurement leads to create spectrum shape for any required density. A significant advantage of the MC code is the creation of the spectrum shape of many gamma emitters like ^{137}Cs and ^{60}Co, for which it difficult to detect these isotopes inside safety storage conditions (Hendriks, A. F., et al., 2002).

Joel and his team devoted the MC code for simulation of the detector diameter and its response function against different gamma emitter of flexible geometries (2D & 3D). The comparison results between practical measurements and computer code show successful agreement for low gamma energies, but for high energy, there is some accepted statistic error. It had concluded that the MC computer program is suitable for determining the quality parameters of gamma spectrometry such as the active area of a scintillation crystal, mathematical response function, and absolute efficiency (Joel, G. S. C., et al., 2018).

Vitorelli and his team used the Monte Carlo code to simulate the mathematical response function of a 7.62cm x 7.62cm NaI(Tl) scintillation crystal. The purpose of the study was collecting unavailable data of gamma associated with (^{241}Am/Be) isotropic neutron emitter. The MC gamma-ray spectrum curve had compared with the experimental gamma curve, in general, the comparison showed a positive agreement between them (Vitorelli, J. C., et al., 2005).

Atallah and his team had investigated the value of the buildup factor experimentally using a gamma spectrometer system for some new chemical compounds (polymer + metal). The results showed that the new chemical compound can used instead of heavy elements used as shielding with lighter weight and low-cost absorber. All in all, the number of scattering gamma-ray decreases with the increasing concentration of the new chemical compound, as well as it increases with increasing the thickness of the attenuator (Atallah, F. S., et al., 2018).

3. MATERIALS AND METHODS

3.1. Calculation Methods

For the measurement technique, the values of the quality parameters of gamma spectrometer are important to calculate. These parameters are usually calculating a function to the gamma-ray energy and source-detector distance. The simulation geometries have been used to analyze the results for many axial distances from the detector surface.

This measurement requires many parameters to consider. Thus in this thesis the main quality parameters of gamma spectrometer had determined experimentally and compared with FLUKA Code.

Since the quality of measurements techniques tasks are important as well as they are difficult to get in ideal structure against radiations, this study will be one of the few ones that incorporates the experimental and Monte Carlo simulation methods of measurements techniques. Thus, it will be a valuable contribution to the literature.

3.1.1. FLUKA Code

FLUKA Monte Carlo code is a multi-particle transport code, the first generation of FLUKA in the CERN SPS project on the last century in 1962-1978, the earlier code used as a tool for shielding purpose-designed against high energy accelerators, at that time the CERN radiation study for 300 GeV. The first Code was called FLUktuierende KAskade. The purpose of FLUKA was to assess the performances of the scintillation crystal NaI(Tl) detector against hadron calorimeters (Ranft, J., 1972).

FLUktuierende KAskade is not toolkit, it is a physical model that fully integrated, it can be defined as "Using a physical computer model to do an impression of the operations of real process or facility according to appropriately developed assumption taking the form of logical, statistical, or mathematical relationships which are developed and shaped into a model" (McHaney, R., 2009; Seco, J., & Verhaegen, F., 2013).

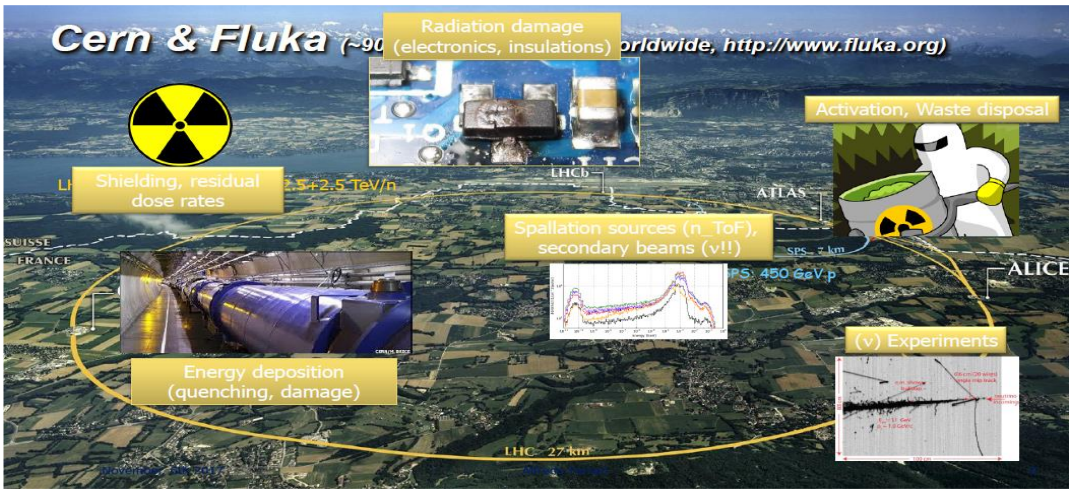

Figure 3.1. Main application of FLUKA Monte Carlo code (Al-obaidi, S. D. S., & Akkurt, I., 2019).

FLUKA estimation is a stochastic numerical simulation method that takes into account all the details of the measurement system aspects of the problem. This procedure is used in radiation transport studies for simulating the transport of neutrons, protons, and electrons, particularly in irregular geometries. In FLUKA code approach, individual particle transport histories are generated by randomly sampling particles as they travel through the geometry of the measurement system. These transport histories are then analyzed to provide information on quantities of interest, such as particle fluence or detector response. The Monte Carlo method is most effective in solving problems that are difficult to simulate with common deterministic methods. This method also provides an answer with a statistical uncertainty associated with it, so that a confidence level in the results can be established (Mohamed, Y. M. B. (2014).

Table 3.1. Comparison between a simulation and experimentally

Experimental	Computer simulation
Sample	model
physical apparatus	computer program
Calibration	testing of program
Measurement	computation
data analysis	data analysis

3.1.2. Basic geometry modelling

The "theory" is a set of assumptions (with perhaps a mathematical formulation of these assumptions) that can be measured in an "experiment". Ideally, the connection between theory and experiment is direct so that the interpretation of the experiment in unambiguous. This happens when the mathematical description of the microscopic interactions and the macroscopic measurement involves no further approximation. When this is not possible, a Monte Carlo simulation enters the picture in a useful way and can serve a two-fold purpose, see Figure 3.2. It can either provide a small correction to an otherwise useful theory or it can be employed directly to verify or disprove the theory of microscopic interactions (Bielajew, A., F., 2001).

The obtained results of the simulation for an idealized model that has no laboratory counterpart would also be quite important. The comparison of the simulation results with an approximate theoretical calculation serves as a stimulus to the development of methods of calculation. On the other hand, a simulation can be done on a realistic model in order to make a more direct comparison with laboratory experiments. Computer simulations, like laboratory experiments, are not substitutes for thinking but are tools that we can use to understand complex phenomena and to seek explanations for them (Gould, H., & Tobochnik, J., 2010).

The probability of an interaction occurring between the incident radiation and a detector increases as the detector volume increasing. A larger volume of the detector offers more “targets” for the incident radiation. Since each kind of radiation has a specific ionization per centimeter, increasing the detector size also increases the length of the path that the radiation traverses through the detector. The longer the path, the larger the number of pulses (RCT 1.05-SG, 2013). The geometry of FLUKA simulation exactly to the experimental properties, the physical volume, the mother volume, and sensitive volume were implemented in the word accordingly using (FLUKA 2011.2 x 7, July 2019), routines as described in FLUKA user manual (Ferrari, A., et al., 2005), the description of interaction of incident particle is important during preparing the input file (Joel, G., S., et al., 2018).

The MC is particularly suitable for complex geometry where analytical methods cannot be applied. Even though FLUKA program does not simulate the detector

process, but scores the number of energy particles absorbed in the detector material (Saraiva, A., et al., 2016).

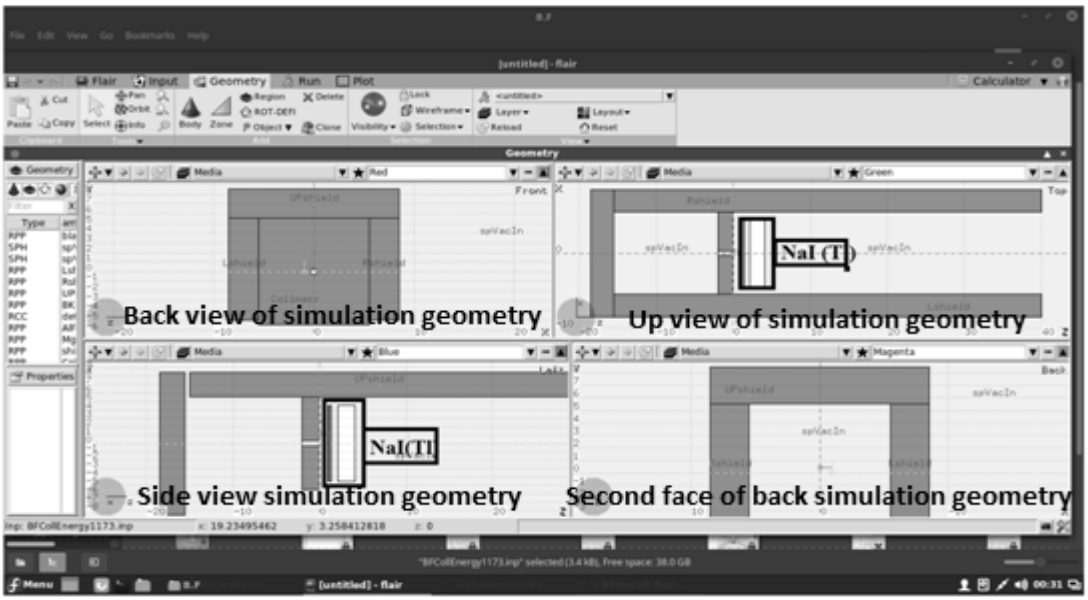

Figure 3.2. The geometry configuration in all dimension.

3.1.3. FLUKA input file

The main feature of FLUKA simulation is described as the mechanism of particle-matter interaction models and the ease of handling with complex geometries. The fact that these advantages stem from a number of drastic simplifications is not so common knowledge. The input file of successful simulation should include information about many parameters such as; the kind of gamma-ray matter interaction that can be implemented in simulation codes, the gamma-ray energy range where simulation results are faithful, each material medium of geometry, isotropic and amorphous, composition and density, the atoms or molecules in the medium, density, see Figure 3.3. In Monte Carlo simulation, the transported (primary and secondary) particles follow straight trajectories between consecutive interactions. That is, wave-like characteristics are disregarded. In principle, individual interaction events should be simulated by random sampling (Al-obaidi, S., & Akkurt, I., 2019).

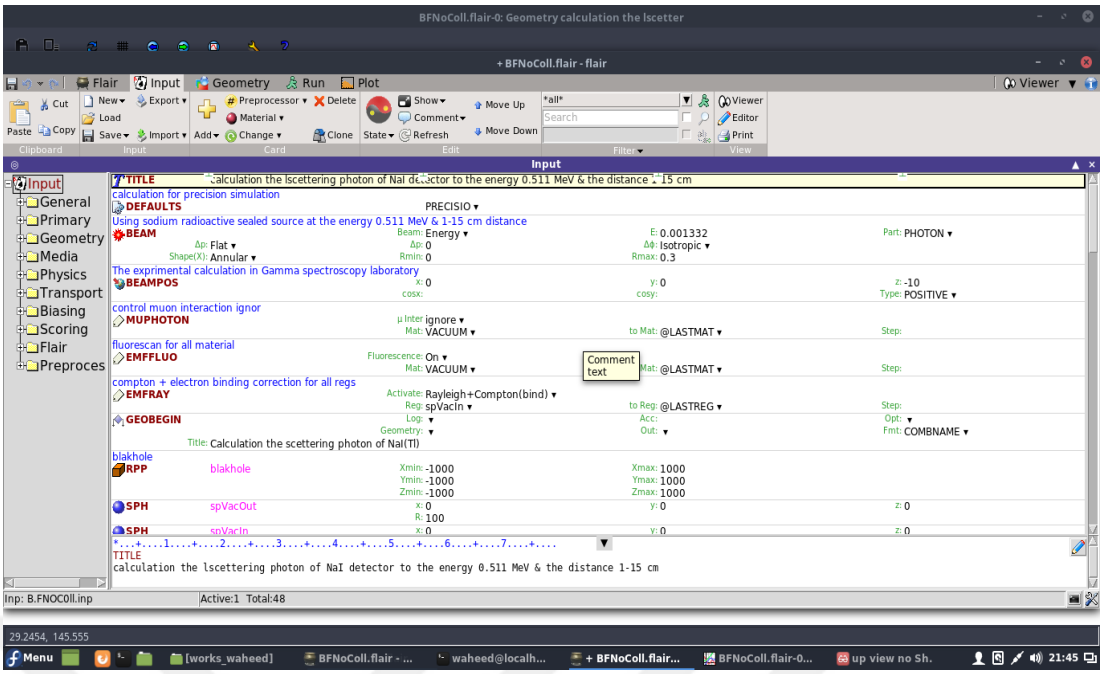

Figure 3.3. The preparation of FLUKA input file

3.1.4. Physical file

The FLUKA physical input file needs many parameters to illustrate almost real measuring system, these physical units which to be understood from simulation should be used as cards, some cards are mandatory and other are options, for example the unite of distance, area, and volume are cm, cm^2, cm^3 respectively. The energy for all incidents particle is GeV, but there is some exemption when using some other cards. For momentum it's united in GeV/c, temperature unite is degree Kelvin, and the dose equivalent is pSv/particle (Ferrari, A., et al., 2005).

3.1.5. Main output

The output data can be manipulated by a set of input files of parameters to help an analyst understand the underlying system's dynamics. The model typically is evaluated numerically over a simulated period of time and data is gathered to estimate real-world system characteristics. Generally, the collected data is interpreted with statistics like any experiment. So, we can say, a simulation is an experiment (Dagpunar, J., S., 2007), or as computer experiments because they share much in common with laboratory experiments. All in all, the main output file of simulation included data or plot of geometry for all material in 3D, basic nuclear data, material

quantities related to multiple scattering, physical model information, distribution of particle concentration in the unite of volume.

3.1.6. Flair

The FLuka Advanced Interface (flair) is an advanced or interface of FLUKA to facilitate the editing of FLUKA input files, see Figure 3.4. Its main purpose to show the input and output file easy for the beginner and experienced user, it used intermediate user's interface level. The Flair of FLUKA can perform many functions that can't see the inner function of the Monte Carlo Code program, but included all related information of comments cards of preceding, continuation, titles, and other related cards. By using flair, the editor will be easily done for many FLUKA features such as; geometry bodies of the region, interface, error, and its correction, plotting in 3D photorealistic figures, import, and export many programs. All in all, it is a dialog to displays card information in a readable way and interpreted (Ferrari, A., et al., 2005).

Figure 3.4. FLuka Advanced Interface (Flair) (Vlachoudis, V., 2006).

3.2. Experimental Detection Method

NaI (Tl) scintillation detectors are commonly used in applications where high gamma sensitivity desired, because of the solid nature of the crystal “offers” more targets to a gamma-ray, On the calculation the quality parameters of gamma spectrometer, prepared requirement that have been tested against gamma-rays using gamma spectrometer in Suleyman Demirel University/ Physics Department. The quality parameters such as; Absolute efficiency, intrinsic energy, resolution, full width at the half of the maximum had measured for gamma rays of five energies (0.511, 0.662, 1.173, 1.275, and 1.332 MeV), the gamma rays for those of energy got from ^{22}Na, ^{137}Cs, and ^{60}Co sources (Waheed, F., & Akkurt, I., 2019).

The geometry had used to analyse spectrums of these sources have been done for axial distances started from 1 cm until to 15 cm from the detector surface. In order to reduce the background level of the system, the detector had shielded by using lead on all sides as illustrate in Figure 3.5. To eliminate or reduce the scattered gamma-rays and Background activity, a lead plate was used to cover the geometry configuration, as shown Figure 3.6.

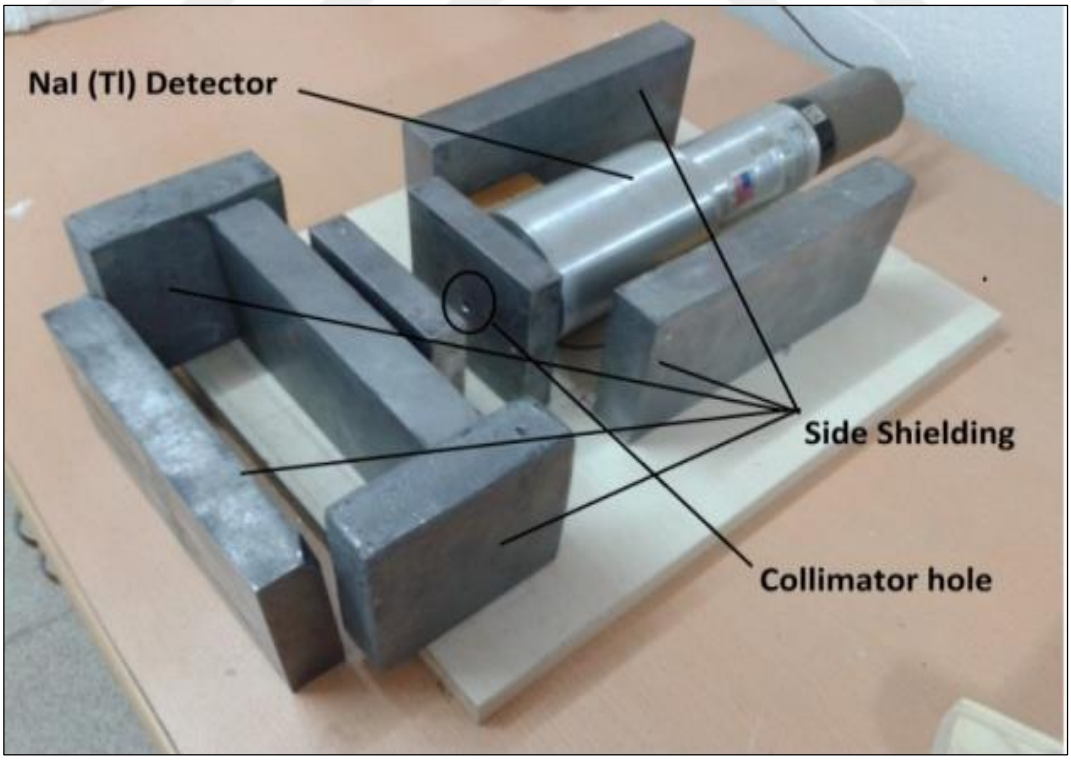

Figure 3.5. Experimenttal geometry setting

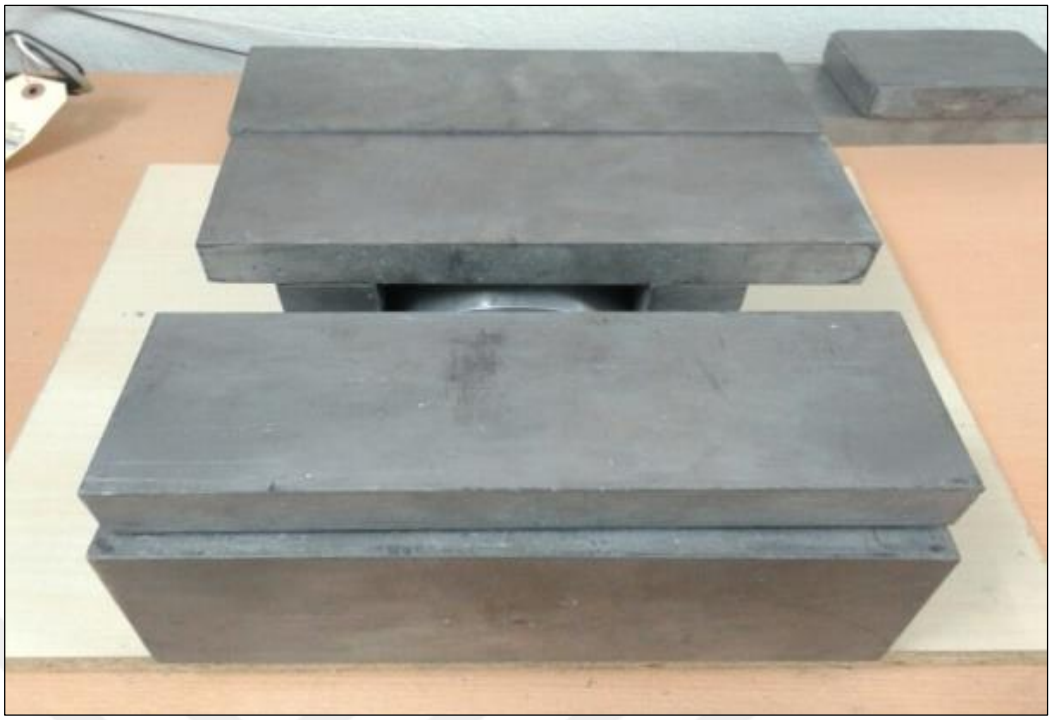

Figure 3.6. Covered the detection system by Lead shielding

3.2.1. Gamma-ray spectrometer system

The detection system has been used in this study to determine the quality parameters by depending on the analysis of the energies and the spectrum areas of the full-energy spectrums of the incoming gamma-rays lines. These mentalities could accepted as non-destructive testing and allow to determine of quality parameters (Kara, Ü., & Akkurt, İ., 2019).

The structure of gamma spectrometer that has been used for all laboratory measurements illustrating in Figure 3.5. It comprises a single crystal of thallium activated sodium iodide detector type 7.62" x 7.62" cm NaI(Tl) by ORTEC Inc., the optical scintillation material is connecting with photocathode of the photomultiplier tube. The Additional equipment needed for experimental calculation included of USB cables, MAESTRO-32 (version 6.06) software package, counting electronic system (high voltage preamplifier, amplifier 16384-channel Multichannel Analyses (MCA)), and a desk-top computer (PC) to read and save spectrum and other related data (Akkurt, I., et al., 2013c). In order to illuminate the bad effected of the background of the gamma spectrometer, the crystal is plate shielded of lead (Albidhani, H., Gunoglu, K., & Akkurt, I., 2019).

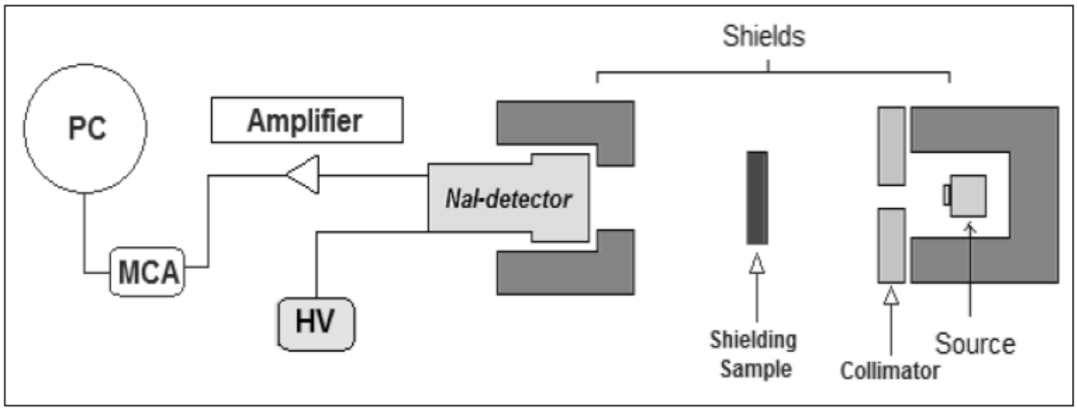

Figure 3.7. The gamma spectrometer system (Abdlhamed, F., & Akkurt, I., 2018).

3.2.2. NaI(Tl) detector

The internal installation of the NaI(Tl) crystal is illustrated in Figure 3.6. When an incident particle such as gamma-ray interacts with the active area, it causing ionization of the scintillation material. These events in the crystal will dissolution by escaping visible light gamma-rays. These phenomena are a scintillation, The thallium activated for converting the wavelength of the visible light for reaching the photocathode. The decay time of the scintillation detector is approximately 250 ns.

The active area of the scintillation detector is covered by a fluffy layer of aluminum, with a glass window at the mediator with the photocathode, to offer a hermetic seal that protects the hygroscopic NaI against moisture absorption. The inside of the fluffy layer of aluminum is lined with a coating that reflects light to enhance the light that touches the photocathode.

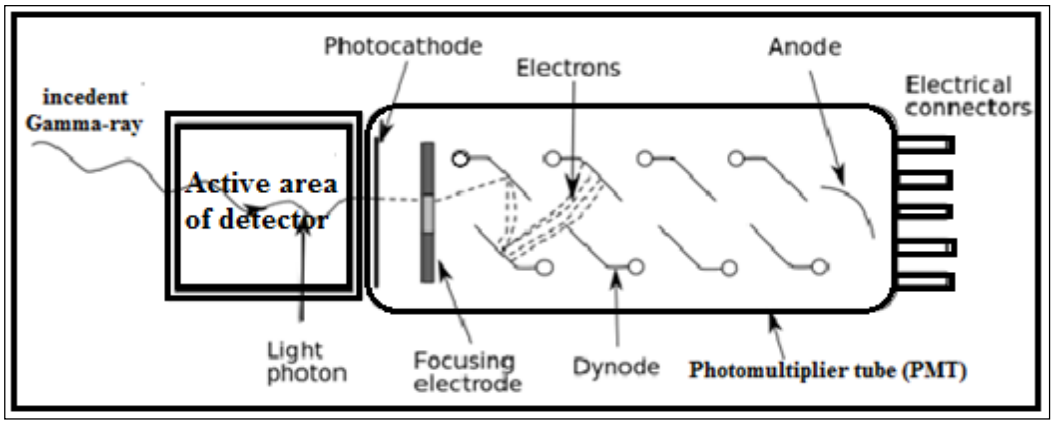

Figure 3.8. The internal structure of the NaI (Tl) detector (Reguigui, N., 2006).

3.2.3. Electronics units

The detection system composes of a scintillation crystal detector, high voltage power supply Unit (HV) that provided the detector with the voltage required to operate, preamplifier that used to collect and integrate the charge from the detector and produce an output voltage pulse and to reduce the noise which lay the nearest point to the scintillation crystal, the main amplifier for amplifying and shaping the pulses which produces from preamplifier and converting the output signals of the preamplifier into a suitable form to the desired measurements multichannel analyzer (MCA) for recording and storing electric pulses according to their height (Knoll, G. F., 2010). All of these electronic units are compacted in one disk top computer (PC) to show the digital signal processing (DSP) as shown in Figure 3.9.

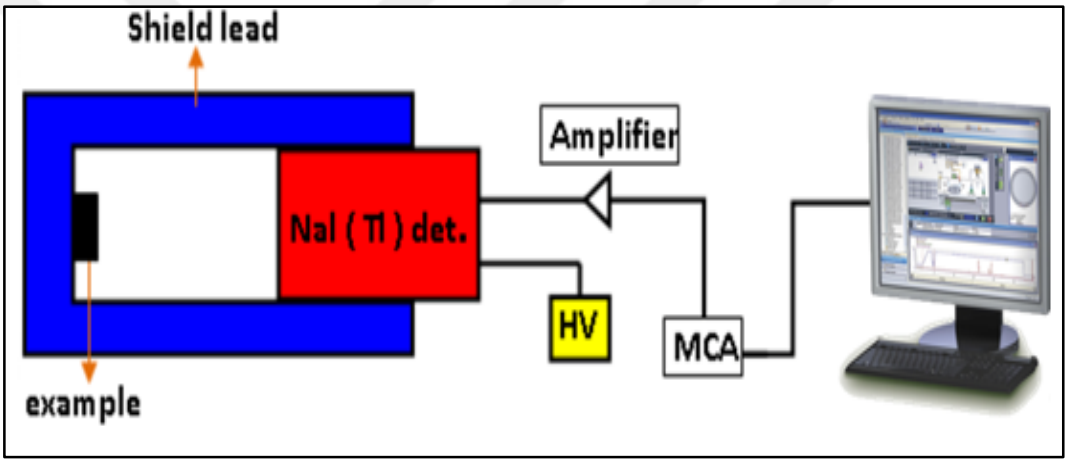

Figure 3.9. Schematic view of gamma spectrometer and electronic units (Akkurt, İ., & Hadi, A. B., 2020).

3.2.4. Energy calibration

The determination of quality parameters for gamma spectrometer depending on the calibrating procedure of NaI(Tl) scintillation detectors before usage. Gamma spectrometer must calibrate in terms of energy in order to obtain reliable results such as radionuclide identification, qualitative and quantitative analysis. This calibration procedure provides more accurate assessment; allow correctly identifying the isotopes and determining the activity of the involved ones (Akkurt, İ., & Günoğlu, K., 2019).

The energy calibration mentality is to determine the energy position of the incident gamma-ray for each channel number (Waheed, F., et al., 2018; Waheed, F., et al., 2019). The energy calibration was conducted to appear the relationship between the

channel numbers and gamma-ray energy, the peaks of the three isotropic sealed sources emitting gamma (^{22}Na, ^{137}Cs, ^{60}Co) was used, see Table 3.2. The standard source were putted in the system for 4000 seconds. The channel number and associated peaks were recorded and the graph between them was plotted. Figure 3.10 shows the spectrum of the gamma-ray of standard calibration sources, while, Figure 3.11 shows the relationship between gamma energy and channel numbers.

Table 3.2. The data of the radionuclides that uses for the determination of the energy calibration

Nuclide	Energy (MeV)	Emission probability (%)	Channel number	Half-life (year)	Activity (Bq)
Cs-137	0.6616	85.1	1808.89	30.08	31515
Na-22	0.511	178.0	825.52	2.6018	5811
	1.2745	99.94	1983.53		
Co-60	1.1732	99.85	2133.05	5.2711	14817
	1.3325	99.9826	2413.15		

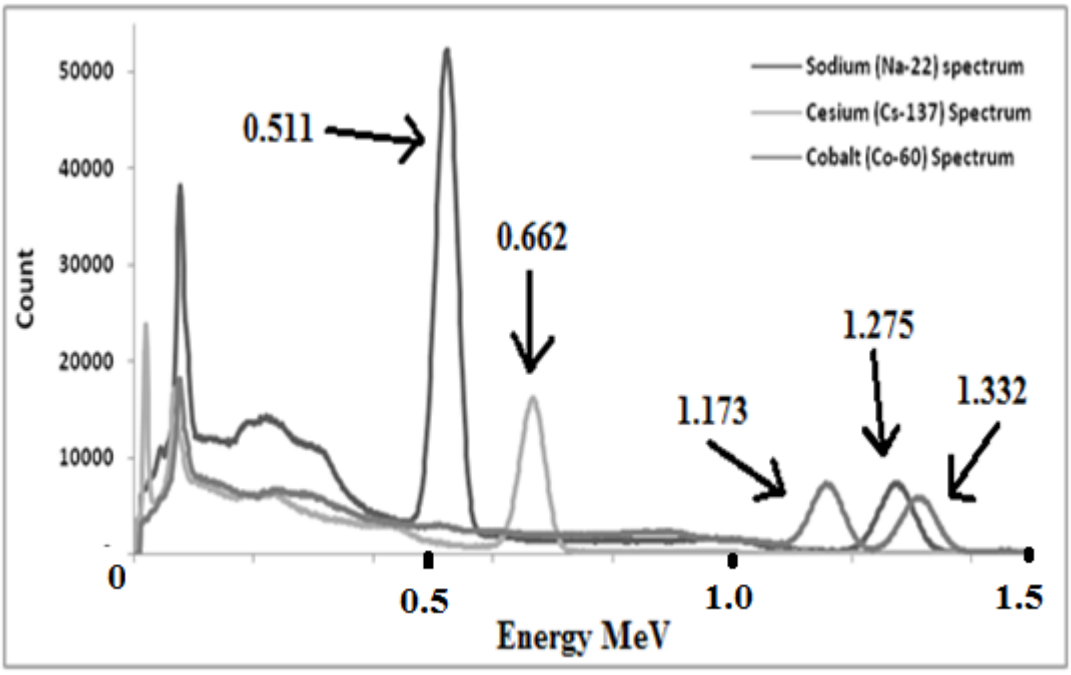

Figure 3.10. The spectrum of the standard calibration sources

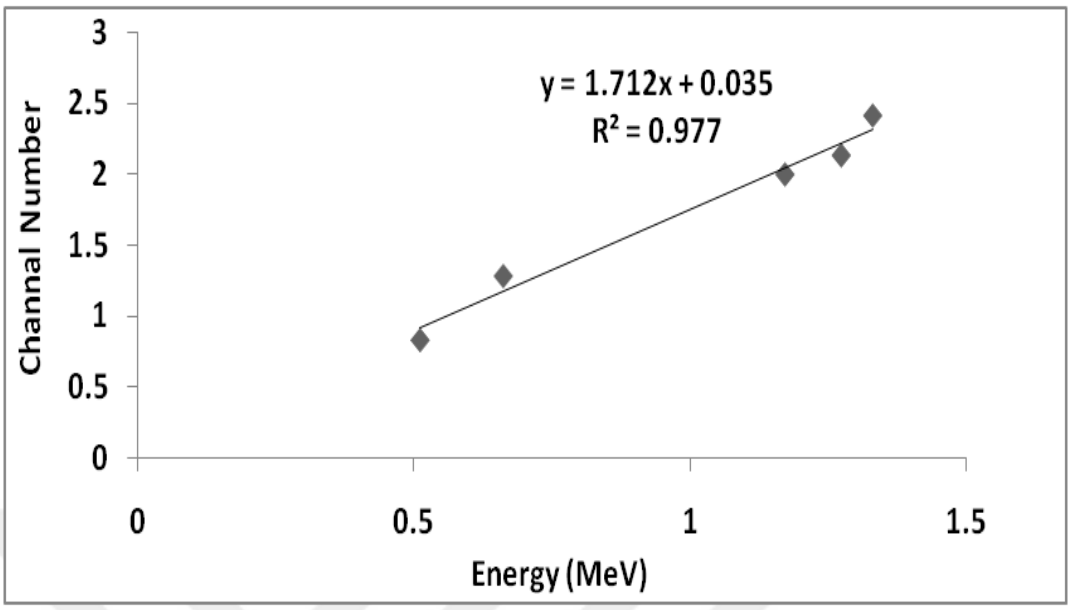

Figure 3.11. Energy calibration with channel number

3.2.5. Determination of detection efficiency

For the gamma-ray spectrometry measurement technique, the absolute efficiency and the intrinsic efficiency are importants parameters take to consider, they are usually referred to the relation between the numbers of the incoming gamma-ray emitted from the isotropic source for all direction to the number of gamma-rays collected in the full-energy spectrum to the same energy. The efficiency calibration allows establishing the detection efficiency of the detector as a function of the gamma-ray energy and source-detector distance (Akkurt, İ., et al., 2020).

The absolute efficiency and the intrinsic of the 3" x 3" scintillation detector have been calculated at 0.511, 0.662, 1.173, 1.275, and 1.332 MeV gamma-ray energy obtained from Sodium (^{22}Na), Cobalt (^{60}Co), and Cesium (^{137}Cs) point isotropic real sources.

The geometry configuration that uses to analyze the spectrum related to its energy has been calculated for many different axial distances starts from 1 cm until 15 cm from the detector surface. It is surrounded by lead shielding to reduce the radiation background effect, see Figure 3.12.

Figure 3.12. The experimental geometry used to analyse the spectroscopy

The physical diameters simulation of the NaI(Tl) crystal by FLUKA code have been modeled with the active area of the real crystal because of the variations of the physical diameters of the real crystal and surrounding shielding geometry impact on the incoming gamma-ray detection efficiency calculation (Nakamura, T., 1983; Sima, Q., 1990). The detector physical data and crystal dimension and other properties as illustrated in Figure 3.13. The geometry of FLUKA simulation is adjusted exactly to the experimental properties, Figure 3.14. Put side and pack shielding, covered all by lead shielding to eliminate the background.

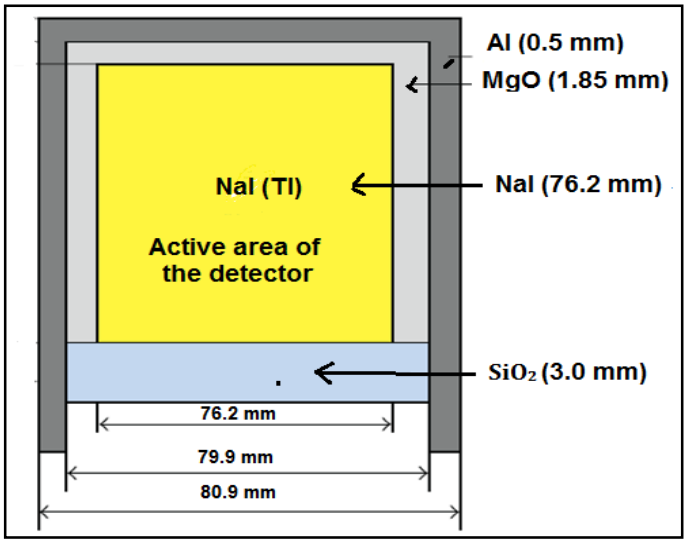

Figure 3.13. The physical data of 3”×3” NaI(Tl) detector (Akkurt, İ., et al., 2020)

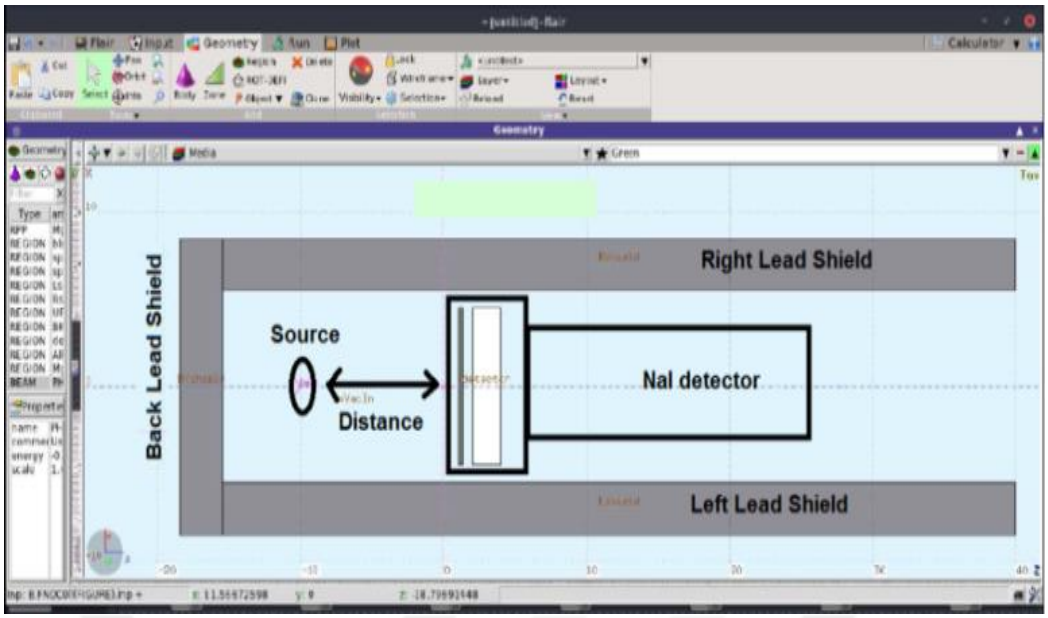

Figure 3.14. The FLUKA simulation geometry configuration

3.2.6. Resolution and FWHM

The energy Resolution (R%) and full width at half of the maximum (FWHM) are other significant parameters of the NaI(Tl) detection system. These parameters calculated using gamma-ray energies emitted by the ^{22}Na, ^{137}Cs, ^{60}Co life isotropic sources, see Figures 3.15. The calculation has been obtained as a function of seven source-detector distance for five gamma-ray energies. The geometry of FLUKA simulation for calculation the resolution and full width at half of the maximum were done according to the experimental properties (Demir, N., et al., 2019).

Figure 3.15. The experimental geometry to calculate the resolution and FWHM.

The energy resolution is an important parameter for a gamma-ray spectrometer because it determines how close energy of two gamma-rays before giving a single

broad peak instead of two distinctly separate peaks, the energy resolution is very important when unknown gamma emitters are recording, since gamma-rays differing in energy by less than the energy resolution will not be separately detectable (Gouda, M. M., et al., 2015; Casanovas, R., et al., 2012).

The 3" x 3" scintillation crystal has a successful energy resolution for plotting the gamma-ray spectrum. The energy resolution of the gamma-ray spectrum is the detection of the variation in the electrical pu□es size resulting from the whole absorption of the incoming gamma-ray energy. A minimum value of energy resolution in the equation below means that the detection system has the ability to recognize between two incoming gamma-ray with nearly energies (Jibiri, N., N., & Abiodun, T., H., 2012; Waheed, F., et al., 2018), (Figure 3.16 & Figure 3.17).

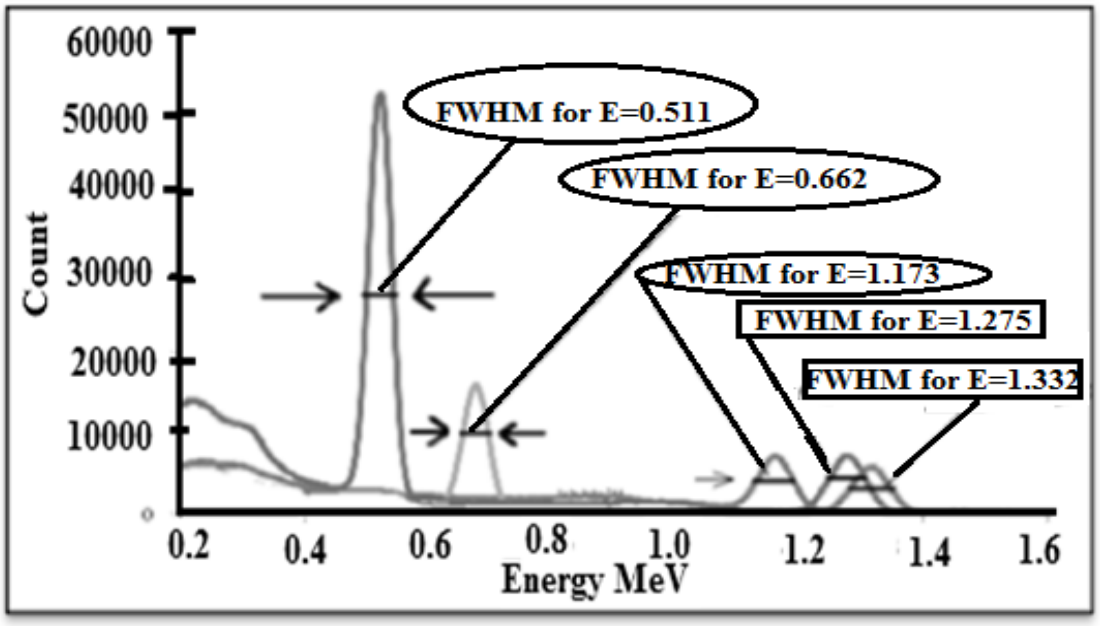

Figure 3.16. FWHM procedure calculation for energy peak.

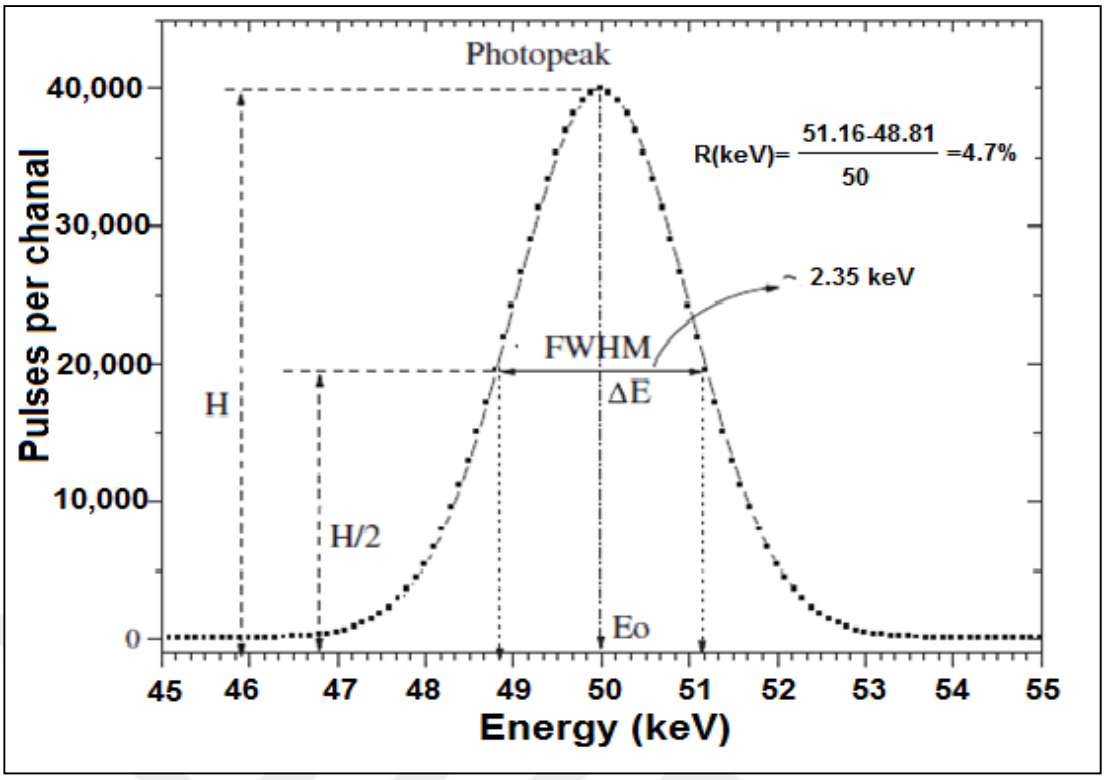

Figure 3.17. Energy resolution and FWHM procedure for calculation the energy peak (Akkurt, I., et al., 2020).

The energy resolution (R) of a NaI detector can be calculate as follow (Sudarshan, M., & Singh, R., 1991).

$$R = FWHM \times \left(\frac{\Delta E}{\Delta ch}\right) x\ 100\ \% \qquad (3\text{-}1)$$

Where:

R:- Energy resolution (keV).

FWHM:- Full width at half the maximum (channel).

ΔE: Variation of the unattached gamma lines (keV).

Δch:- Variation between the spectrums of the unattached gamma lines (channel).

The energy resolution of the detection system can be determined from the width of a spectrum at half i□maximum height of the counted value (FWHM) of the spectrum depending during below formula:-

$$R = \frac{FWHM}{E_0} \times 100 \qquad (3\text{-}2)$$

Here *R* is energy resolution and E_0 is the related energy. The experimental full energy peak efficiency at energy *E* was determined depending as below formula:-

$$\varepsilon_{fep}(E) = \frac{N(E)}{A \cdot t \cdot p(E)} \quad (3\text{-}3)$$

Where *N(E)* is the net coun□ calculated under the spectrum for that energy, *A* is the activity of the real isotropic source, *t* is the real time that used to analyze the spectrum (in seconds) and *p(E)* is the eventuality for each gamma-ray emission of the used source.

In the practicle spectra shape plotting, the data for plotting the real spectrum according to the Gaussian distribution for the energy lines. However, the FLUKA simulation method for plotting the spectrum shape is not directly. It doesn't have the ability to show physical effects or electric noise that leads to the broadening spectrum, but it uses a mathematical response function technique for plotting the spectrum shape related to the real resolution of the experimentally detection system. Thus, for more realistic for plotting spectrum shape obtained by FLUKA simulation, it is important to consider the resolution of the spectrum shape by applying a Gaussian function as a mathematical response function, this technique according to the use of the "USRBDX" card and calculating the FWHM of the spectrum. For this purpose, the experimental value of the FWHM as a function of the incoming gamma-ray energy and source-detector distance was calculated and compared with simulation results.

The mathematical response function that uses to plot the spectrum shape of the simulation method is done by below formula (Hakimabad, H. M., et al., 2007; Waheed, F. Q. et al., 2019):-

$$\text{f (E)} = Ce\ \left(\frac{-(2\sqrt{Ln2}\,(E-Eo)}{FWHM}\right)^2 \quad (3\text{-}4)$$

$$FWHM = a + b\sqrt{E + cE^2} \quad (3\text{-}5)$$

Equation (3-5) is the value of FWHM as a function of energy, in order to get the value of *a, b,* and *c* to be applied in the Gaussian Energy Broadening command of FLUKA simulation. The adjustment coefficients of energy resolution for the detection system, a=-0.0024, b=0.05165, and c=2.85838, were calculated after adjusting a function of formula (3-4). Where: *E*: the broadened energy; E_0: the

unbroadened energy of the tally; *C*: normalization constant. A non-linear function adjusted by least-squares method was used to determine the numerical numbers of the *"a", "b"* and *"c"* coefficients, that is important when preparing the MC simulation, according to mathematical response function that shown in formula (3-4) (Salgado, C. M., 2015; Waheed, F., 2019; Pelowitz, D., B., 2005).

These numerical values should be use with the GEB command in order to consider the energy resolution of the physical diameters of the crystal in the simulation (Hakimabad, H. et al., 2007).

3.2.7. Energy buildup factor.

For the gamma-ray detection technique, the buildup factor is important to be determined to govern the quality parameters of the gamma spectrometer. This parameter is usually done using a function to the energy range and detector-source distance, The geometry was used to analysis spectroscopy of these sources to determination the buildup factor have been done for many different axial distances starts from 1 cm until 15 cm from the detector surface. For the determination the value of the buildup factor; lead collimator had been used to illuminate scattering gamma-ray, the difference between the number of particles arrived at scintillation detector referred the number of scattering gamma-ray with geometry materials, but when used lead collimator, the main equation of Beer-Lambert low can be directly applied. The lead collimator and other geometry properties as illustrated in Figure 3.18. In order to reduce the background level of the system, the detector is shielded using lead on all sides as, to eliminate or reduce the scattered gamma-rays and Background activity, a lead plate was used to cover the geometry configuration.

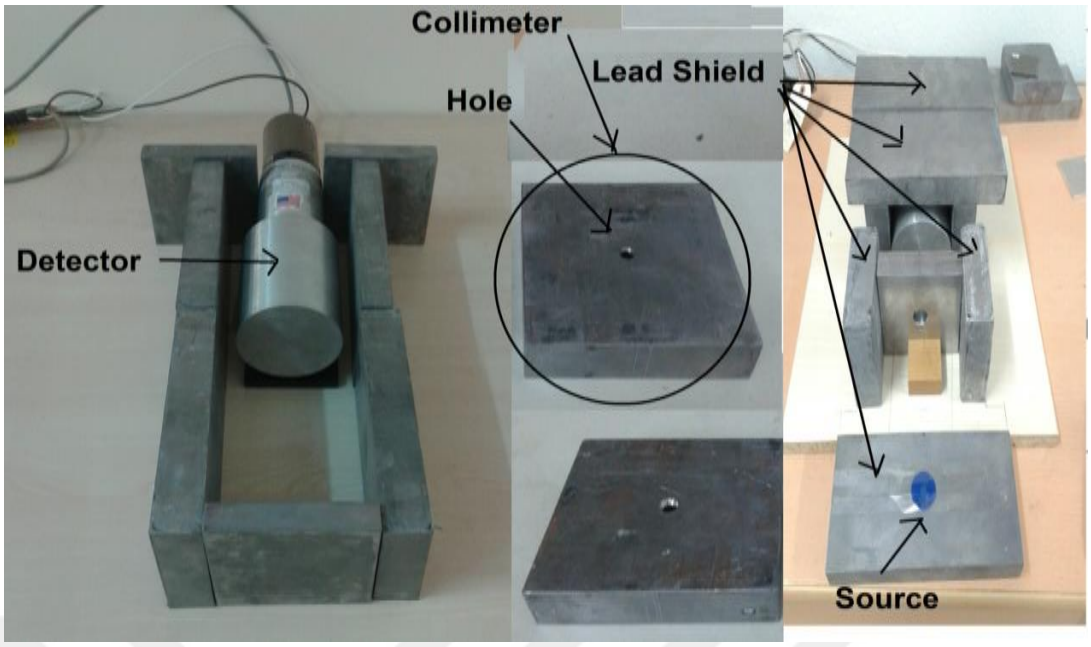

Figure 3.18. The lead collimator and other experimental geometry properties.

The geometry of FLUKA simulation for calculation the buildup factor is exactly to the experimental properties to get acceptable results, the description of the interaction of incident particle is important during preparing the input file of simulation (**Joel, G., 2018**). Figure 3.19 illustrates simulation geometry structure related to experimental selection configuration when using a lead collimator, put side and pack shielding and covered all by lead shielding to illumination background, while, Figure 3.20 illustrates simulation without a lead collimator.

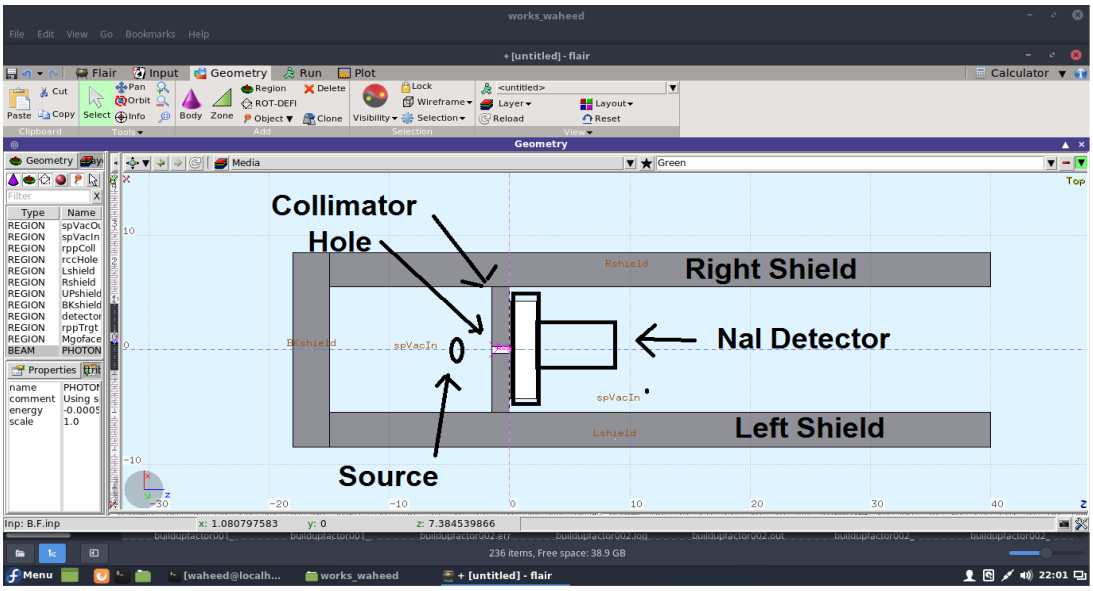

Figure 3.19. The lead collimator and other simulation geometry properties

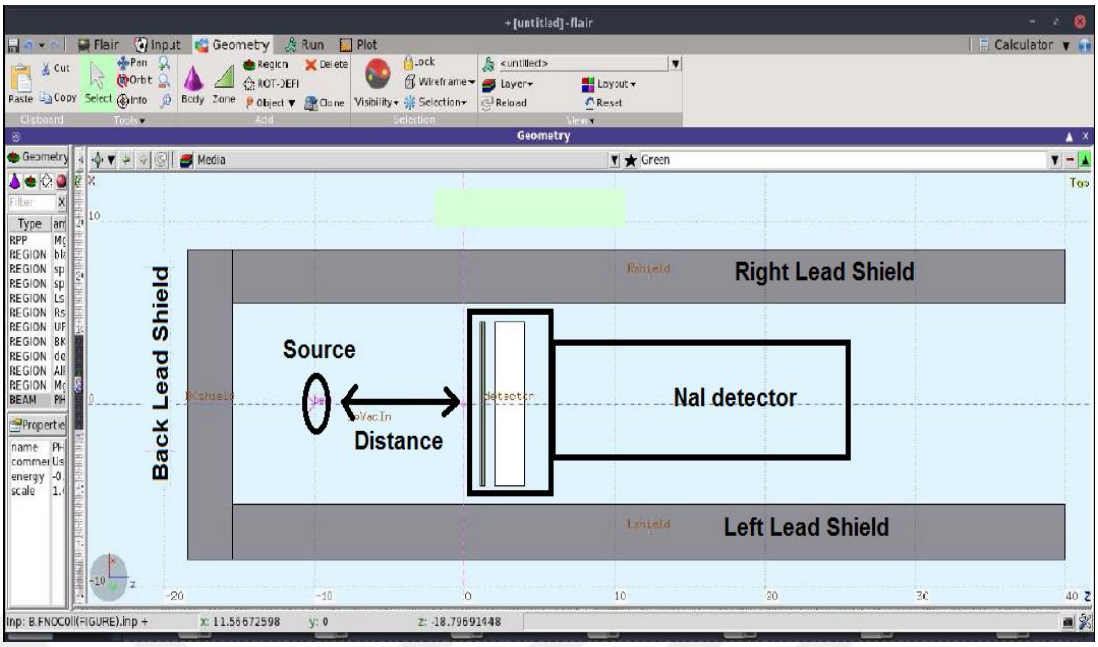

Figure 3.20. Simulation geometry properties without using the lead collimator.

4. RESULTS AND DISCUSSIONS

The important quality parameters of gamma spectrometer have been determined for a 3" x 3" NaI(Tl) detector (Canberra Inc.). These parametrs are; the detector intrinsic efficiency, detector absolute efficiency, energy resolution (R), the full width at the half of maximum (FWHM), buildup factor, and also the source-detector distance impact to the each value of all of these quality parameters. The measurements have been performed at seven axial source-detector-distances for five gamma-ray energies emit by three isotropic sources (^{22}Na, ^{137}Cs, and ^{60}Co). Thus, fundamental data for further works obtained.

FLUKA (2011.2 x 7, July 2019) code have been used to obtain the results of quality parameters of 3" x 3" NaI scintillation detector exposed to gamma-ray energy emit from life radioactive real source. The detector was modeled with the FLUKA code and the results were compared to experimental calculations of radiation sources to the same conditions.

4.1. Energy Spectrum

Figure 4.1 shows the energy spectrum curve of Cesium isotropic source (^{137}Cs) which emit 0.662 MeV gamma-ray and comparison with the simulated spectrum curve using FLUKA Code after applying the mathematical response functions to the same gamma-ray energy (FLUKA spectrum is Gaussian distribution pulses broadened). The activity of the life Cesium source was 31.515 kBq at measuring time. The result shows a high background count in low energy region mainly originating from Compton scattering because of interaction with geometry materials. The successful agreement has been appeared in the spectrum.

Figure 4.2 shows the experimental spectrum curve of Sodium isotropic source (^{22}Na) which emit 0.511 and 1.275 MeV gamma-rays and comparison with the simulated spectrum using FLUKA code after applying the mathematical response functions to the same gamma-ray energy (FLUKA spectrum is Gaussian distribution pulses broadened). The activity of life Sodium source was 2.6018 kBq at the measuring time. The result shows a high background count in low energy region mainly originating from Compton scattering because of interaction with geometry materials. The successful agreement has been appeared in the spectrum curve.

Figure 4.3 shows the experimental spectrum of Cobalt isotropic source (^{60}Co) which emit 1.173 and 1.332 MeV gamma-rays and comparison with the simulated spectrum using FLUKA code after applying the mathematical response functions to the same gamma-ray energy (the FLUKA spectrum is Gaussian distribution pulses broadened). The activity of life Sodium source was 5.2711 kBq at the measuring time. The result shows a high background count in low energy region mainly originating from Compton scattering because of interaction with geometry materials. The successful agreement has been appeared in the spectrum curve.

Figure 4.4 shows the impact of the source-detector distance of the experimental gamma-ray spectrum of the Cesium source (^{137}Cs) which emit 0.662 MeV gamma-ray. It can be seen the height of the gamma-ray spectrum decreases with increasing the source-detector distance. It can be seen that, at short source-detector distance (1cm), the height of the gamma-ray spectrum shape at maximum level, and for long distance (15cm) the height of the gamma-ray spectrum at minimum level.

Figure 4.5 shows the impact of the source-detector distance of the experimental gamma-ray spectrum of the Sodium source (^{22}Na) which emit 0.511 and 1.275 MeV gamma-rays. It can be seen from this result that the height of the gamma spectrum decreases with increasing the source-detector distance. It can be seen that, at short source-detector distance (1cm) the height of the gamma-ray spectrum at maximum level, and for long distance (15cm), the height of the gamma spectrum at minimum level.

Figure 4.6 shows the impact of the source-detector distance of the experimental gamma-ray spectrum of the Cobalt source (^{60}Co) which emit 1.173 and 1.332 MeV gamma-rays. It can be seen the height of the gamma spectrum decreases with increasing the source-detector distance. It can be seen that, at short source-detector distance (1cm) the height of the gamma-ray spectrum at maximum level, and for long distance (15cm) , the height of the gamma spectrum at minimum level.

Figure 4.7 shows the impact of the source-detector distance of FLUKA simulation gamma-ray spectrum of the Cesium source (^{137}Cs) which emit 0.662 MeV gamma-ray after applying the mathematical response function. It can be seen the height of the gamma-ray spectrum decreases with increasing source-detector distance. It can be seen that, at short source-detector distance (1cm), the height of the gamma-ray

spectrum at maximum level, and for long distance (15cm), the height of the gamma-ray spectrum at minimum level.

Figure 4.8 shows impact of the source-detector distance of FLUKA simulation gamma-ray spectrum of the Sodium source (^{22}Na) which emit 0.511 and 1.275 MeV gamma-rays after applying the mathematical response function. It can be seen the height of the gamma spectrum decreases with increasing source-detector distance. It can be seen that, at short source-detector distance (1cm), the height of the gamma-ray spectrum at maximum level, and for long distance (15cm), the height of the gamma-ray spectrum at minimum level.

Figure 4.9 shows impact the of source-detector distance of FLUKA simulation gamma-ray spectrum of the Cobalt source (^{60}Co) which emit 1.173 and 1.332 MeV gamma-rays after applying the mathematical response function. It can be seen the height of the gamma-ray spectrum decreases with increasing source-detector distance. It can be seen that, at short source-detector distance (1cm), the height of the gamma-ray spectrum at maximum level, and for long distance (15cm), the height of the gamma-ray spectrum at minimum level.

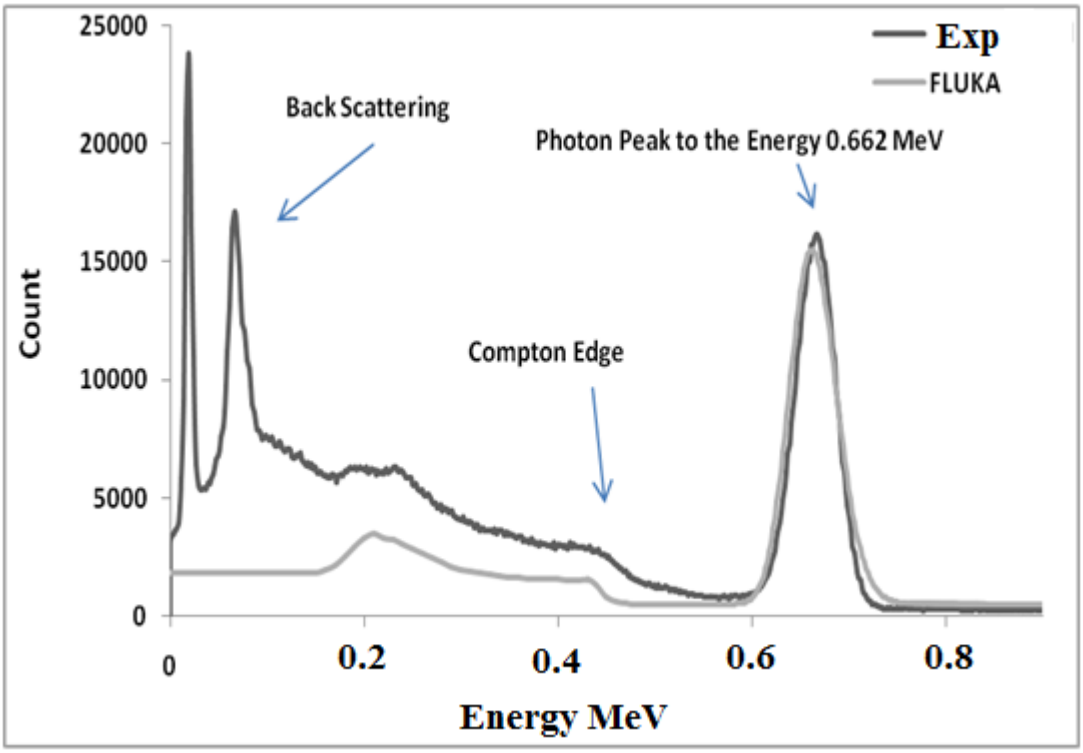

Figure 4.1. FLUKA Simulated gamma-ray spectrum for Cesium (^{137}Cs) in comparison with the experimental spectrum

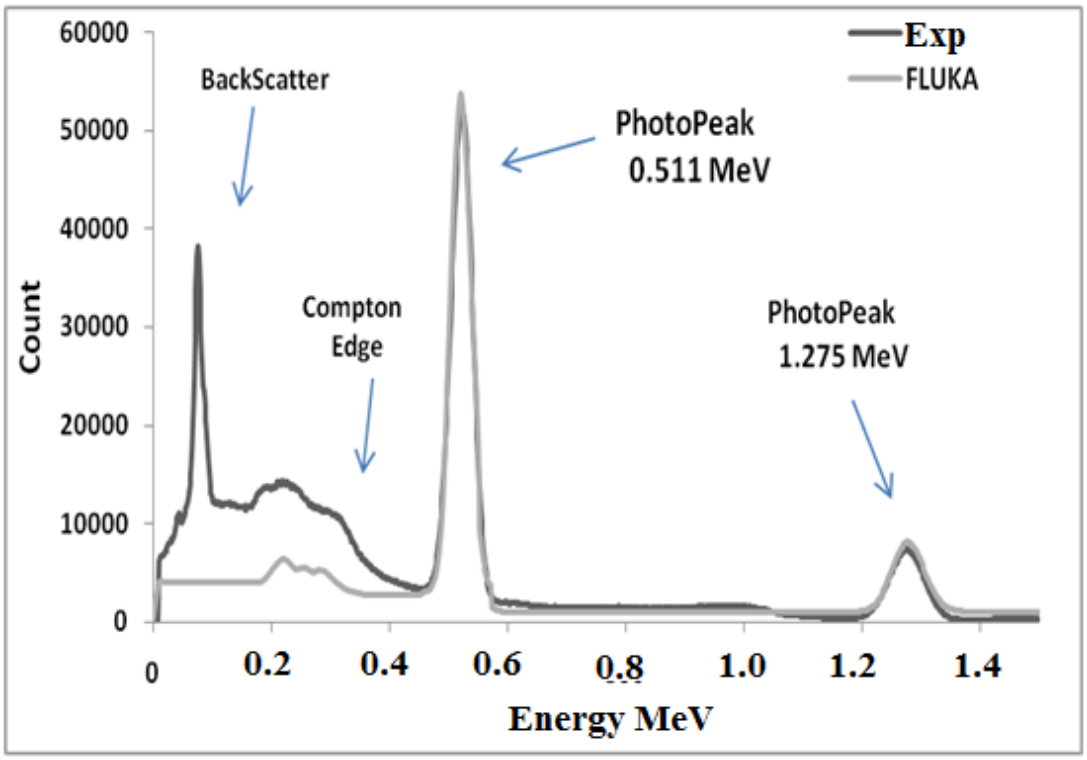

Figure 4.2. FLUKA Simulated gamma-ray spectrum for Sodium (^{22}Na) in comparison with the experimental spectrum.

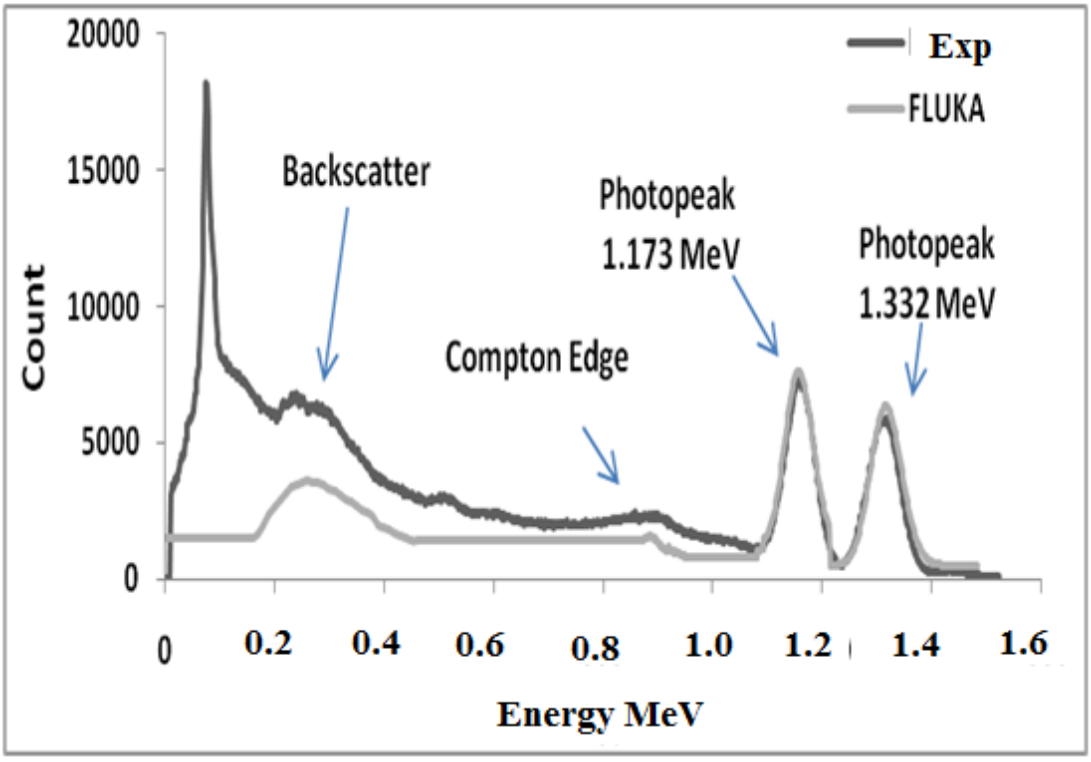

Figure 4.3. FLUKA Simulated gamma-ray spectrum for Cobalt (^{60}Co) in comparison with the experimental spectrum.

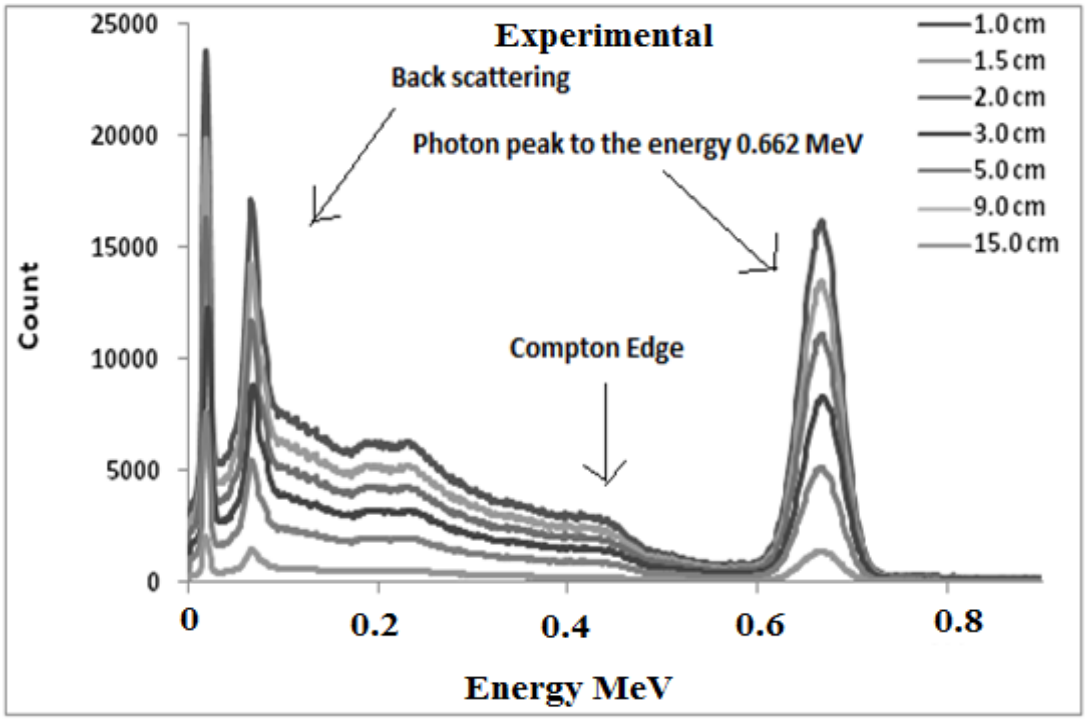

Figure 4.4. Experimentally gamma-ray spectrum for Cesium source (^{137}Cs)

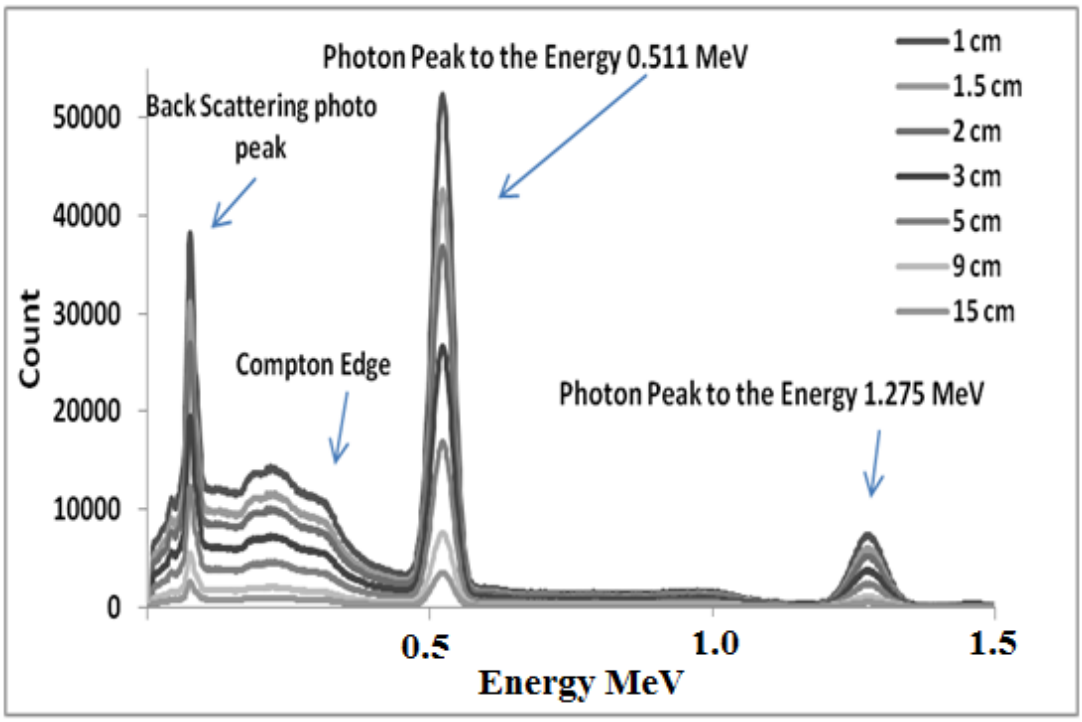

Figure 4.5. Experimental gamma-ray spectrum for Sodium source (^{22}Na)

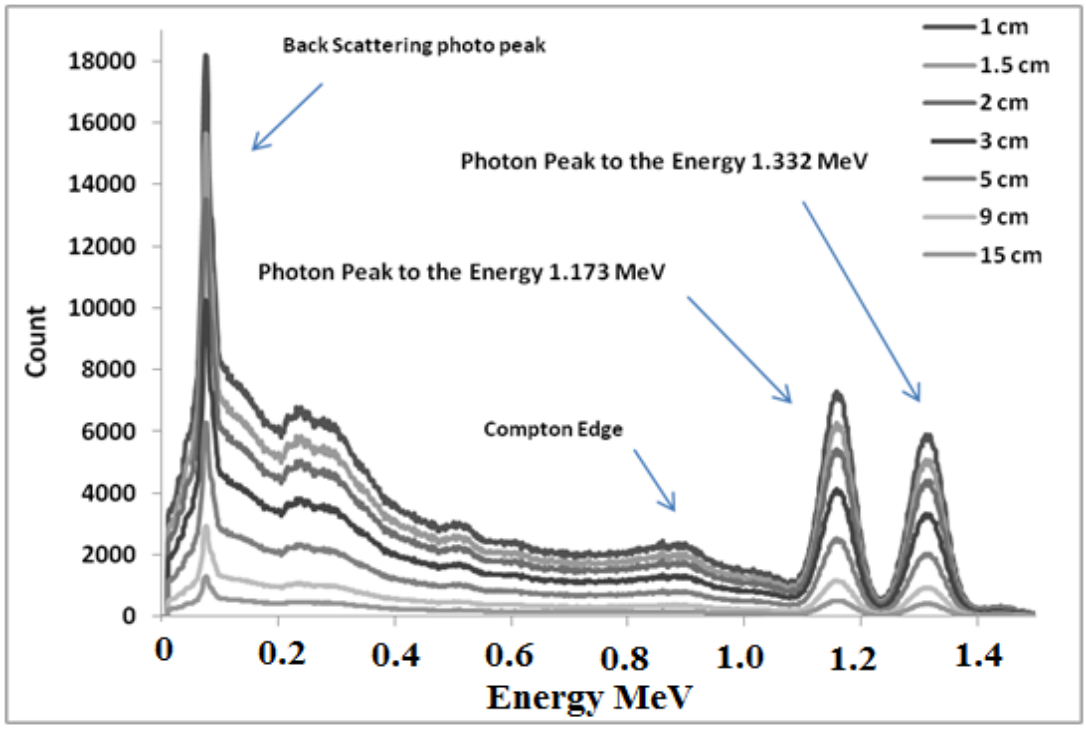

Figure 4.6. Experimental gamma-ray spectrum for Cobalt source (^{60}Co)

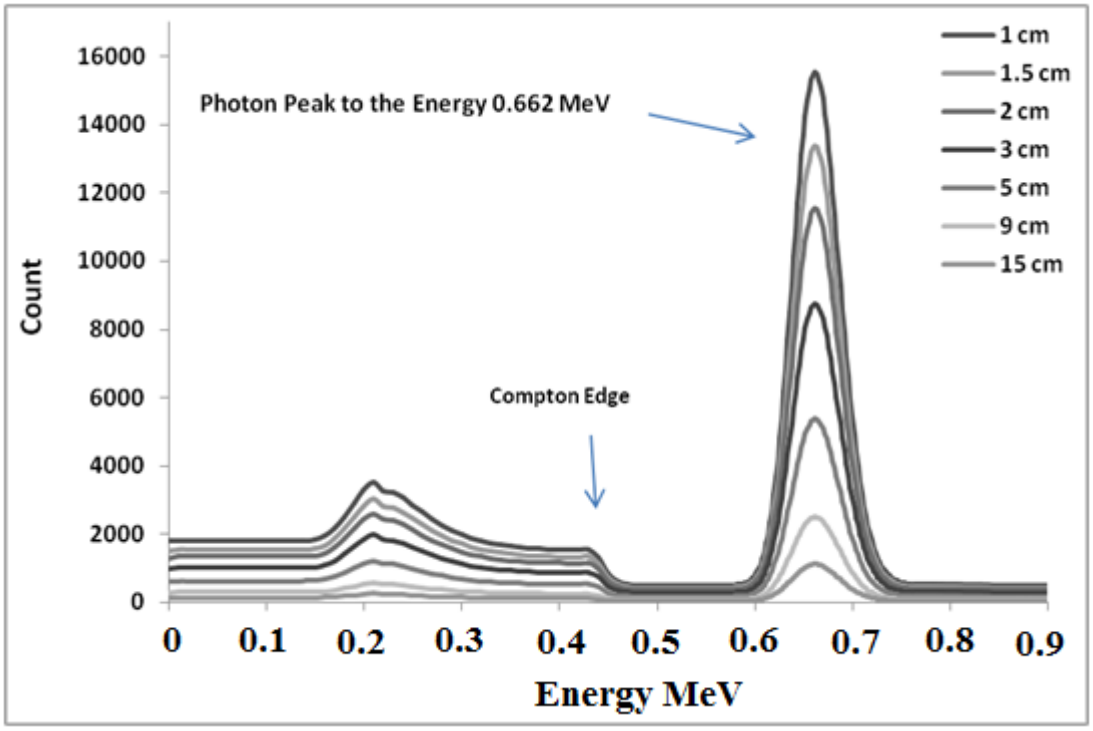

Figure 4.7. FLUKA gamma-ray spectrum for Cesium source (^{137}Cs)

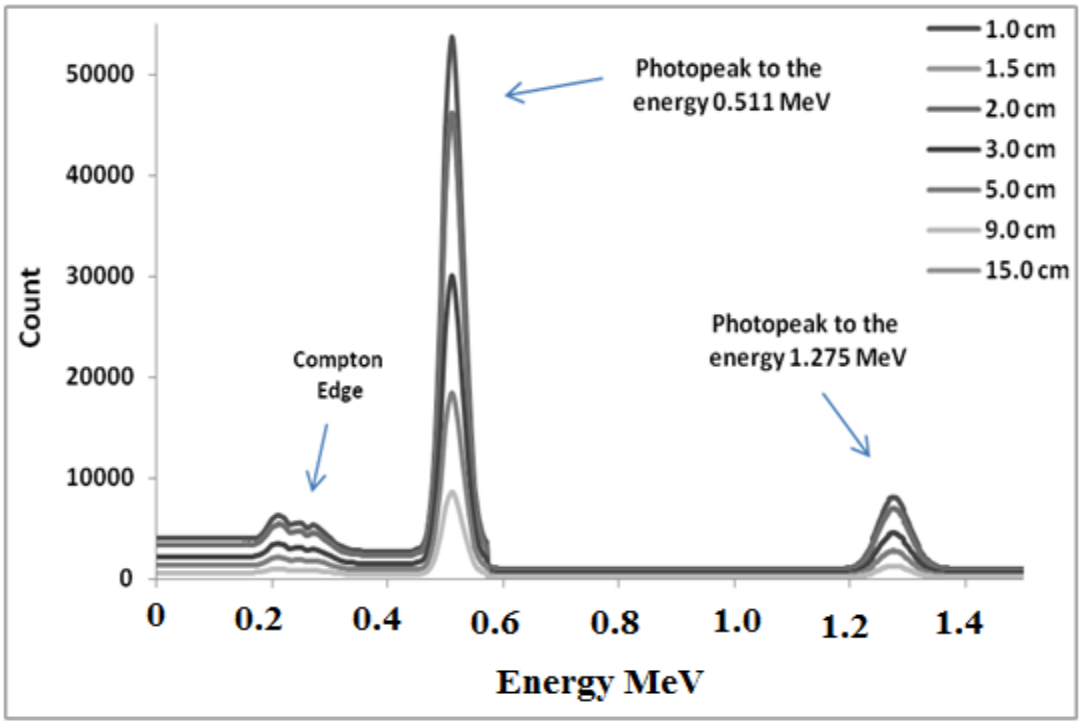

Figure 4.8. FLUKA gamma-ray spectrum for Sodium source (^{22}Na)

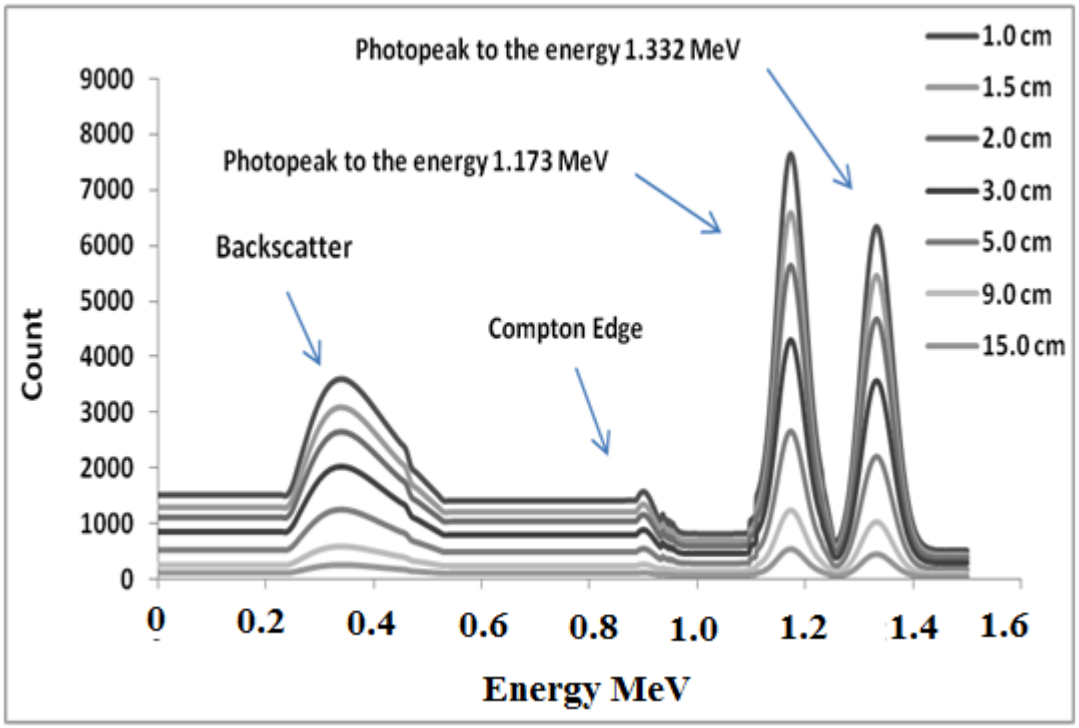

Figure 4.9. FLUKA gamma-ray spectrum for Cobalt source (^{60}Co)

4.2. Detector Effifiency Results

Figure 4.10 shows the detector intrinsic efficiency as a function of gamma-ray energy. From this result, the variation of intrinsic efficiency as a function of the gamma-ray

energies has been obtained to the five energies. It can be seen that the intrinsic efficiency decreases with increasing the gamma-ray energy.

Figure 4.11 shows the high different variation of the absolute efficiency as a function of the gamma-ray energy (MeV) and source-detector distance (cm) experimentally. From these results. It can be seen that the absolute efficiency decreases with increasing the gamma-ray energy to the same source-detector distance, and it decreases with increasing the gamma-ray energy to the same source-detector distance.

Figure 4.12 shows the high different variation of the absolute efficiency as a function of the gamma-ray energy (MeV) and source-detector distance (cm) of FLUKA simulation. From this result. It can be seen that the absolute efficiency decreases with increasing the gamma-ray energy to the same source-detector distance, and it decreases with increasing the gamma-ray energy to the same source-detector distance.

Figure 4.13 shows the high different variation of the absolute efficiency as a function of gamma-ray energy and source-detector distance experimentally and the comparison with FLUKA simulation. From this result. It can be seen that the absolute efficiency decreases with increasing the gamma-ray energy to the same source-detector distance, and it decreases with increasing the gamma-ray energy to the same source-detector distance. It can be seen that, at low energy 0.511 MeV and short source-detector distance 1cm, the absolute efficiency is 11.3% experimentally and it is 10.6% by FLUKA simulation. While the absolute efficiency at high energy 1.332 MeV and far distance 15cm, it is 0.76 and 0.75% experimentally and by FLUKA simulation, respectively.

Figure 4.14 shows the comparison of the absolute efficiency as a function of the source-detector distance (cm) to the gamma-ray energy (0.511 MeV) experimentally and FLUKA simulation. It can be seen that the absolute efficiency decreases with increasing the source-detector distance.

Figure 4.15 shows the comparison of the absolute efficiency as a function of the source-detector distance (cm) to the gamma-ray energy (0.662 MeV) experimentally and FLUKA simulation. It can be seen that the absolute efficiency decreases with increasing the source-detector distance.

Figure 4.16 shows the comparison of the absolute efficiency as a function of the source-detector distance (cm) to the gamma-ray energy (1.173 MeV) experimentally and FLUKA simulation. It can be seen that the absolute efficiency decreases with increasing the source-detector distance.

Figure 4.17 shows the comparison of the absolute efficiency as a function of the source-detector distance (cm) to the gamma-ray energy (1.275 MeV) experimentally and FLUKA simulation. It can be seen that the absolute efficiency decreases with increasing the source-detector distance.

Figure 4.18 shows the comparison of the absolute efficiency as a function of the source-detector distance (cm) to the gamma-ray energy (1.332 MeV) experimentally and FLUKA simulation. It can be seen that the absolute efficiency decreases with increasing the source-detector distance.

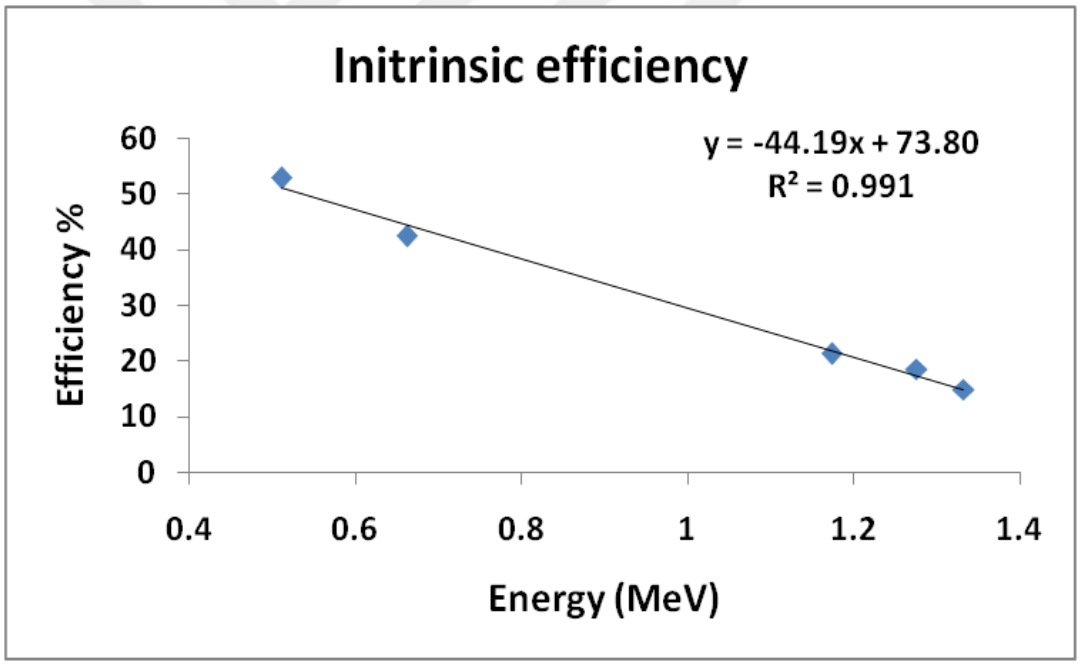

Figure 4.10. Intrinsic efficiency of the NaI Detector

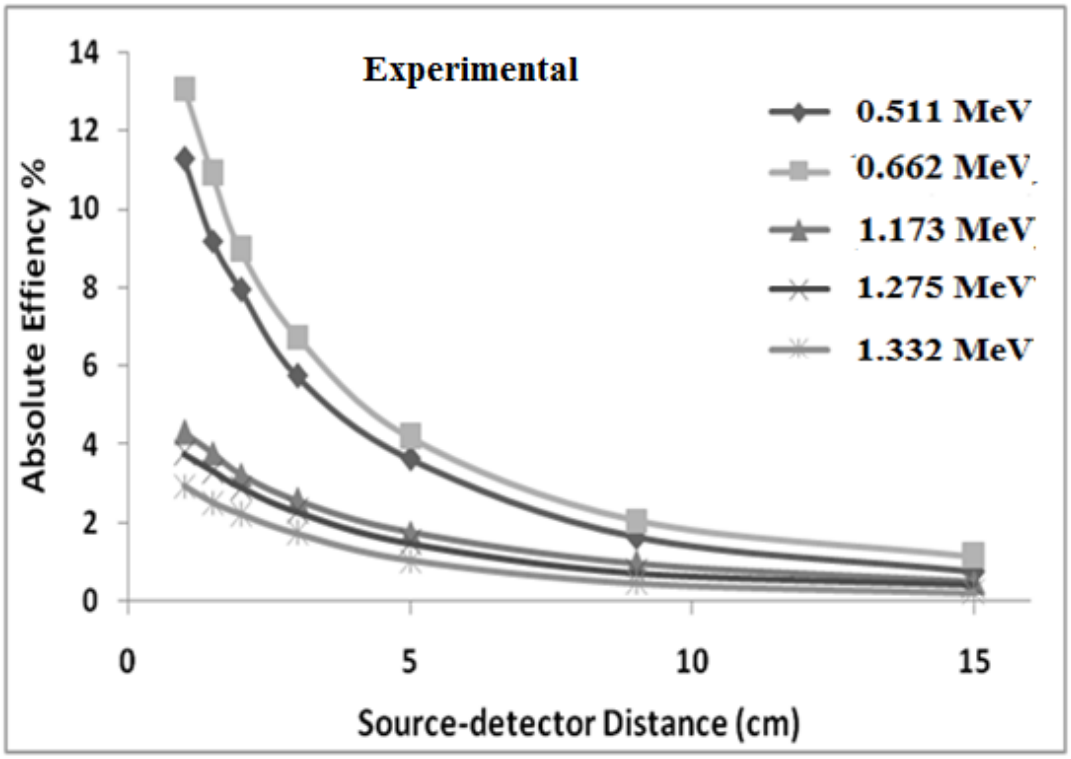

Figure 4.11. Experimentally absolute efficiency as a function of gamma-ray energy (MeV) and Source-detector distance (cm).

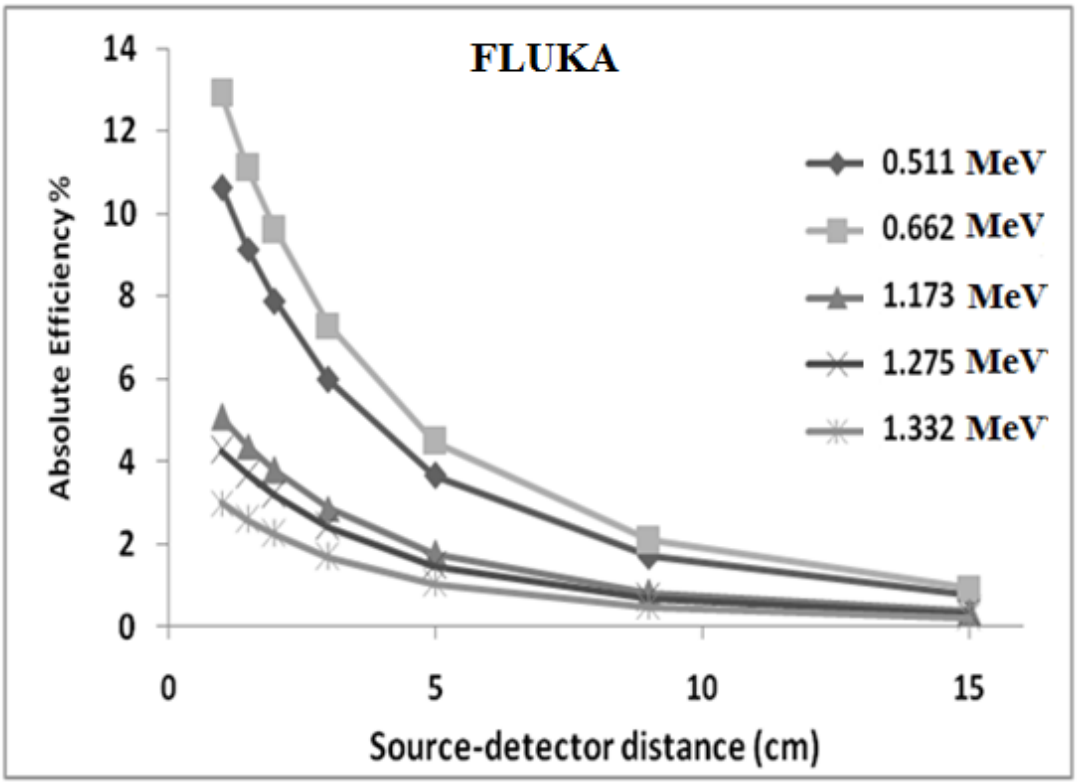

Figure 4.12. FLUKA absolute efficiency as a function of gamma-ray energy (MeV) and Source-detector distance (cm).

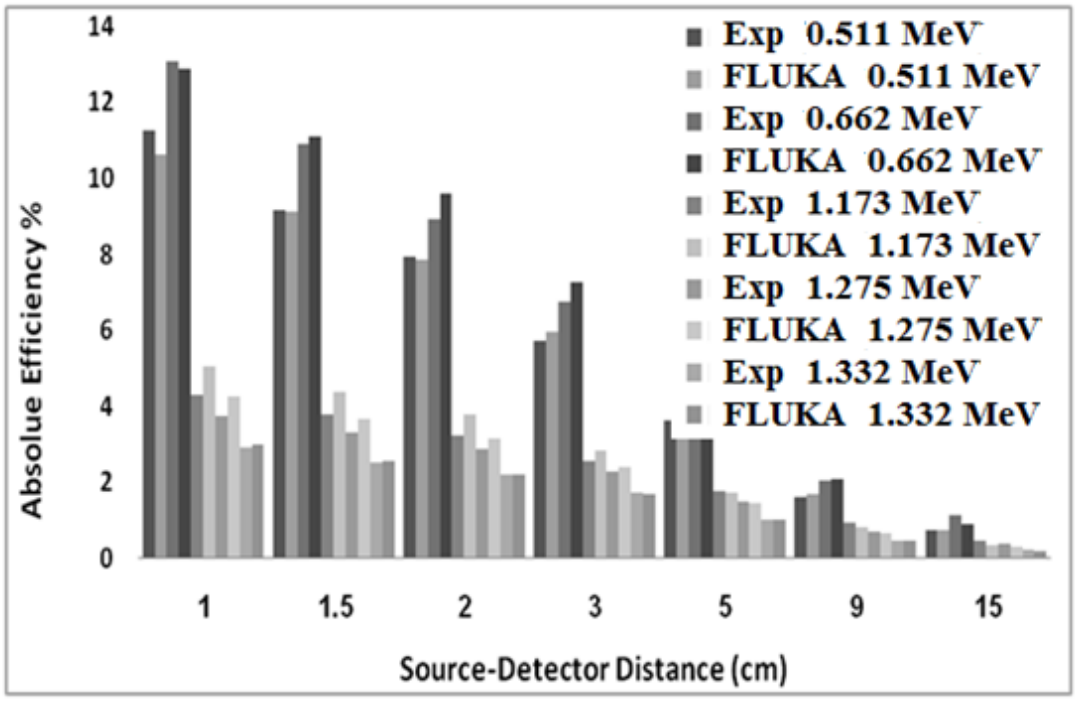

Figure 4.13. Absolute efficiency as a function of gamma-ray energy and source-detector distance experimentally and FLUKA simulation

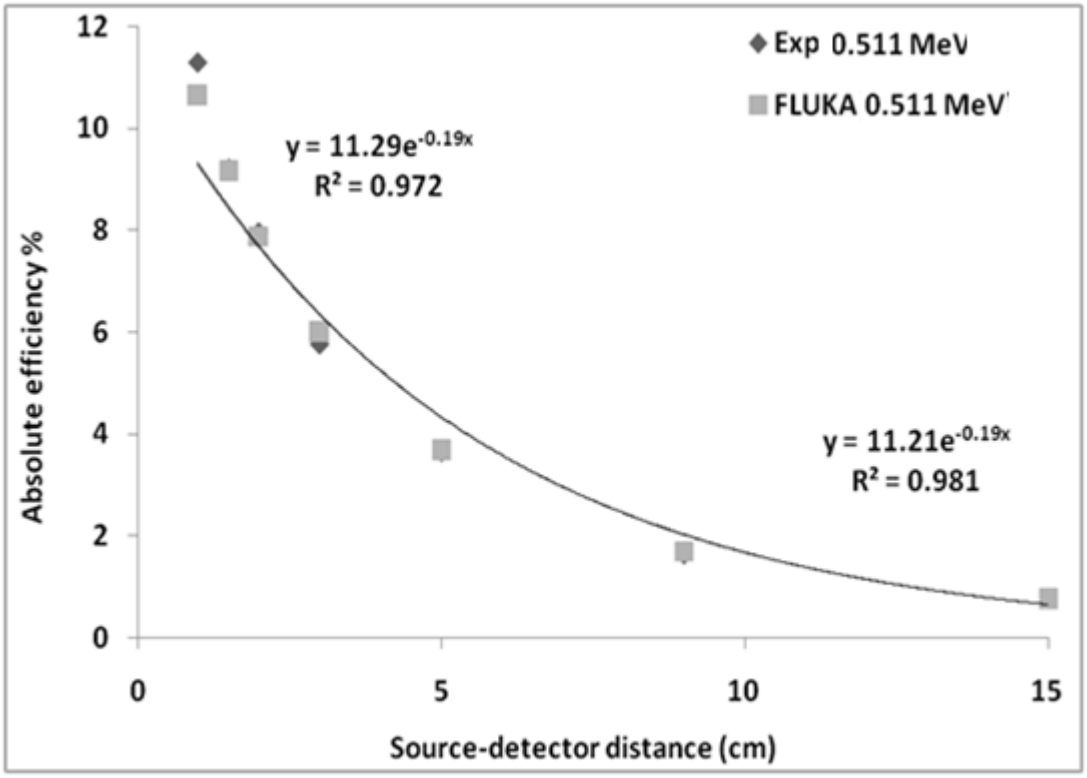

Figure 4.14. The comparison of the absolute efficiency as a function of the distance to the energy (0.511 MeV)

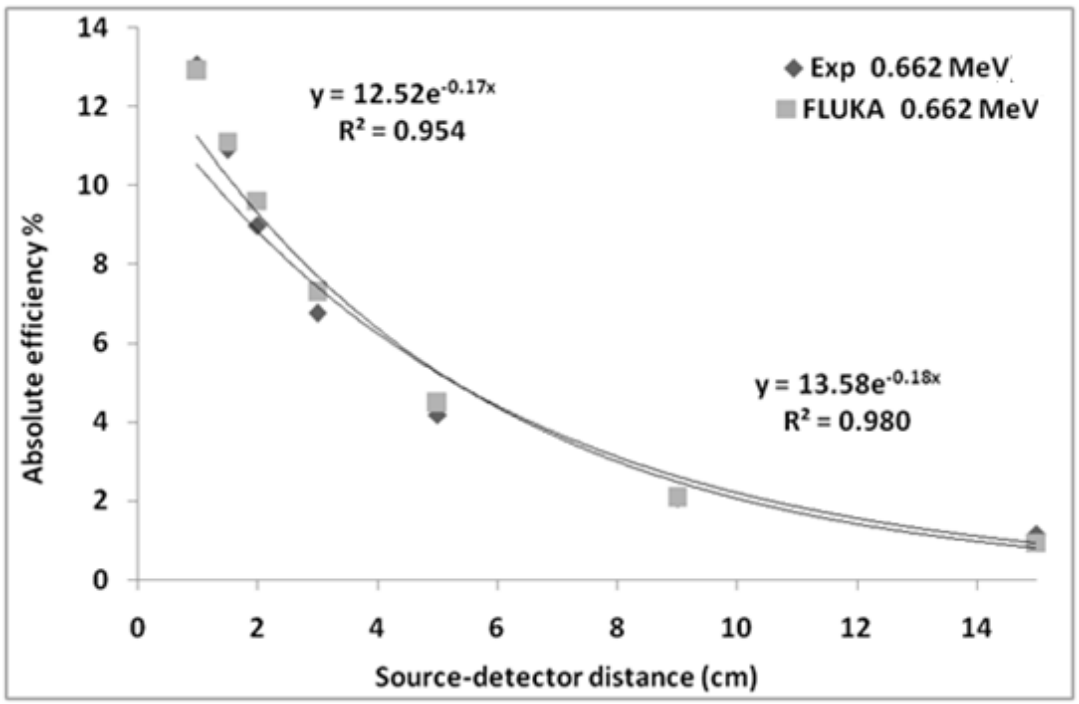

Figure 4.15. The comparison of the absolute efficiency as a function of the distance to the energy (0.662 MeV).

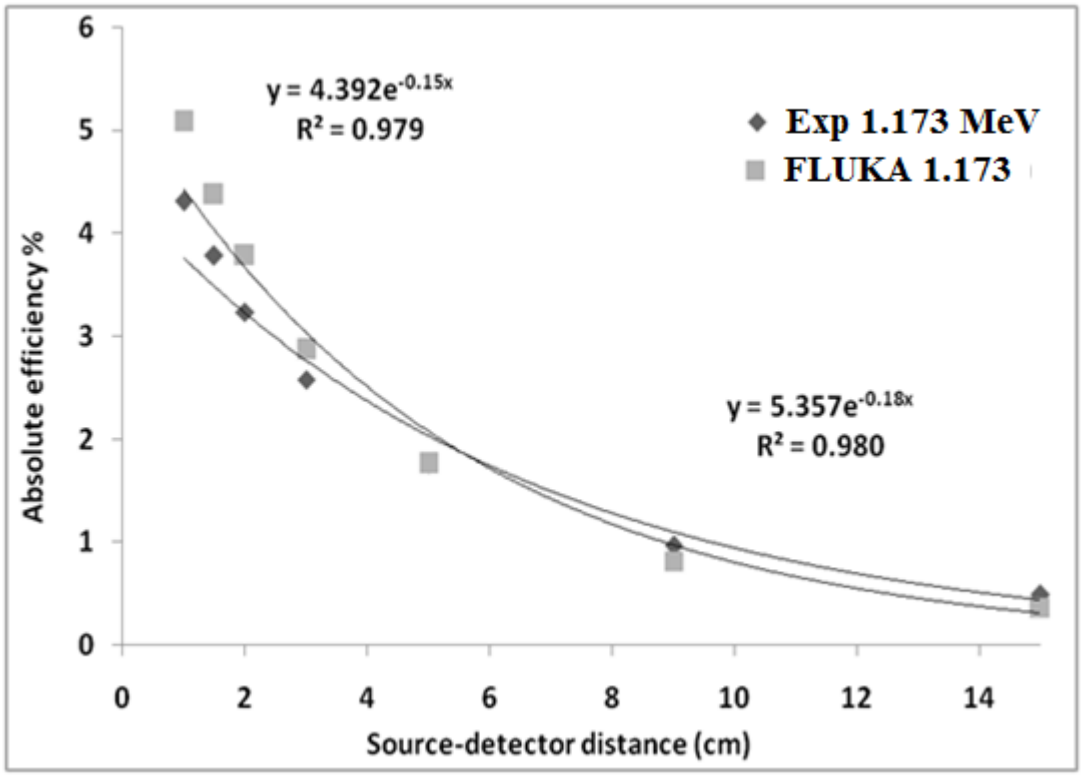

Figure 4.16. The comparison of the absolute efficiency as a function of the distance to the energy (1.173 MeV).

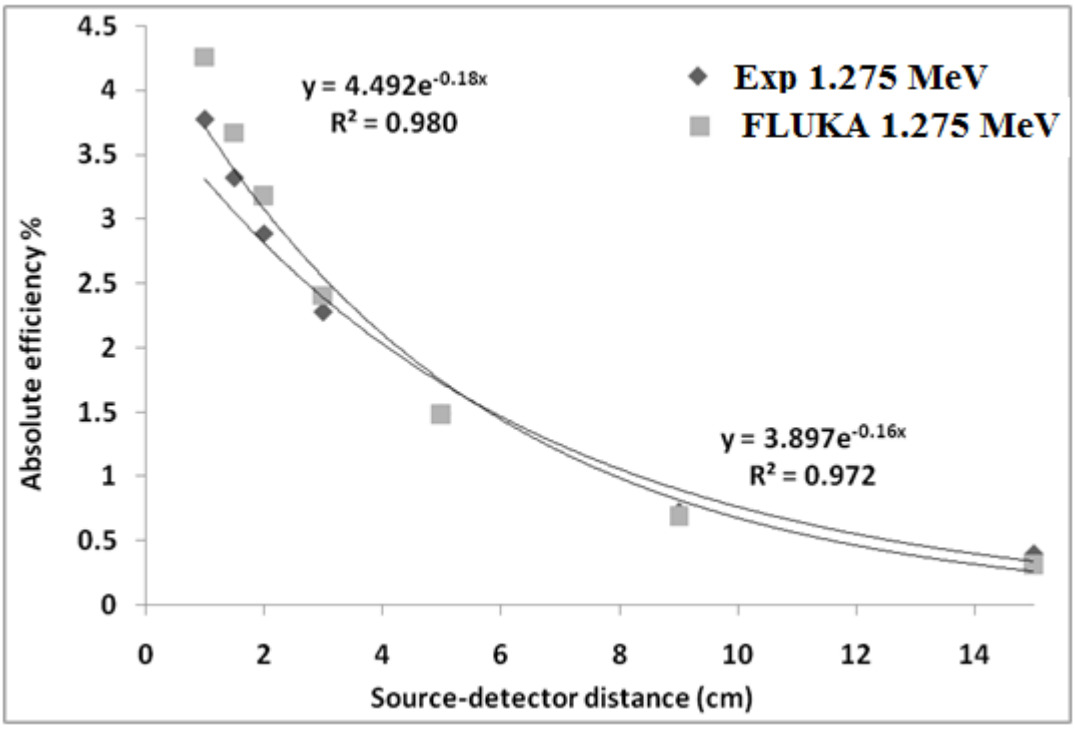

Figure 4.17. The comparison of the absolute efficiency as a function of the distance to the energy (1.275 MeV).

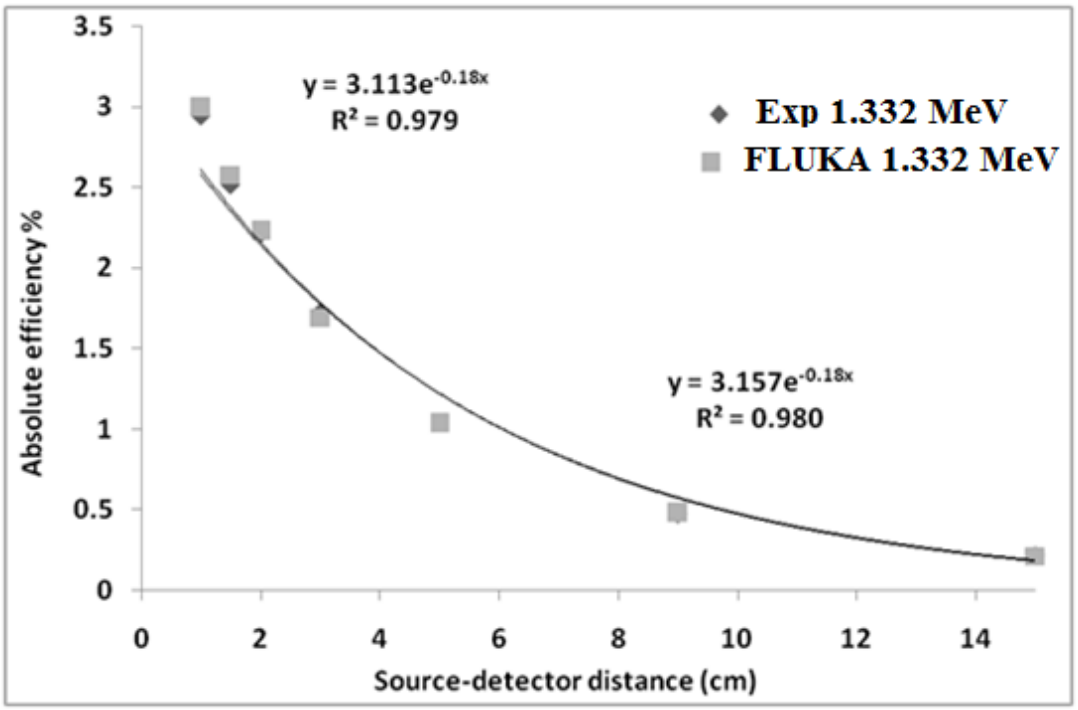

Figure 4.18. The comparison of the absolute efficiency as a function of the distance to the energy (1.332 MeV).

Figure 4.19 shows the energy resolution (R%) as a function of gamma-ray energy and source-detector distance experimentally. The result shows a great variety of analytical

function that is used to describe the energy resolution depending on the gamma-ray energy and source-detector distance. It can be seen that the energy resolution decreases with increasing the gamma-ray energy to the same source-detector distance, and it decreases with increasing the source-detector distance to the same gamma-ray energy.

Figure 4.20 shows the energy resolution (R%) as a function of gamma-ray energy and source-detector distance of FLUKA simulation after applying the response function. The result shows a great variety of analytical function that is used to describe the energy resolution depending on the gamma-ray energy and source-detector distance. It can be seen that the energy resolution decreases with increasing the gamma-ray energy to the same source-detector distance, and it decreases with increasing the source-detector distance to the same gamma-ray energy.

Figure 4.21 shows the energy resolution (R%) as a function of gamma-ray energy and source-detector distance experimentally and the comparison with FLUKA simulation (after applying the response function). The result shows a great variety of analytical function that is used to describe the energy resolution depending on the gamma-ray energy and source-detector distance. It can be seen that the energy resolution decreases with increasing the gamma-ray energy to the same source-detector distance, and it decreases with increasing the gamma-ray energy to the same source-detector distance for both procedures; experimentally and for simulation. The result shows a successfully agreement although it had done in different gamma-ray energy and source-detector distance.

Figure 4.22 shows the comparison of the energy resolution (R%) as a function of the source-detector distance (cm) to the gamma-ray energy (0.511 MeV) experimentally and FLUKA simulation. It can be seen that the energy resolution decreases with increasing the source-detector distance.

Figure 4.23 shows the comparison of the energy resolution (R %) as a function of the source-detector distance (cm) to the gamma-ray energy (0.662 MeV) experimentally and FLUKA simulation. It can be seen that the energy resolution decreases with increasing the source-detector distance.

Figure 4.24 shows the comparison of the energy resolution (R%) as a function of the source-detector distance (cm) to the gamma-ray energy (1.173 MeV) experimentally and FLUKA simulation. It can be seen that the energy resolution decreases with increasing the source-detector distance.

Figure 4.25 shows the comparison of the energy resolution (R%) as a function of the source-detector distance (cm) to the gamma-ray energy (1.275 MeV) experimentally and FLUKA simulation. It can be seen that the energy resolution decreases with increasing the source-detector distance.

Figure 4.26 shows the comparison of the energy resolution (R%) as a function of the source-detector distance (cm) to the gamma-ray energy (1.332 MeV) experimentally and FLUKA simulation. It can be seen that the energy resolution decreases with increasing the source-detector distance.

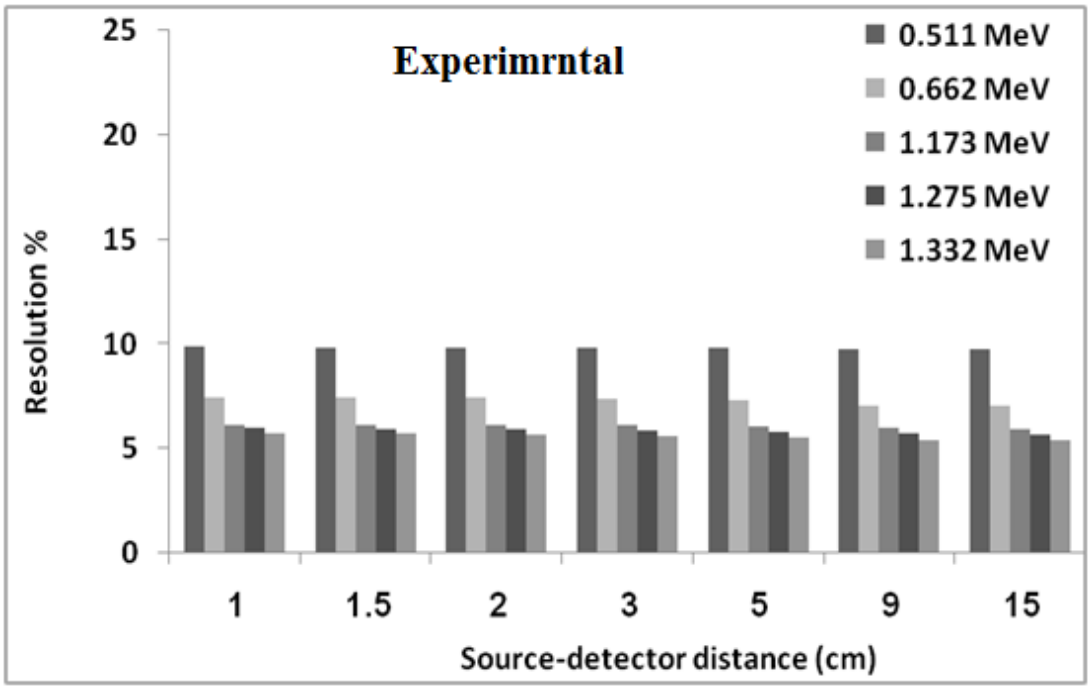

Figure 4.19. Experimentally energy resolution as a function of gamma-ray energy (MeV) and source-detector distance (cm).

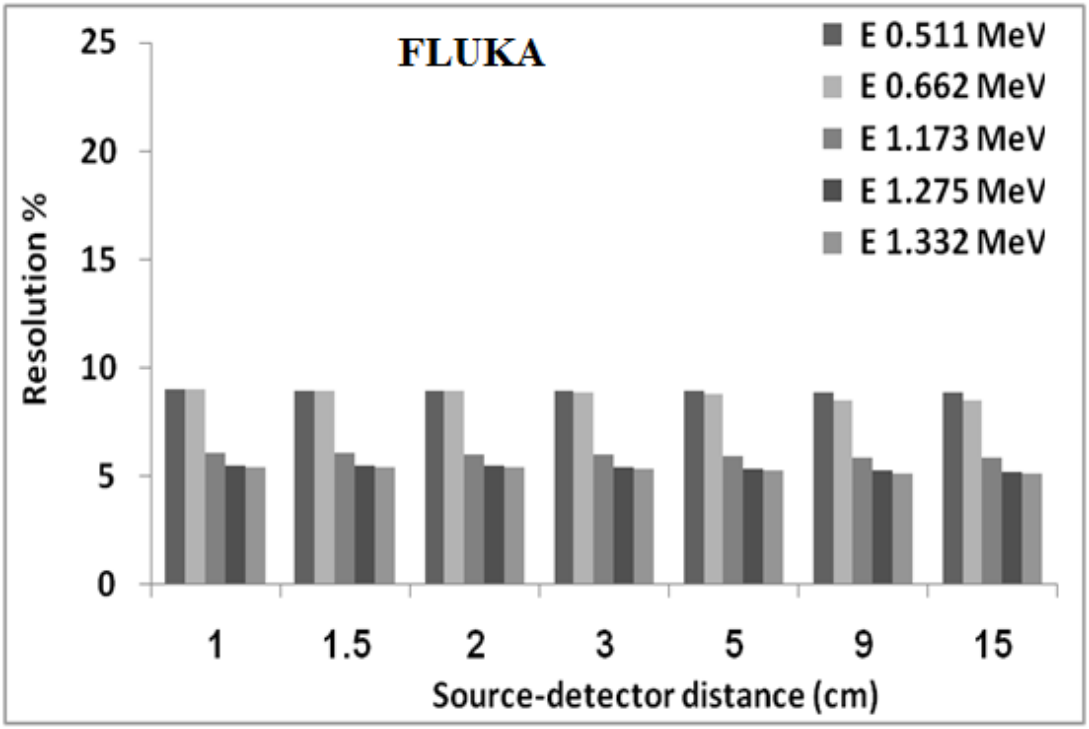

Figure 4.20. FLUKA energy resolution as a function of gamma-ray energy (MeV) and source-detector distance (cm)

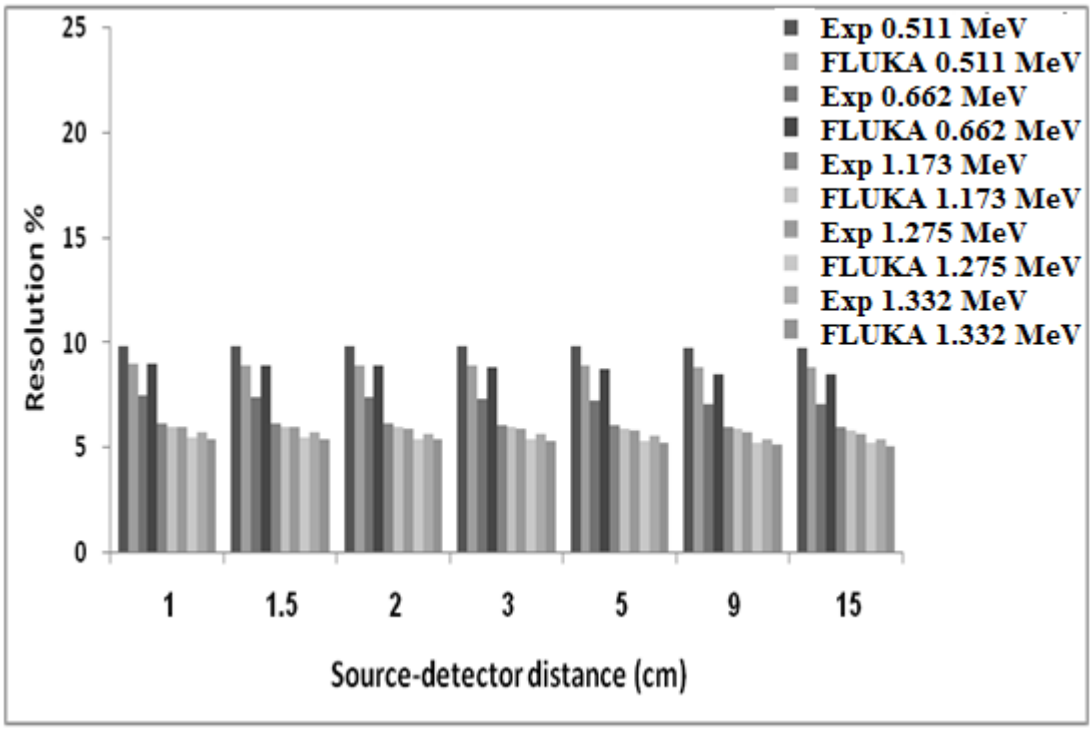

Figure 4.21. The energy resolution as a function of gamma-ray energy and source-detector distance experimentally and FLUKA simulation

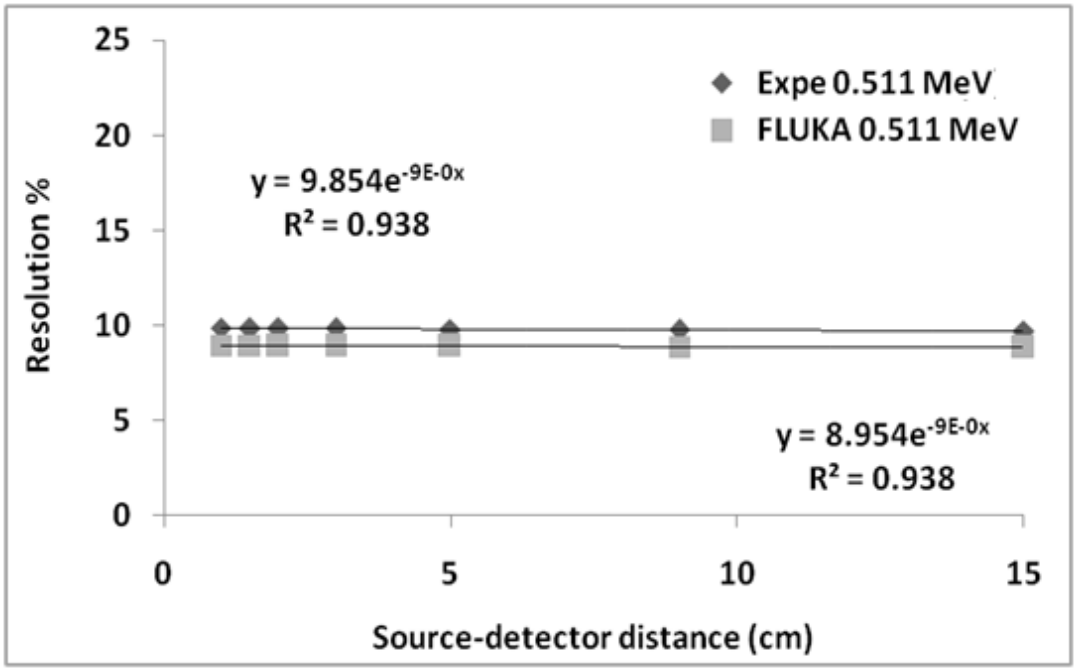

Figure 4.22. The comparison of the energy resolution as a function of the distance to the energy (0.511 MeV) experimentally and FLUKA simulation

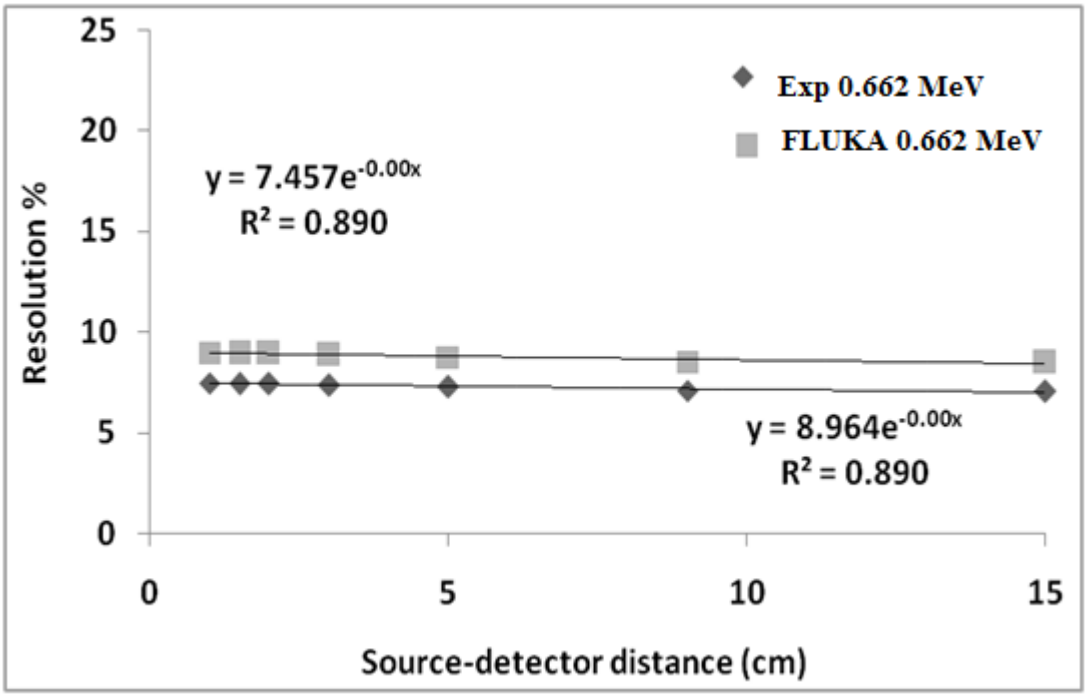

Figure 4.23. The comparison of the energy resolution as a function of the distance to the energy (0.662 MeV) experimentally and FLUKA simulation.

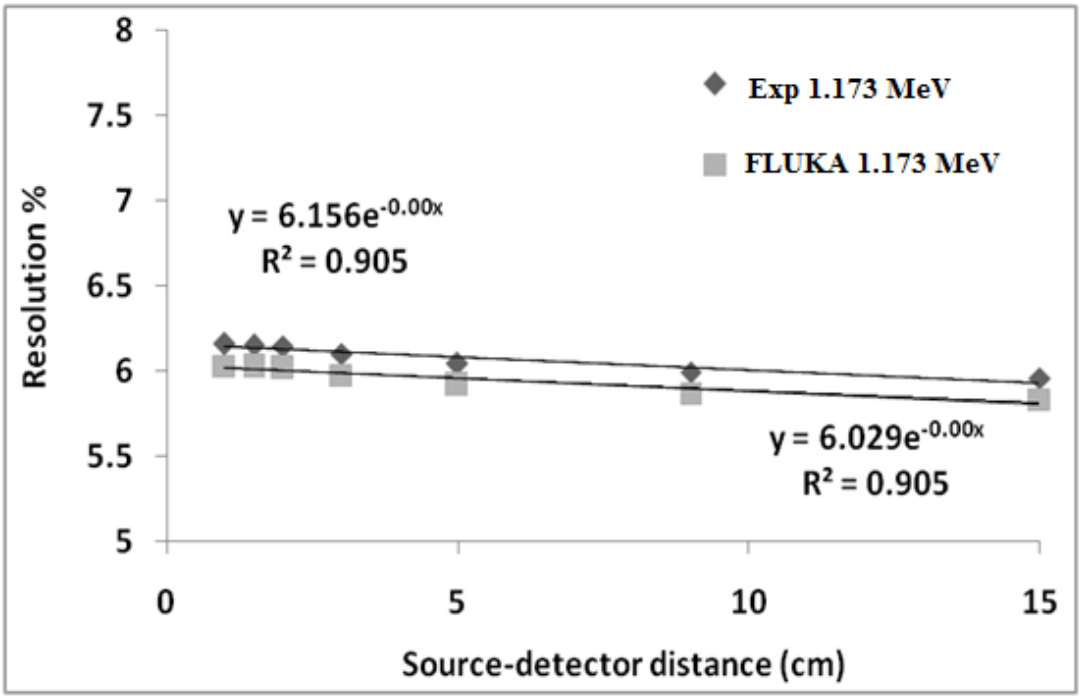

Figure 4.24. The comparison of the energy resolution as a function of the distance to the energy (1.173 MeV) experimentally and FLUKA simulation.

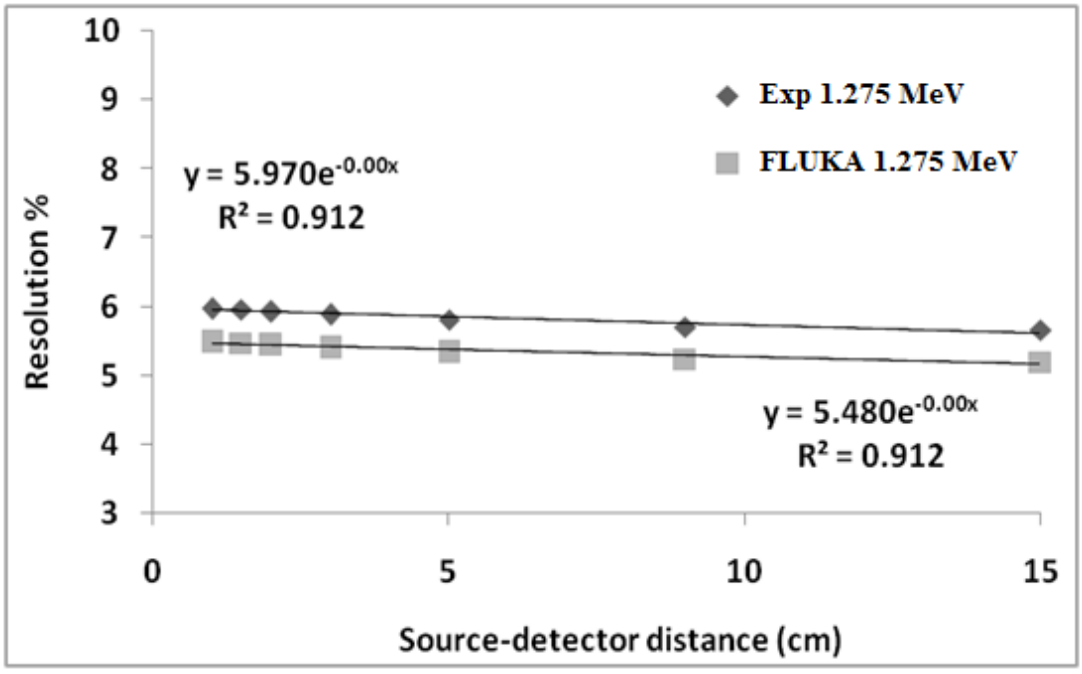

Figure 4.25. The comparison of the energy resolution as a function of the distance to the energy (1.275 MeV) experimentally and FLUKA simulation.

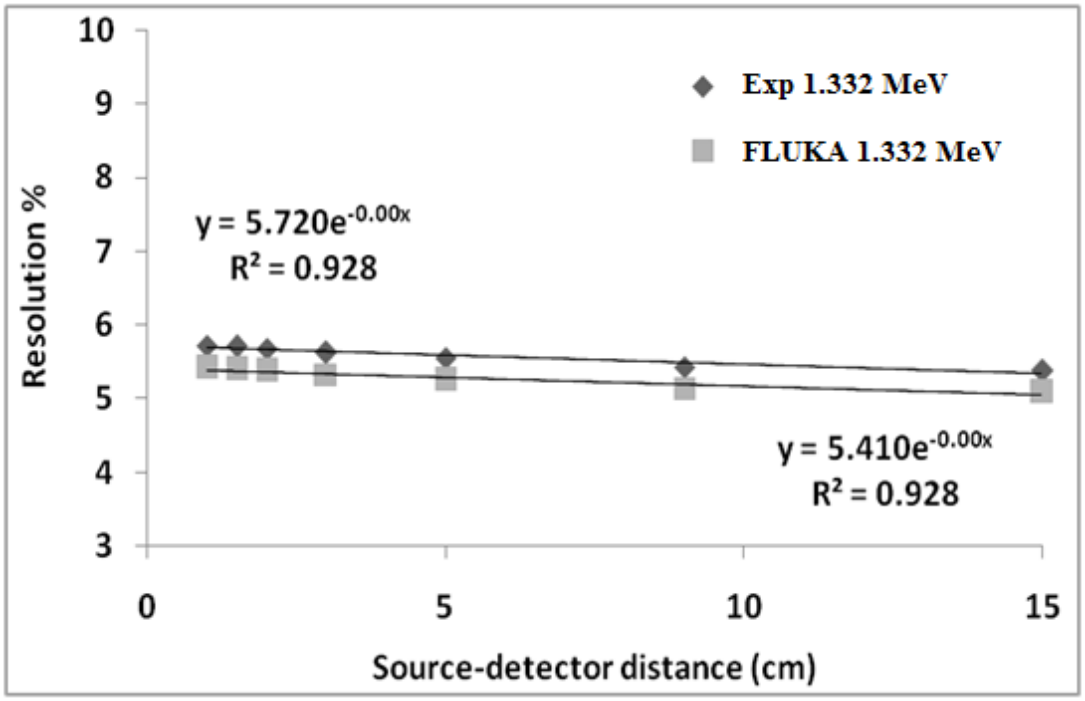

Figure 4.26. The comparison of the energy resolution as a function of the distance to the energy (1.332 MeV) experimentally and FLUKA simulation.

4.3. FWHM Results

Figure 4.27 shows FWHM as a function of gamma-ray energy and source-detector distance experimentally. The result shows a great variety of analytical function that is used to describe the FWHM depending on the gamma-ray energy and source-detector distance. It can be seen that FWMH increases with increasing the gamma-ray energy to the same source-detector distance, and it decreases with increasing source-detector distance to the same gamma-ray energy.

Figure 4.28 shows FWHM as a function of gamma-ray energy and source-detector distance of FLUKA simulation. The result shows a great variety of analytical function that is used to describe FWHM depending on the gamma-ray energy and source-detector distance. It can be seen that FWMH increases with increasing the gamma-ray energy to the same source-detector distance, and it decreases with increasing source-detector distance to the same gamma-ray energy.

Figure 4.29 shows FWHM as a function of gamma-ray energy and source-detector distance experimentally and comparison with FLUKA simulation. The result shows a great variety of analytical function that is used to describe FWHM depending on the gamma-ray energy and source-detector distance. It can be seen that FWMH increases

with increasing the gamma-ray energy to the same source-detector distance, and it decreases with increasing source-detector distance to the same gamma-ray energy for both procedures; experimentally and for FLUKA simulation. The result shows a successfully agreement of the simulation although the measurement had done in different gamma-ray energies and source-detector distances.

Figure 4.30 shows the comparison of FWHM as a function of the source-detector distance (cm) to the gamma-ray energy (0.511 MeV) experimentally and FLUKA simulation. It can be seen that FWHM decreases with increasing the source-detector distance.

Figure 4.31 shows the comparison of FWHM as a function of the source-detector distance (cm) to the gamma-ray energy (0.662 MeV) experimentally and FLUKA simulation. It can be seen that FWHM decreases with increasing the source-detector distance.

Figure 4.32 shows the comparison of FWHM as a function of the source-detector distance (cm) to the gamma-ray energy (1.173 MeV) experimentally and FLUKA simulation. It can be seen that FWHM decreases with increasing the source-detector distance.

Figure 4.33 shows the comparison of FWHM as a function of the source-detector distance (cm) to the gamma-ray energy (1.275 MeV) experimentally and FLUKA simulation. It can be seen that FWHM decreases with increasing the source-detector distance.

Figure 4.34 shows the comparison of FWHM as a function of the source-detector distance (cm) to the gamma-ray energy (1.332 MeV) experimentally and FLUKA simulation. It can be seen that FWHM decreases with increasing the source-detector distance.

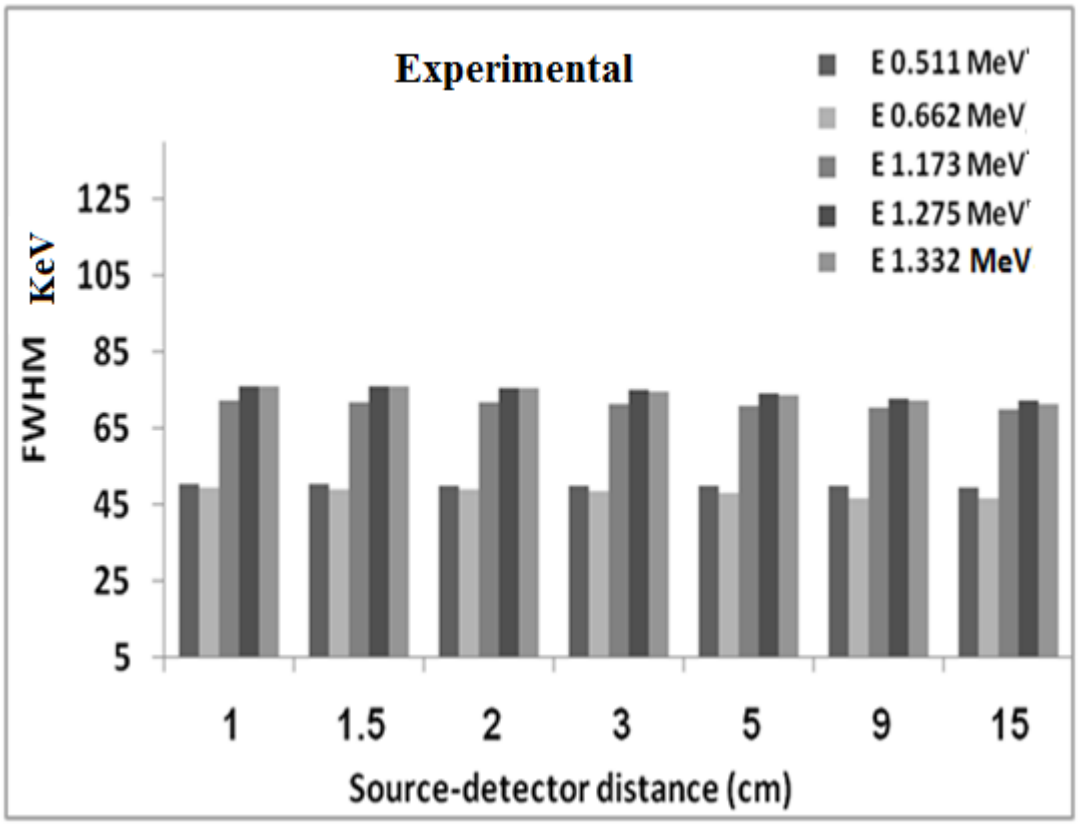

Figure 4.27. Experimentally FWHM as a function of gamma-ray energy (MeV) and source-detector distance (cm).

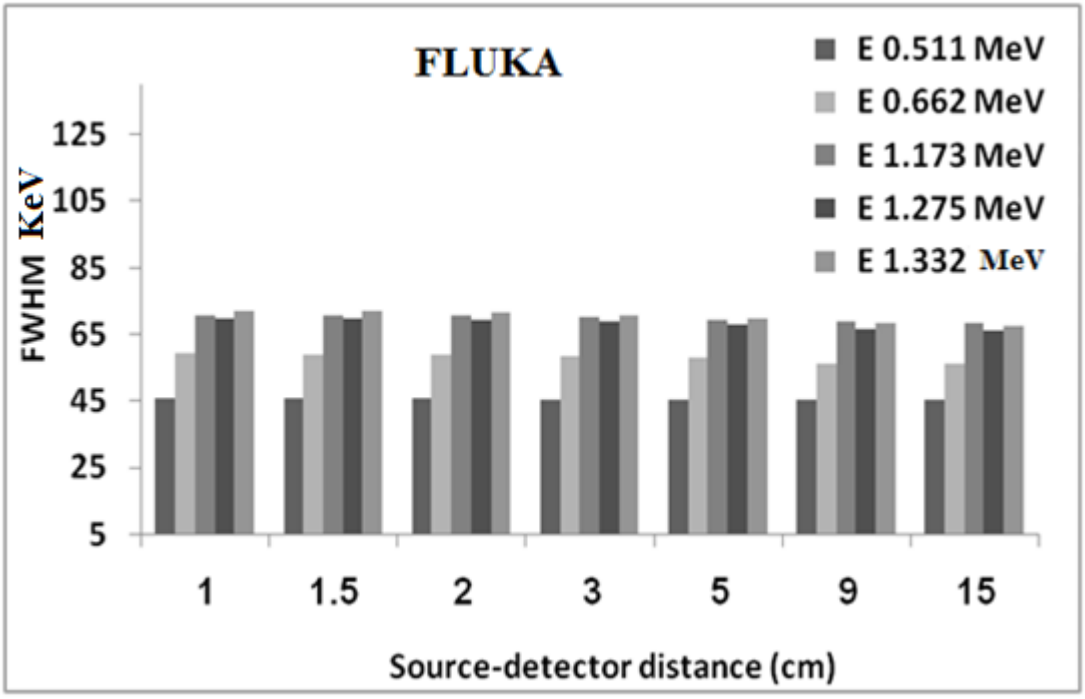

Figure 4.28. FLUKA FWHM as a function of gamma-ray energy (MeV) and source-detector distance (cm)

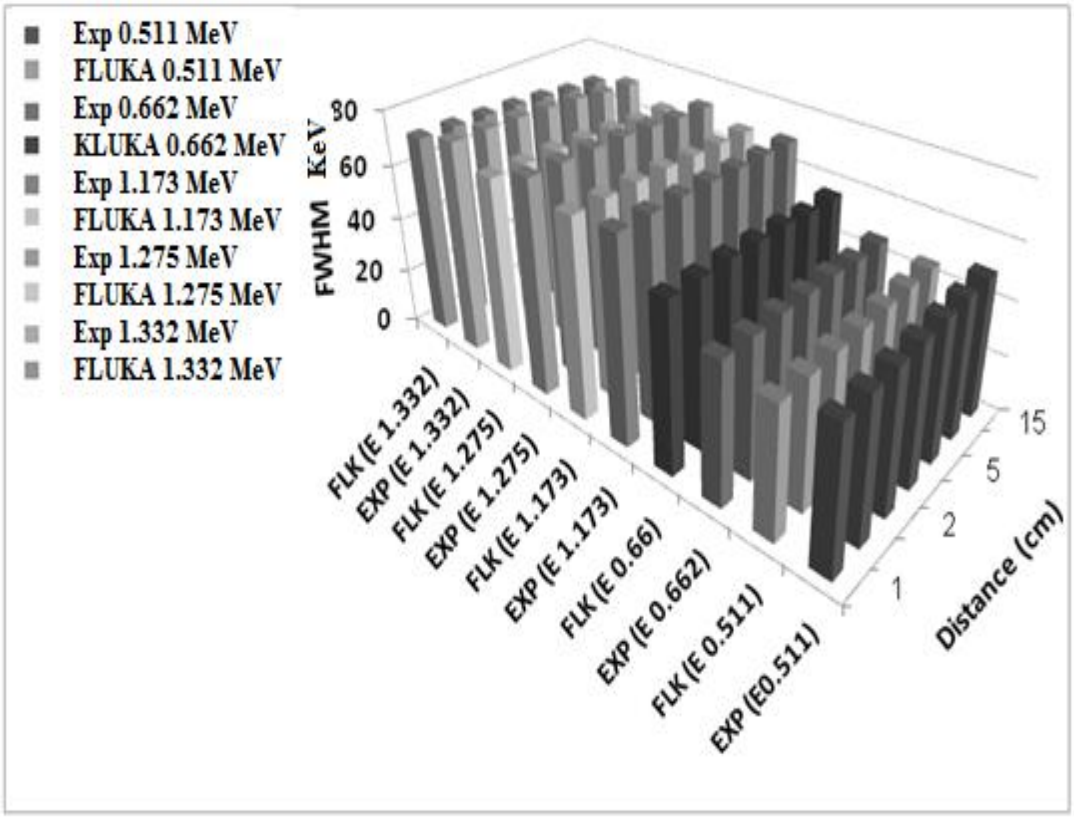

Figure 4.29. FWHM as a function of gamma-ray energy and source-detector distance experimentally and FLUKA simulation

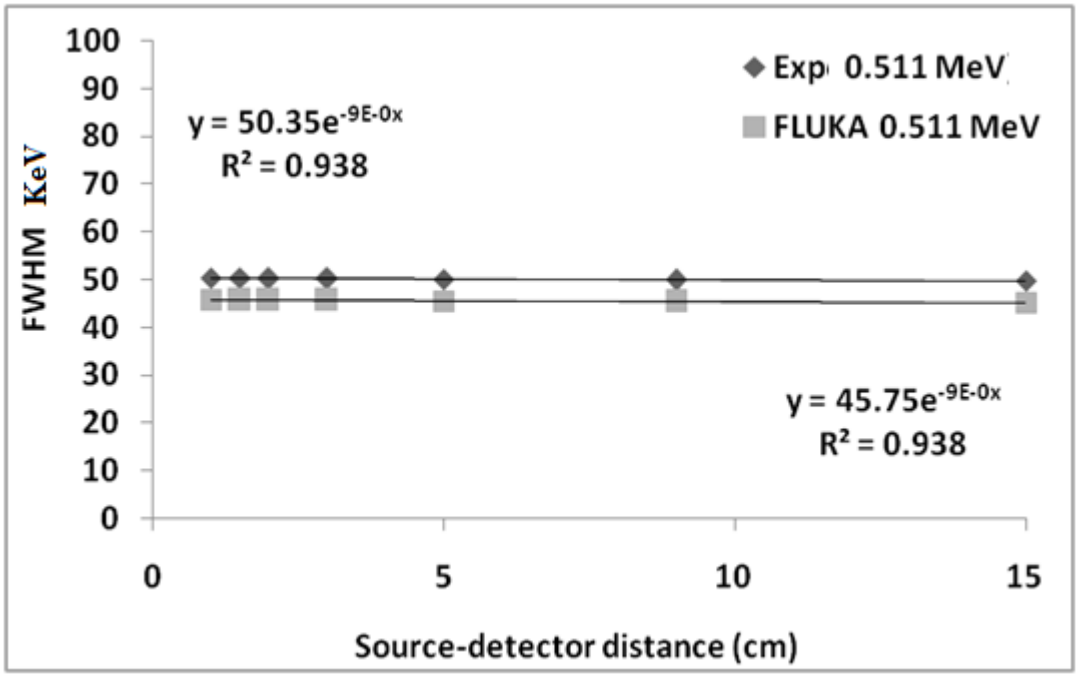

Figure 4.30. The comparison of FWHM as a function of the distance to the energy (0.511 MeV)

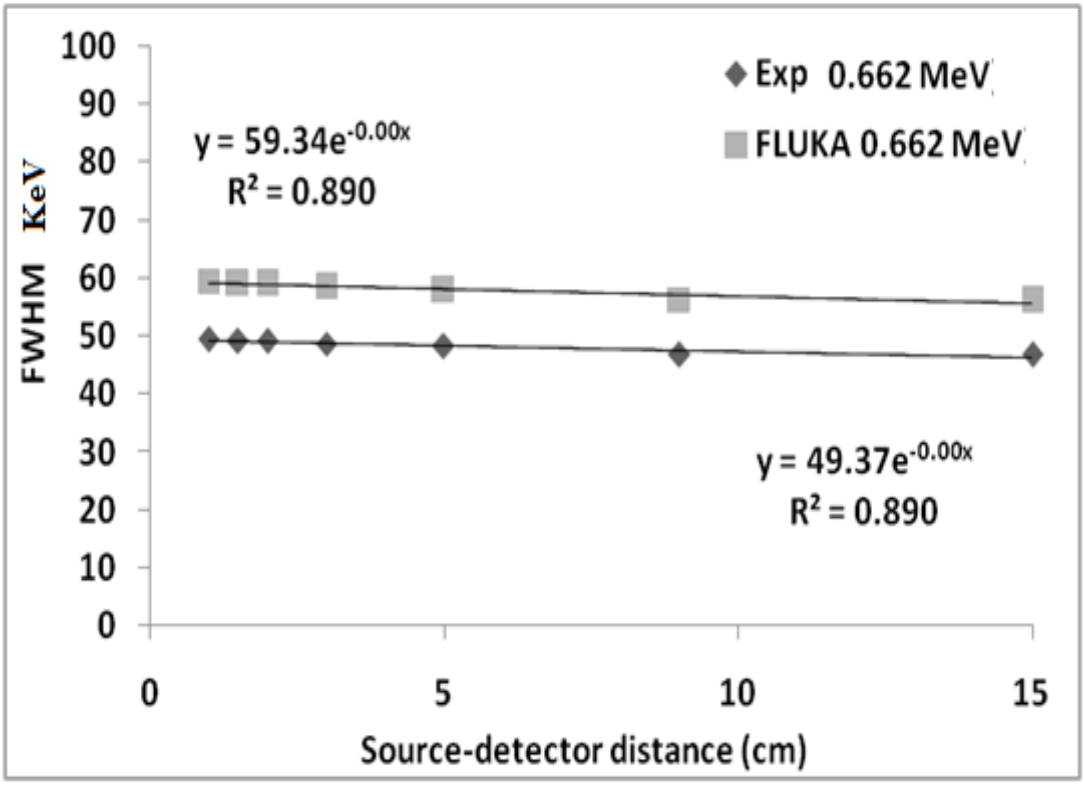

Figure 4.31. The comparison of FWHM as a function of the distance to the energy (0.662 MeV)

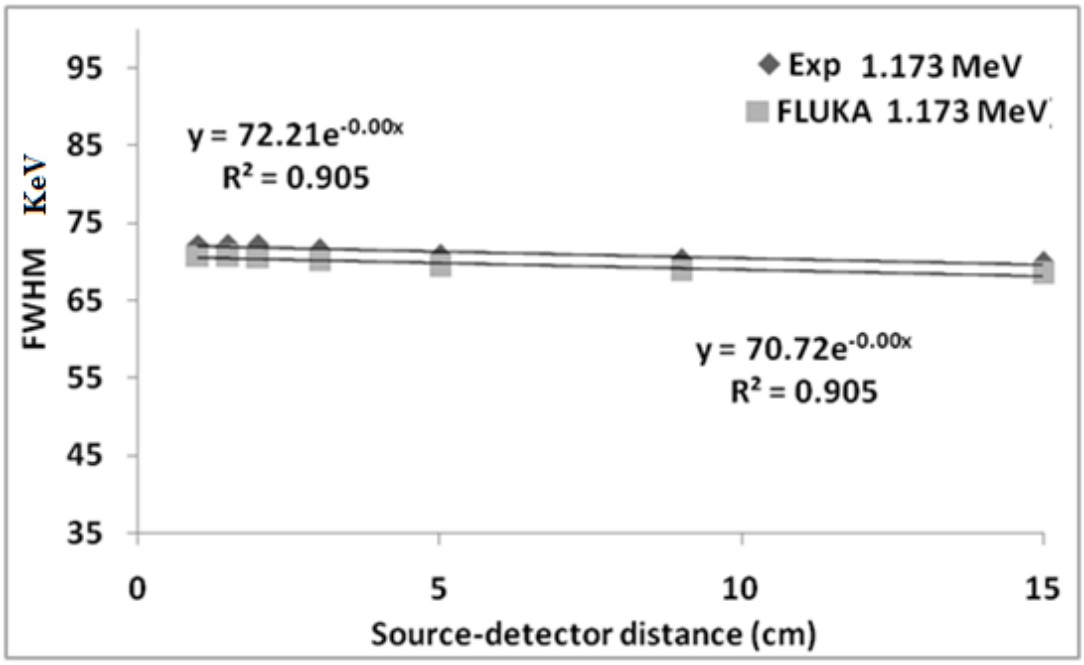

Figure 4.32. The comparison of FWHM as a function of the distance to the energy (1.173 MeV).

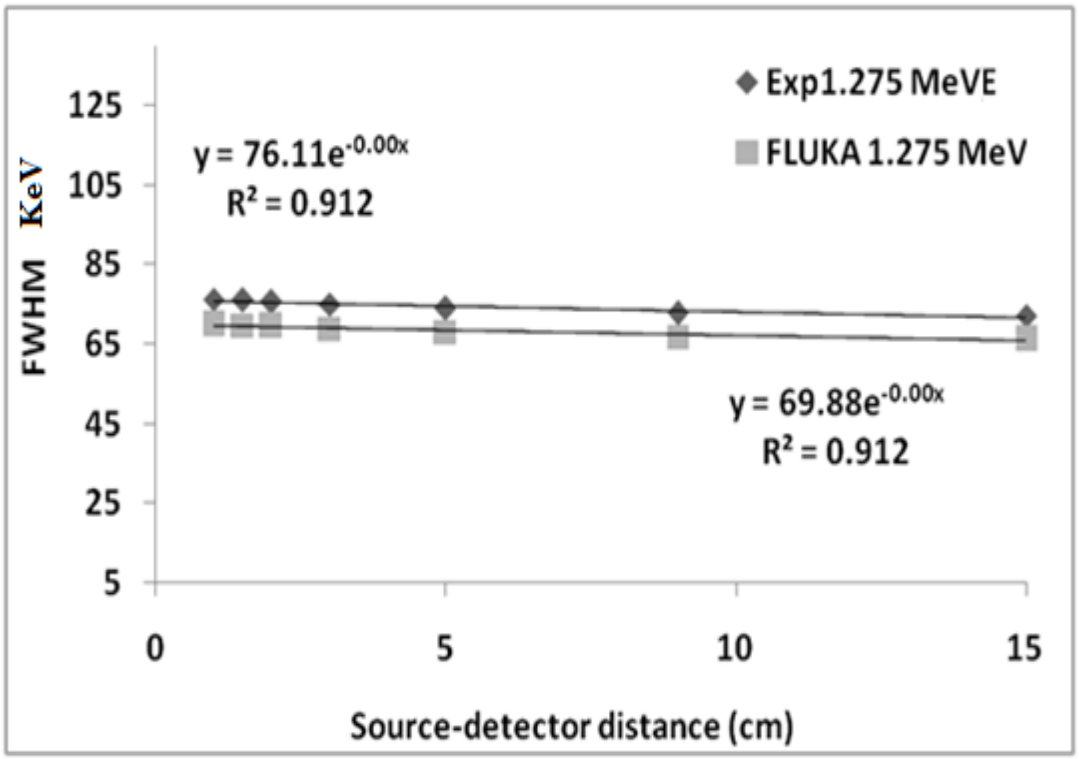

Figure 4.33. The comparison of FWHM as a function of the distance to the energy (1.275 MeV)

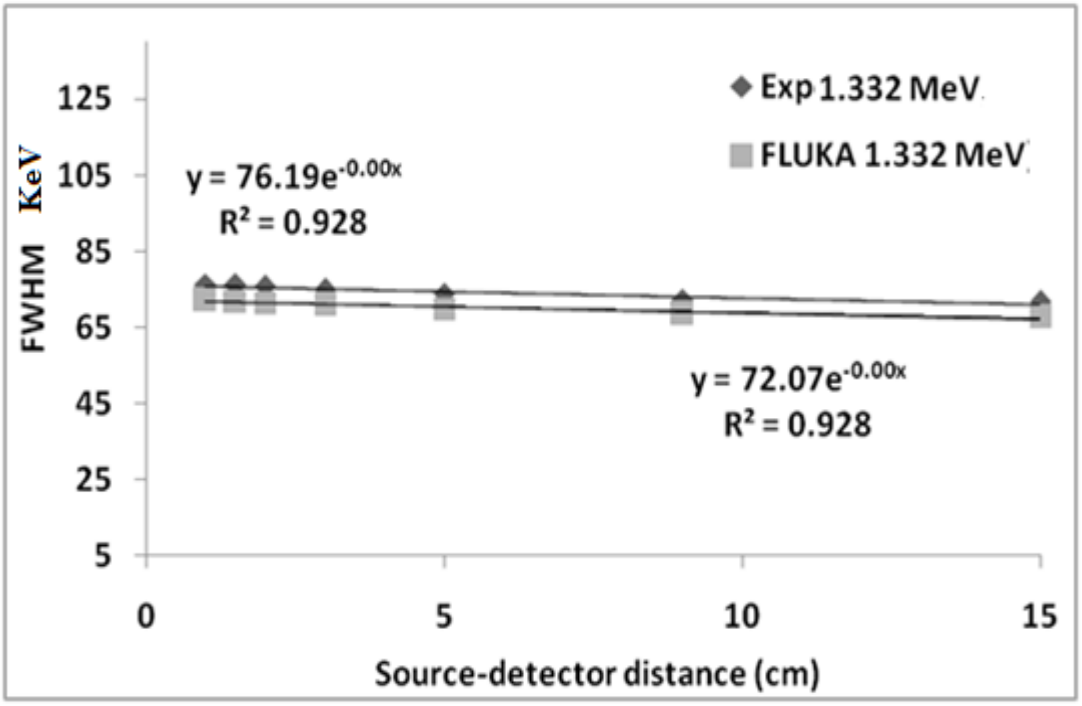

Figure 4.34. The comparison of FWHM as a function of the distance to the energy (1.332 MeV).

Figure 4.35 shows the buildup factor as a function of gamma-ray energy and source detector-distance experimentally. The result has been calculated with two conditions (with and without using the Lead collimators). It can be seen that the

value of buildup factor decreases with increasing the gamma-ray energy to the same source-detector distance, and it decreases with increasing the source-detector distance to the same gamma-ray energy.

Figure 4.36 shows the buildup factor as a function of gamma-ray energy and source detector-distance of FLUKA simulation. The result has been calculated with two conditions (with and without using the Lead collimators). It can be seen that the value of buildup factor decreases with increasing the gamma-ray energy to the same source-detector distance, and it decreases with increasing the source-detector distance to the same gamma-ray energy.

Figure 4.37 shows the buildup factor as a function of gamma-ray energy and source detector-distance experimentally and comparison with FLUKA simulation to the same the geometry conditions (with and without using the Lead collimators). It can be seen that the value of buildup factor decreases with increasing the gamma-ray energy to the same source-detector distance, and it decreases with increasing the source-detector distance to the same gamma-ray energy for both procedures; experimentally and for FLUKA simulation. The result shows a successfully agreement although the measurement had done in different gamma-ray energies and source-detector distances.

Figure 4.38 shows the comparison of the energy buildup factor as a function of the source-detector distance (cm) to the gamma-ray energy (0.511 MeV) experimentally and FLUKA simulation. It can be seen that the energy buildup factor decreases with increasing the source-detector distance.

Figure 4.39 shows the comparison of the energy buildup factor as a function of the source-detector distance (cm) to the gamma-ray energy (0.662 MeV) experimentally and FLUKA simulation. It can be seen that the energy buildup factor decreases with increasing the source-detector distance.

Figure 4.40 shows the comparison of the energy buildup factor as a function of the source-detector distance (cm) to the gamma-ray energy (1.173 MeV) experimentally and FLUKA simulation. It can be seen that the energy buildup factor decreases with increasing the source-detector distance.

Figure 4.41 shows the comparison of the energy buildup factor as a function of the source-detector distance (cm) to the gamma-ray energy (1.275 MeV) experimentally and FLUKA simulation. It can be seen that the energy buildup factor decreases with increasing the source-detector distance.

Figure 4.42 shows the comparison of the energy buildup factor as a function of the source-detector distance (cm) to the gamma-ray energy (1.332 MeV) experimentally and FLUKA simulation. It can be seen that the energy buildup factor decreases with increasing the source-detector distance.

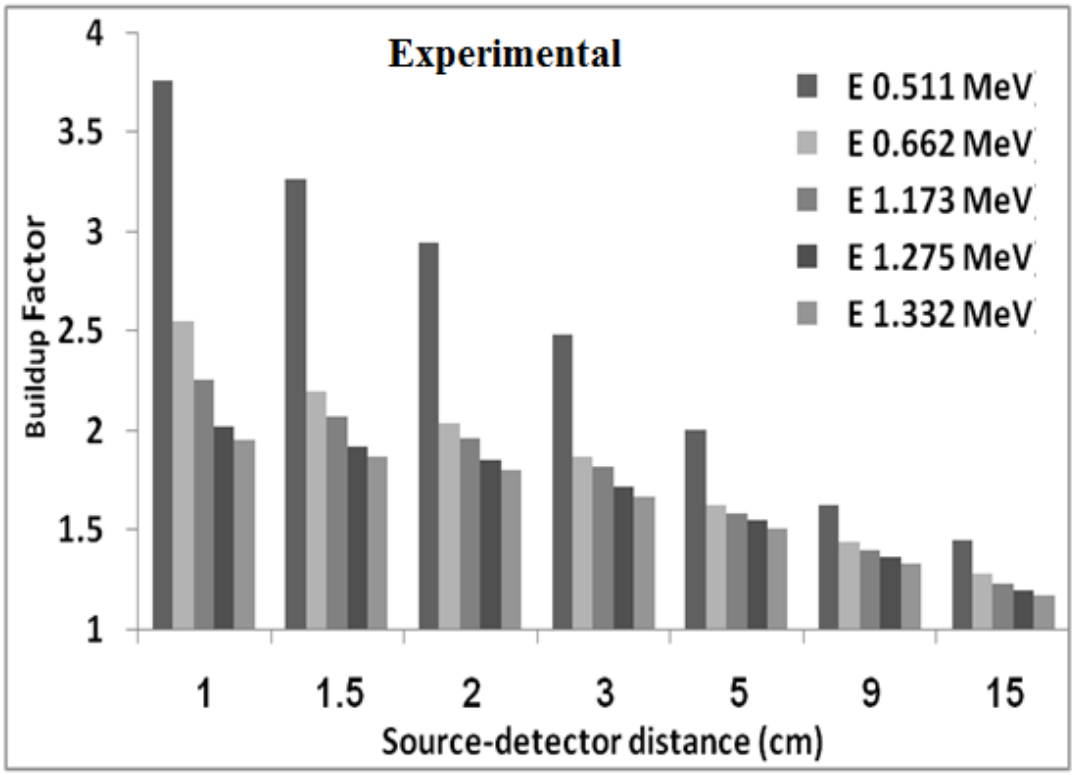

Figure 4.35. Experimentally buildup factor as a function of gamma-ray energy (MeV) and source-detector distance (cm).

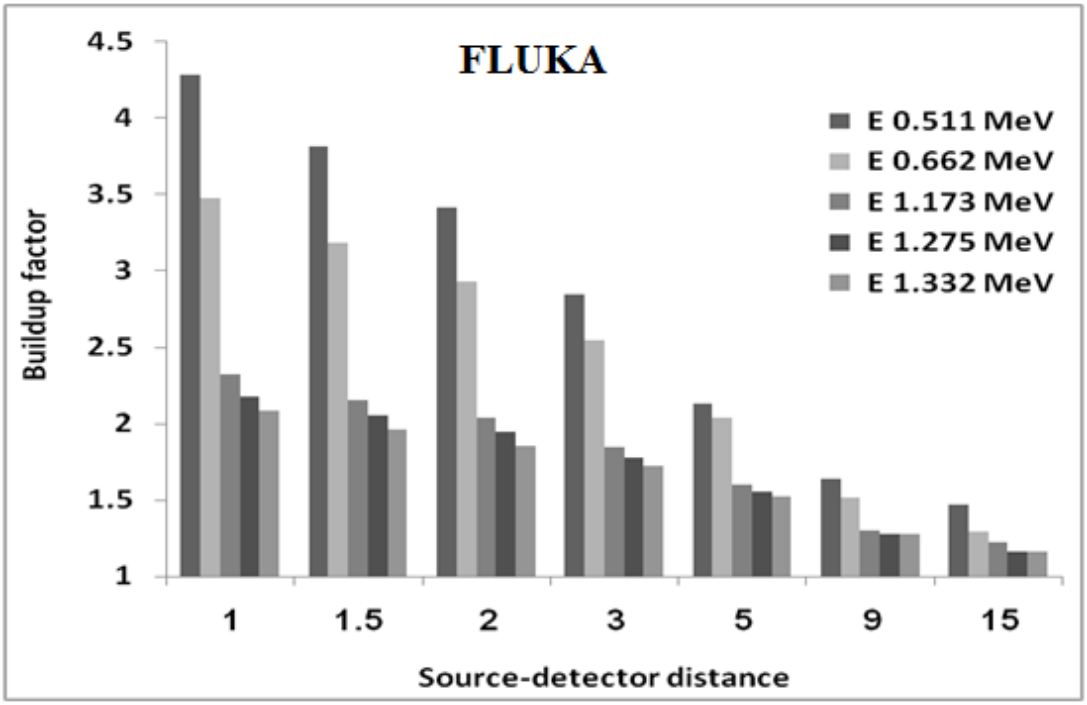

Figure 4.36. FLUKA buildup factor as a function of gamma-ray energy (MeV) and source-detector distance (cm).

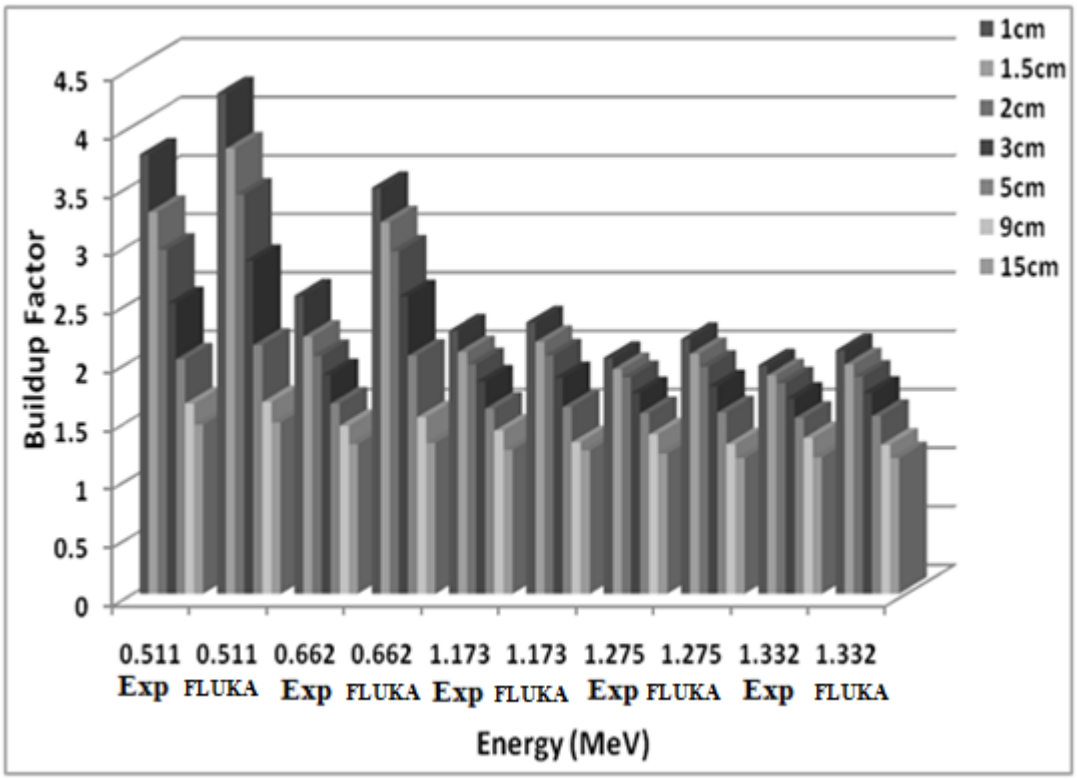

Figure 4.37. The buildup factor as a function of gamma-ray and source-detector distance experimentally and FLUKA simulation.

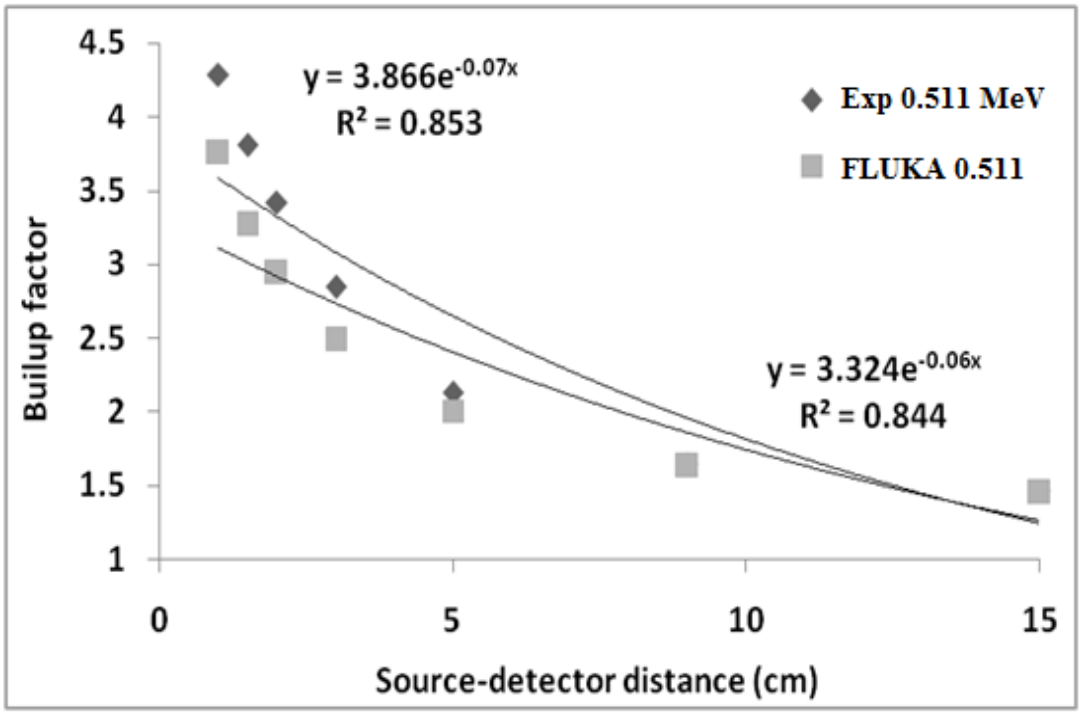

Figure 4.38. The comparison of the buildup factor as a function of the distance to the energy (0.511 MeV) experimentally and FLUKA simulation.

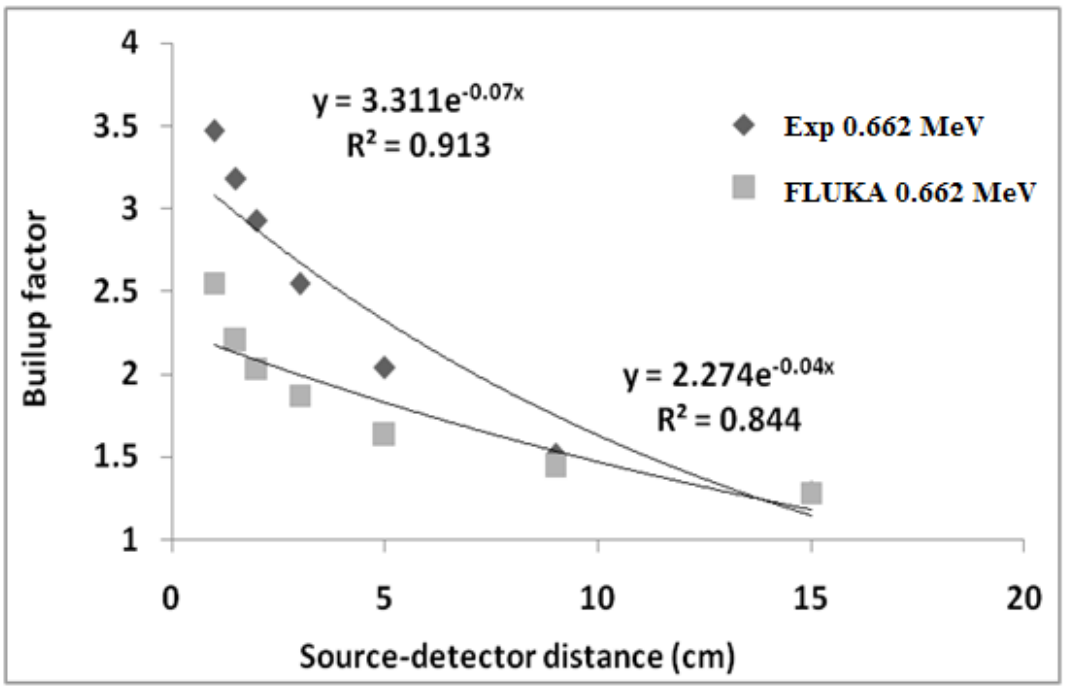

Figure 4.39. The comparison of the buildup factor as a function of the distance to the energy (0.662 MeV) experimentally and FLUKA simulation

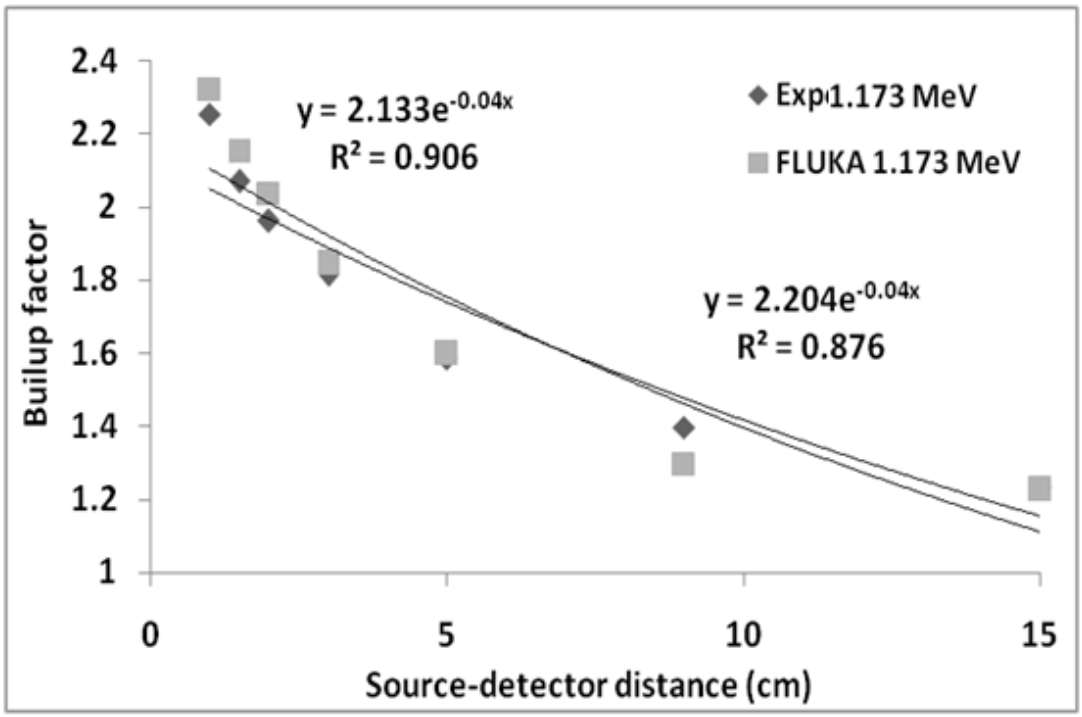

Figure 4.40. The comparison of the buildup factor as a function of the distance to the energy (1.173 MeV) experimentally and FLUKA simulation.

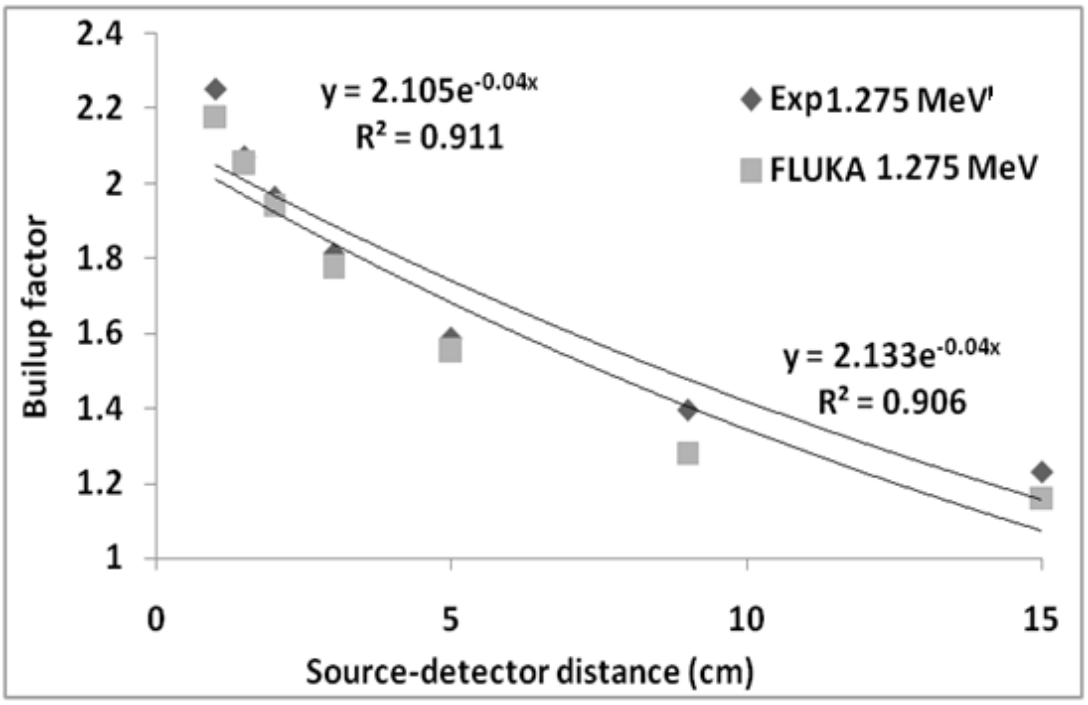

Figure 4.41. The comparison of the buildup factor as a function of the distance to the energy (1.275 MeV) experimentally and FLUKA simulation

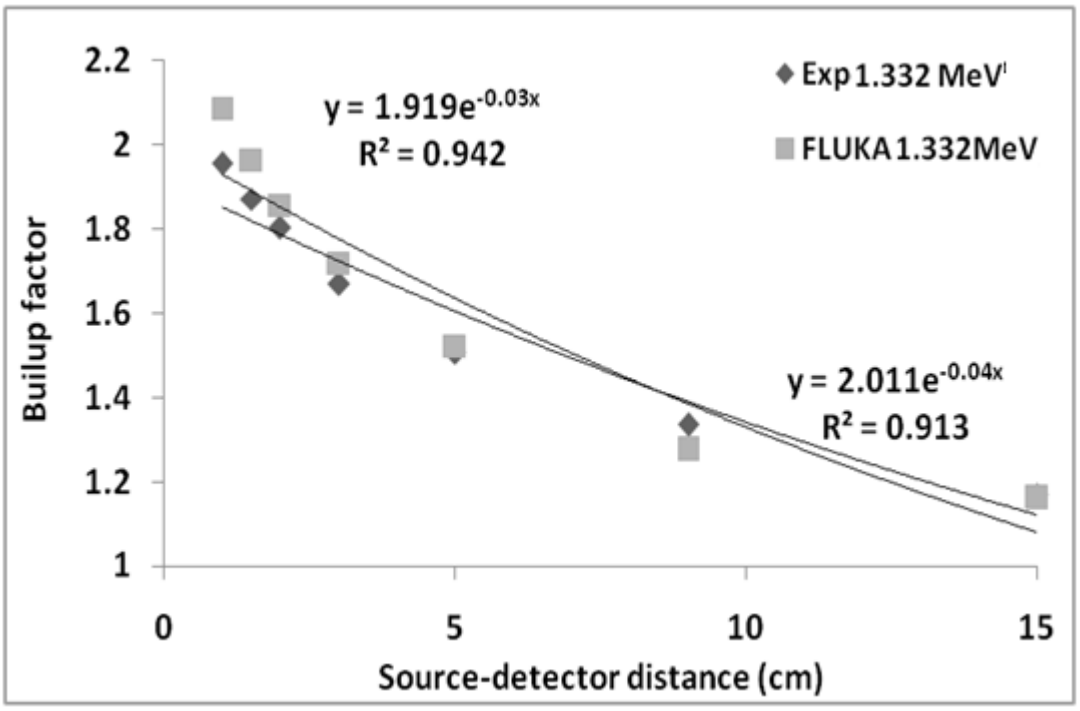

Figure 4.42. The comparison of the buildup factor as a function of the distance to the energy (1.332 MeV) experimentally and FLUKA simulation

4.4. Gamma-ray map density distribution

Figure 4.43 shows FLUKA map density distribution for ^{137}Cs which emit 0.662 MeV gamma-ray, the image of the map has been created using 10^6 number of gamma-ray. The activity corresponded to an acquisition lasting 2000s. The simulation beam of gamma-ray energy has been based on a flying point in space, no surrounding material against beam distribution. It can be seen that when no scattering (ideal situation) the circle of gamma-rays distribution concentrations is in normal shape.

Figure 4.44 shows up view of FLUKA map density distribution for ^{137}Cs which emit 0.662 MeV gamma-ray, the image of the map has been created using ^{10}6 number of gamma-ray and the activity corresponded to an acquisition lasting 2000s. The simulation beam of gamma-ray energy has been based inside geometry surrounded by lead shielding, the path of a collimated gamma-ray suffered from scattering after interaction with shielding. From this result, it can be seen that, when gamma-ray scattered (normal scattering phenomena) the circle of gamma-rays distribution concentrations have been changed as a result of the interaction. From this point, it can get an idea about the buildup factor effect.

Figure 4.45 shows up view of FLUKA map density distribution for ^{137}Cs which emit 0.662 MeV gamma-ray, the image of the map has been created using ^{10}6 number of gamma-ray and the activity corresponded to an acquisition lasting 2000s. The simulation of the map density has been based inside geometry surrounded by lead shielding, the path of the collimated gamma-ray (using lead Collimator) suffered from scattering after interaction with shielding. From this results, it can be seen that; when gamma-ray scattered (normal scattering phenomena) the circle of gamma-rays distribution concentrations have been changed as a result of the interaction. From this point, it can get an idea about buildup factor effect.

Figure 4.46 shows back view of FLUKA map density distribution for ^{137}Cs which emit 0.662 MeV gamma-ray, the image of the map has been created using ^{10}6 number of gamma-ray and the activity corresponded to an acquisition lasting 2000s. The simulation of map density has been based inside geometry surrounded be lead shielding, the path of gamma-ray suffered from scattering after interaction with up and side lead shielding (No down shielding). From this result, it can be seen that when gamma-ray scattered (normal scattering phenomena) the circle of gamma-rays distribution concentrations have been changed as a results of scattering. From this point, it can get an idea about the buildup factor effect.

Figure 4.47 shows side view FLUKA map density distribution for ^{137}Cs which emit 0.662 MeV gamma-ray, the image of the map has been created using ^{10}6 number of gamma-ray and the activity corresponded to an acquisition lasting 2000s. The simulation of map density has been based inside geometry surrounded by lead shielding, the path of gamma-rays suffered from scattering after interaction with up and side lead shielding (No down shielding). From this result, it can be seen that; when gamma-rays scattered (normal scattering phenomena) the circle of gamma-rays distribution concentrations have been changed as a result of scattering. From this point, it can get an idea about the buildup factor effect.

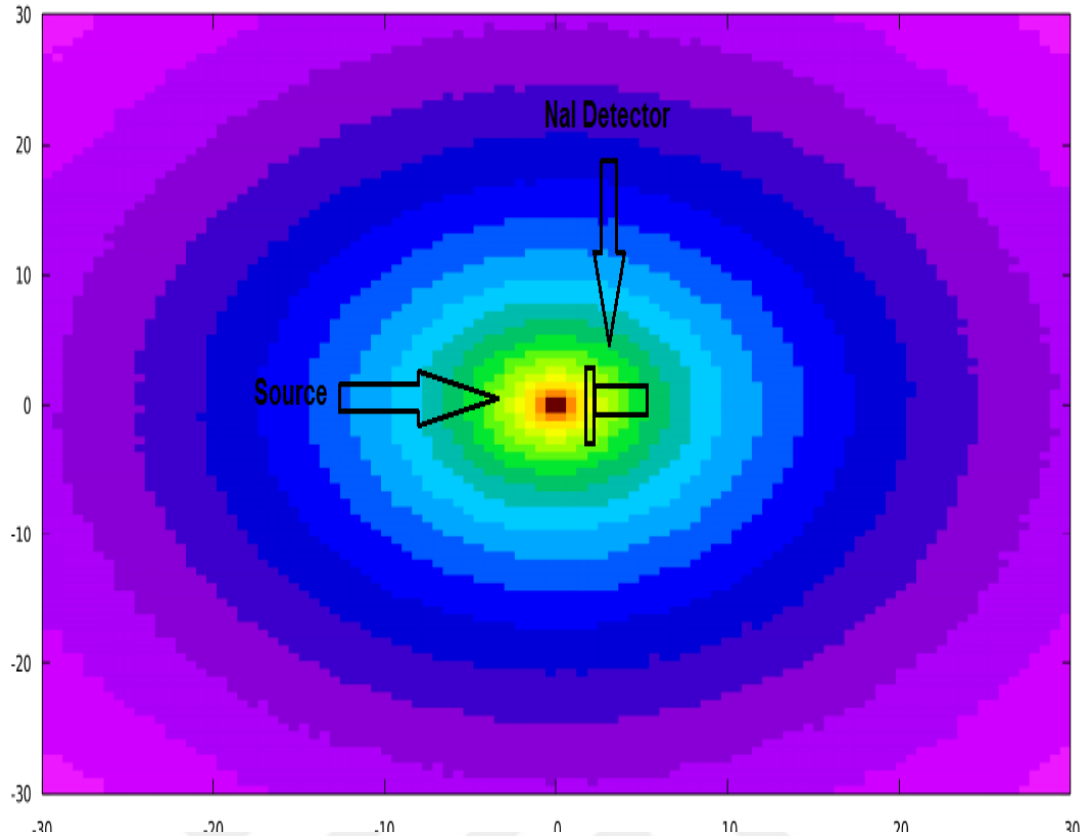

Figure 4.43. FLUKA ideal situation of gamma-rays map density distribution

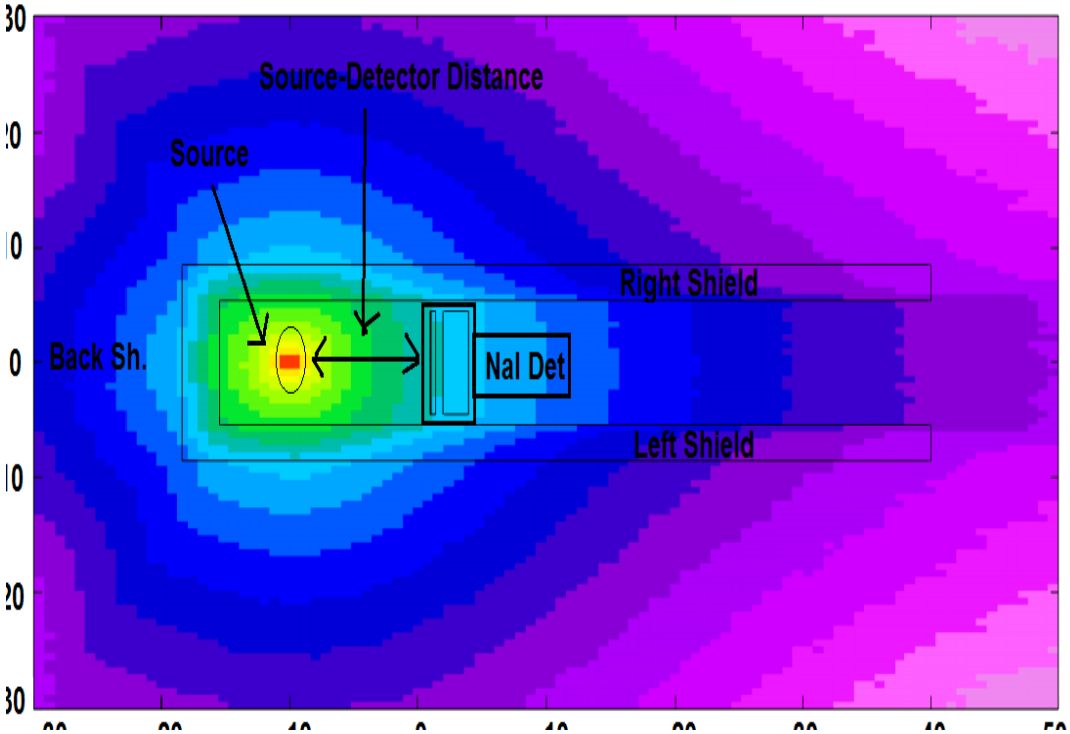

Figure 4.44. FLUKA up view of gamma-rays map density distribution (No Lead collimator)

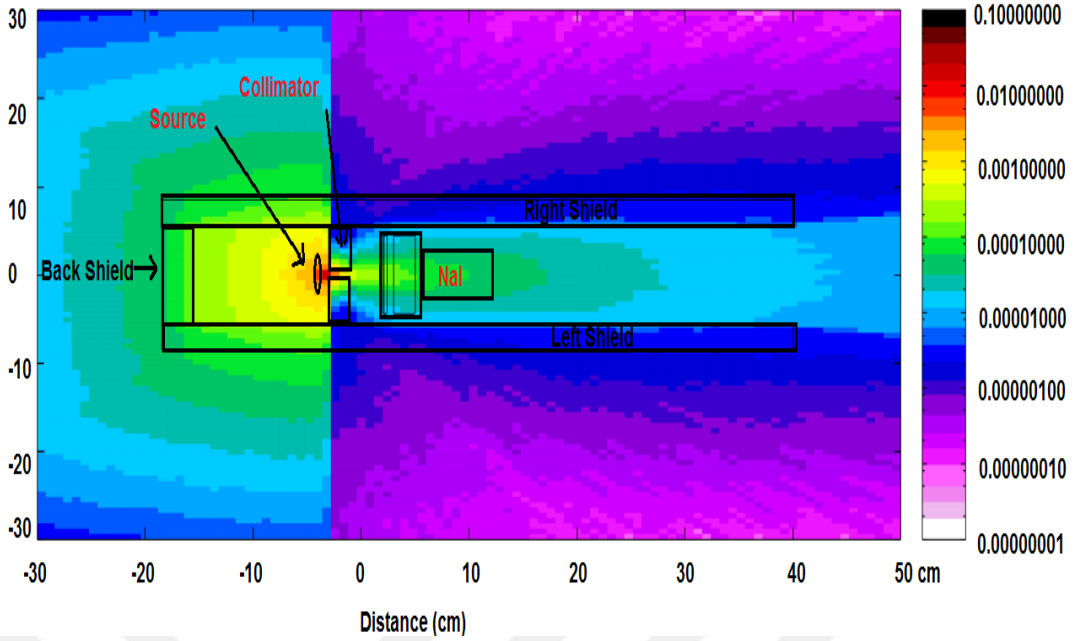

Figure 4.45. FLUKA up view of gamma-rays map density distribution (using Lead collimator)

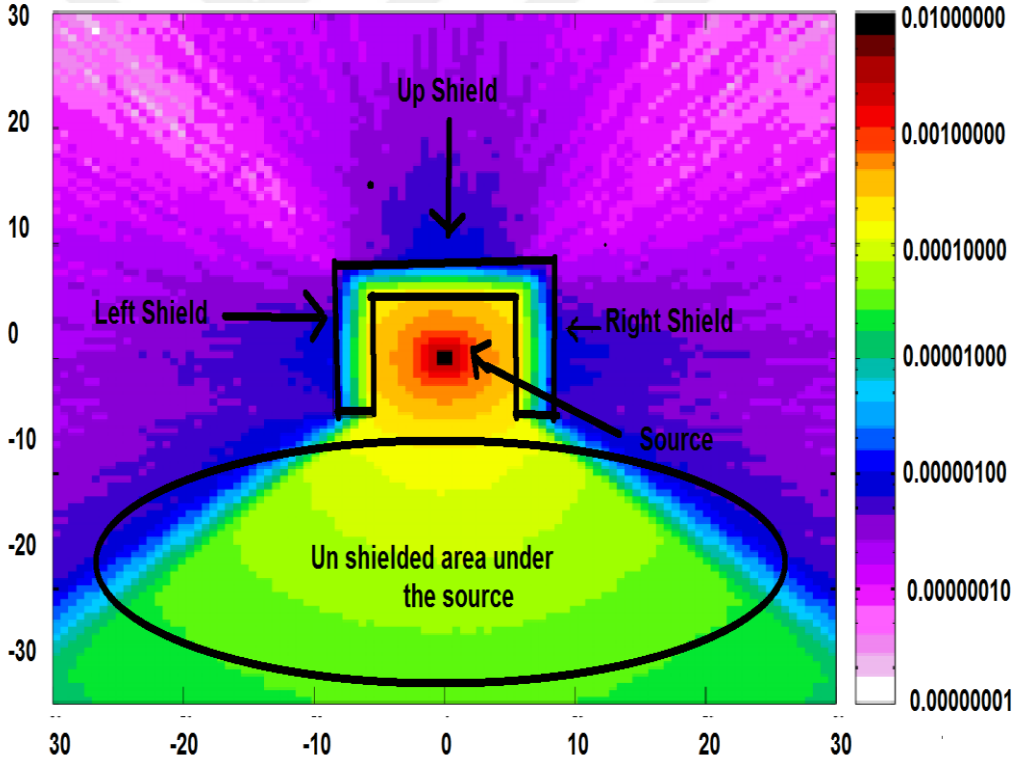

Figure 4.46. FLUKA back view of gamma-rays map density distribution

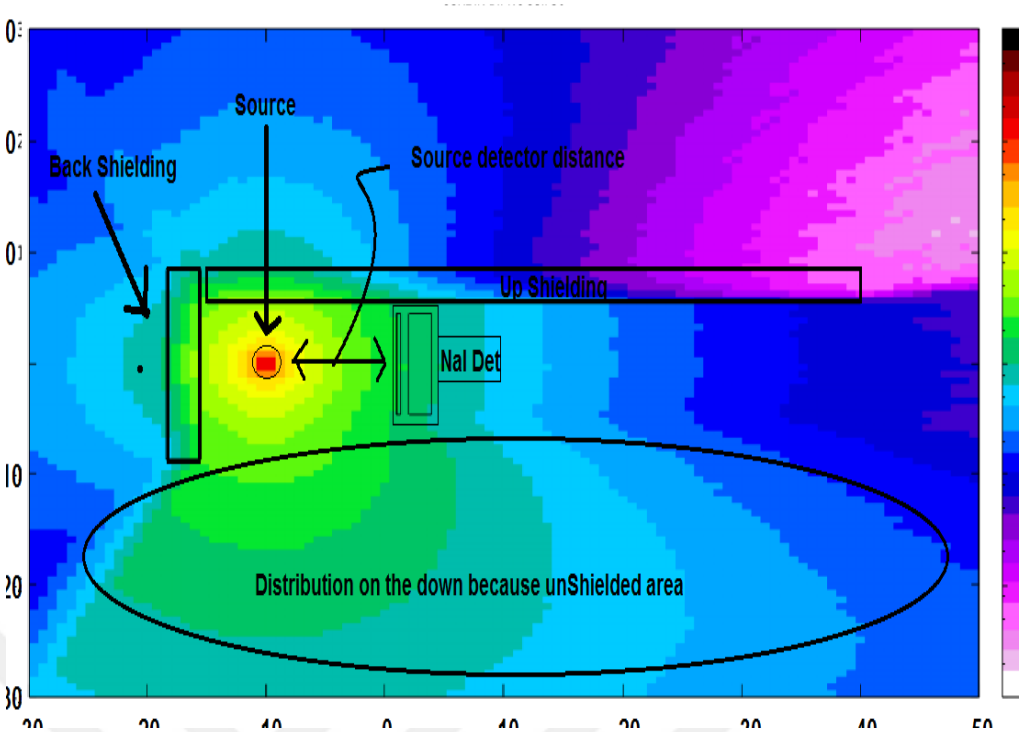

Figure 4.47. FLUKA side view of gamma-rays map density distribution

5. CONCLUSIONS

As the detector performance is important for radiation measurements, in this work important quality parameters such as; the energy calibration, the intrinsic efficiency, the absolute efficiency, the energy resolution (R), FWHM, the energy buildup factor have been obtained both experimentally and simulation to five different gamma-ray energies useing a collimated 3" x 3" NaI(Tl) and FLUKA Monte Carlo Code modelling.

The results first validated through the comparison of experimentally and FLUKA simulated for three isotropic referent sources. Once FLUKA input file was validated, the Monte Carlo was applied to scale experimental results for activity area with ^{60}Co, ^{137}Cs, and ^{22}Na radionuclides. The obtained results demonstrate that FLUKA simulated quality parameters of the collimated scintillation crystal can be used for prompt and direc perfect investigation of quality parameters in the presence of the interfering radiation fields measurements.

FLUKA is a powerful tool for calculating the detector efficiency, energy buildup factor, FWHM, energy resolution (R%), detector responsibility the applicability of this method depends on the reality input file of the source, geometry, composition, density distribution of experimental calculation, and the simulation calculation. The results show a good agreement between them, the results of this study demonstrate that FLUKA can be applied for various energies and source-detector distance when it is difficult to set up an experimentally. It was found from this work that the gamma spectroscopy detection efficiency depends on energy and also source-detector distance.

It have been concluded for both procedures; experimentally and for FLUKA simulation that the:-

1. NaI(Tl) detectors are usually preferred when compared with other kinds of detection systems and used commonly in applications where high gamma sensitivity desired.
2. The intrinsic efficiency decreases with increasing the gamma-ray energy.

3. The absolute efficiency decreases with increasing the gamma-ray energy to the same source-detector distance, and it decreases with increasing the gamma-ray energy to the same source-detector distance.
4. The height of the gamma-ray spectrum shape decreases with increasing source-detector distance.
5. the energy resolution decreases with increasing the gamma-ray energy to the same source-detector distance, and it decreases with increasing the source-detector distance to the same gamma-ray energy.
6. The FWMH increases with increasing the gamma-ray energy to the same source-detector distance, and it decreases with increasing source-detector distance to the same gamma-ray energy.
7. the value of buildup factor decreases with increasing the gamma-ray energy to the same source-detector distance, and it decreases with increasing the source-detector distance to the same gamma-ray energy.
8. There parameters are important for gamma-ray detection system and after this work any measurement will be done depending on this system should be take in to account of these parameters.
9. Any future study for calculation efficiency for unknown gamma-ray energy may be needed to use obtained fitting function.

REFERENCES

A., Das and T., Ferbel. Introduction to Nuclear and Particle Physics Second Edition, University of Rochester, World Scientific Publishing Co. Pte. Ltd. 2003.

Abdlhamed, A. F. A. (2018). *Graduate School Of Natural And Applied Sciences* (Doctoral Dissertation, Süleyman Demirel University).

Abdul Haneefa, K., Cyriac, T. S., Musthafa, M. M., Ganapathi Raman, R., Hridya, V. T., Siddhartha, A., & Shakir, K. K. (2014). FLUKA Monte Carlo for basic dosimetric studies of dual energy medical linear accelerator. Journal of Radiotherapy, 2014

Akkurt, I ., Akyildirim, H., Mavi, B., Kılınçarslan, Ş., Basyigit, C., 2010. Photon Attenuation Coefficients Of Concrete Includes Barite In Different Rate ,Annals of Nuclear Energy (Impact Factor: 0.96). 07/2010; 37 (7): 910-914. DOI: 10.1016 / j.anucene.2010.04.001.

Akkurt, İ., & Günoğlu, K. (2019). Radioactivity Levels of Some Natural Stones in Burdur, Turkey. Advanced Science, Engineering and Medicine, 11(11), 1060-1063.

Akkurt, I., & Tekin, H. O. (2020). Radiological parameters of bismuth oxide glasses using the Phy-X/PSD software. *Emerging Materials Research*, *9*(3), 1020-1027.

Akkurt, I., Calik, A., & Akyıldırım, H. (2011). The boronizing effect on the radiation shielding and magnetization properties of AISI 316L austenitic stainless steel. *Nuclear engineering and design*, *241*(1), 55-58.

Akkurt, I., Calik, A., Akyıldırım, H., 2011. The boronizing effect on the radiation shielding and magnetization properties of AISI 316L austenitic stainless steel. Nuclear Engineering and Design 241, 55–58.

Akkurt, İ., Günoğlu, K., & Hadi, A. B. (2020). Basra Petrol Sahasındaki Atık Toprak-Yağ Karışımının Doğal Radyonüklid İçeriği ve Radyolojik Tehlike Seviyeleri. *Avrupa Bilim ve Teknoloji Dergisi*, (19), 715-721.

Akkurt, I., Kılıncarslan, Ş., Basyigit, C., Mavi, B., Akyıldırım, H., 2009. Investigation of photon attenuation coefficient for pumice, Int., J., Phys. Sci 4 (10), 588-591, international Journal of Physical Sciences Vol. 4 (10), pp. 588-591, October 2009 Available online at http://www.academicjournals.org/IJPSISSN 1992 - 1950 © 2009 Academic Journals.

Akkurt, I., Mavi, B., Akkurt, A., Basyigit, C., Kilincarslan, S., Yalim, H., A., 2005. Study on Z-dependence of partialand total mass attenuation coefficients. J. Quant. Spectrosc. Radiat. Transfer 94 (3–4), 379–385.

Akkurt, I., Tekin, H., O., & Mesbahi, A. (2015). Calculation of detection efficiency for the gamma detector using MCNPX. *Acta Phys. Pol. A*, *128*(2-B), 332-334.

Akkurt, İ., Waheed, F., Akyildirim, H., & Gunoglu, K. (2020). Monte Carlo simulation of a NaI (Tl) detector efficiency. *Radiation Physics and Chemistry*, *176*, 109081.

Akkurt, I., Gunoglu, K., and Arda, S., S., 2014. Detection Efficiency of NaI (Tl) Detector in 0.511–1.332 MeV Energy Range, research Article. Science and Technology of Nuclear Installations. Volume 2014 (2014), Article ID 186798, 5 pages. http://dx.doi.org/10.1155/2014/186798

Akyıldırım, H. Attenuation Parameters and Effective Atomic Numbers of Concretes Containing Pumice for Some Photon Energies by Experiment, Simulation and Calculation. *Avrupa Bilim ve Teknoloji Dergisi*, (14), 90-95.

Akyildirim, H., Kavaz, E., El-Agawany, F. I., & Rammah, Y. S. (2020). WITHDRAWN: Assessment of ionizing radiation attenuation features of zirconolite silicate glasses using XCOM and FLUKA simulation code.

Akyildirim, H., Waheed, F., Günoğlu, K., & Akkurt, İ. (2017). Investigation of Buildup Factor in Gamma-Ray Measurement. *Acta Physica Polonica A*, *132*(3), 1203-1206.

Albidhani, H., Gunoglu, K., & Akkurt, I. (2019). Natural radiation measurement in some soil samples from Basra oil field, IRAQ State. International Journal of Computational and Experimental Science and Engineering, 5(1), 48-51.

Al-obaidi, S. D. S., & Akkurt, I., (2019). Investigation of neutron shielding properties from ^{252}Cf source.

Al-Sarray, E., & Akkurt, İ. (2016). Investigation Of Radiation Shielding Properties Of Some Composite Materials (Doctoral Dissertation, Msc Thesis Fen Bilimleri Enstitusu-Sdu).

Androulakaki, E. G., Kokkoris, M., Skordis, E., Fatsea, E., Patiris, D. L., Tsabaris, C., & Vlastou, R. (2016). Implementation of FLUKA for γ-ray applications in the marine environment. Journal of environmental radioactivity, 164, 253-257.

ANSI/ANS-6.4.3, 1991. Gamma attenuation coefficient and buildup factor for engineering materials. American Nuclear Society. La. Grange Park., IL.

Atallah, F. S., Alrubaye, H. H., Khalaf, M. K., & Ahmed, M. S. (2018). Promote Scientific Research is Our Way to Serve the Community.

Baccouche, S., Al-Azmi, D., Karunakara, N., & Trabelsi, A. (2012). Application of the Monte Carlo method for the efficiency calibration of CsI and NaI detectors for gamma-ray measurements from terrestrial samples. Applied Radiation and Isotopes, 70(1), 227-232.

Bagatelas, C., Tsabaris, C., Kokkoris, M., Papadopoulos, C. T., & Vlastou, R. (2010). Determination of marine gamma activity and study of the minimum detectable activity (MDA) in 4pi geometry based on Monte Carlo simulation. Environmental monitoring and assessment, 165(1-4), 159-168.

Beer, J., McCracken, K., & Steiger, R. (2012). *Cosmogenic radionuclides: theory and applications in the terrestrial and space environments*. Springer Science & Business Media.

Bentayeb, K. (2013). Les Radiations Naturelles Des Matériaux De Construction: Ciment De Beni Saf (Doctoral Dissertation).

Bielajew, A. F. (2001). Fundamentals of the Monte Carlo method for neutral and charged particle transport. The University of Michigan.

Böhlen, T. T., Cerutti, F., Chin, M. P. W., Fassò, A., Ferrari, A., Ortega, P. G., ... & Vlachoudis, V. (2014). The FLUKA code: developments and challenges for high Energy and medical applications. Nuclear data sheets, 120, 211-214.

Boson, J., Ågren, G., & Johansson, L. (2008). A detailed investigation of HPGe detector response for improved Monte Carlo efficiency calculations. Nuclear Instruments and Methods in Physics Research Section A: Accelerators, Spectrometers, Detectors and Associated Equipment, 587(2-3), 304-314.

Brar, G., S., Sidhu, G., S., Singh, P., S., Mudahar, G., S., 1997. Buildup factor studies of HCO-materials as a function of weight fraction of constituent elements, Radiation Physics and Chemistry: Vol.49, No.8,pp.977-980,1998.

Byun, S. H., Prestwich, W. V., Chin, K., McNeill, F. E., & Chettle, D. R. (2004). Efficiency calibration and coincidence summing correction for a 4π NaI (Tl) detector array. Nuclear Instruments and Methods in Physics Research Section A: Accelerators, Spectrometers, Detectors and Associated Equipment, 535(3), 674-685.

Canadian Nuclear Safety Commission, 2017. Types and source of radiation. Available at:- http://nuclearsafety.gc.ca/eng/resources/radiation/introduction-to-radiation/radioisotopes.cfm.

Casanovas, R., Morant, J. J., & Salvadó, M. (2012). Energy and resolution calibration of NaI (Tl) and LaBr3 (Ce) scintillators and validation of an EGS5 Monte Carlo user code for efficiency calculations. Nuclear Instruments and Methods in Physics Research Section A: Accelerators, Spectrometers, Detectors and Associated Equipment, 675, 78-83.

Categorization of radioactive source. Revision of IAEA-TECHDOC-1191, international Atomic energy Agency, Vienna (Austria). Available at: http://www.iaea.org/inis/collection/NCLCollectionStore/_public/34/065/34065394.pdf.

Cember, H., Johnson, T. E., & Alaei, P. (2008). Introduction to health physics. Medical Physics, 35(12), 5959.

Cember, Herman, 1996. Introduction to Health Physics, 3rd Edition, Mc Graw Hill, New York.

Chandani, Z., Prestwich, W. V., & Byun, S. H. (2017). Development of low level 226Ra analysis for live fish using gamma-ray spectrometry. Radiation Physics and Chemistry, 135, 23-27.

Cherry, S., R., Sorenson, J., A., & Phelps, M., E., (2012). Physics in nuclear medicine e-Book. Elsevier Health Sciences.

Chilton, A., B., Shultis, J., K., & Faw, R., E., (1984). Principles of Radiation Shielding Prentice Hall. Inc., New Jersey, 90-92.

Copenhaver, E. D., Houser, B. S., Butler Jr, H. M., Bogard, J. S., Fair, M. F., Haynes, C. E., & Parzyck, D. C. (1986). *Technical qualification requirements and training programs for radiation protection personnel at Oak Ridge National Laboratory* (No. ORNL/TM-10119). Oak Ridge National Lab., TN (USA). Environmental and Occupational Safety Div.

Cottingham, W., N., Greenwood, D. A., & Greenwood, D. A. (2001). An introduction to nuclear physics. Cambridge University Press.

Dagpunar, J. S. (2007). Simulation and Monte Carlo: With applications in finance and MCMC. John Wiley & Sons.

Daniel, G., 2008. Basic radiation protection technology, 5 th ed: pacific radiation corporation.

Davis, J. R. (Ed.). (2000). Corrosion: Understanding the basics. Asm International.

Demir, N., Kuluöztürk, Z. N., & Akkurt, İ. (2019). FLUKA Monte Carlo calculations for angular distribution of bremsstrahlung photons from thin targets. Nuclear Instruments and Methods in Physics Research Section B: Beam Interactions with Materials and Atoms, 443, 19-24.

Dhillon, J. S., Singh, B., Sindhu, G., S., 2012. Gamma Ray Photon Energy Absorption Buildup Factor Study In Some Soils. IOSR Journal of Applied Physics (IOSRJAP) ISSN – 2278-4861 Volume 1, Issue 6 (Sep-Oct. 2012), PP 14-21 www.iosrjournals.org.

Dickstein, P., & Vanunu, S. (2016). Nuclear Terror: The Essentials, Threats, Effects and Resilience. *International Institute for Counter-Terrorism*, 4.

DOE-HDBK-1019/1-93, 1993. Nuclear Physics and Reactor Theory. Volume 1 of 2; DOE, Fundamentals Hand book Series, January.

El-Khayatt A., M., Akkurt I., 2013. Photon Interaction. Energy Absorption And Neutron Removal Cross Section Of Concrete Including Marble. Annals of Nuclear Energy Volume 60, October 2013, Pages 8–14.

Evans, R. D., & Evans, R. D. (1955). The atomic nucleus.

Faanu, A., Emi-Reynolds, G., Darko, E. O., Awudu, R., Glover, E. T., Adukpo, O. K., ... & Lawluvi, H. (2011). Calibration and performance testing of sodium iodide, NaI (Tl), detector at the food and environmental laboratory of the radiation protection institute of the Ghana atomic energy commission. West African Journal of Applied Ecology, 19(1).

Ferrari, A., Sala, P. R., Fasso, A., & Ranft, J. (2005). FLUKA: A multi-particle transport code (Program version 2005) (No. INFN-TC-05-11).

Friedberg, W., Copeland, K., Duke, F. E., O'Brien III, K., & Darden Jr, E. B. (1999). Guidelines and technical information provided by the US Federal Aviation Administration to promote radiation safety for air carrier crew members. Radiation Protection Dosimetry, 86(4), 323-327.

from ORTEC, E. N. High-Resolution Gamma-Ray Spectroscopy. ORTEC Experiment 3. Gamma-Ray Spectroscopy Using NaI(Tl) Equipment Required. Purpose. Gamma Emission. Available at:- https://pdfs.semanticscholar.org/41f6/de956ddbe9e838925b92ec7092133285c406.pdf.

Gardner, R. P., & Sood, A. (2004). A Monte Carlo simulation approach for generating NaI detector response functions (DRFs) that accounts for non-linearity and variable flat continua. Nuclear Instruments and Methods in Physics Research Section B: Beam Interactions with Materials and Atoms, 213, 87-99.

Gilmore, G. (2011). experimental gamma-ray spectroscopy. John Wiley & Sons.

Gouda, M. M., Badawi, M. S., El-Khatib, A. M., Mohamed, M. M., Thabet, A. A., & Abbas, M. I. (2015). Calibration of well-type NaI (Tl) detector using a point sources measured out the detector well at different axial distances. *Journal of Instrumentation*, *10*(03), P03022.

Gould, H., & Tobochnik, J. (2010). Statistical and thermal physics: with computer applications. Princeton University Press.

Grujić, S., Đorđević, I., Milošević, M., & Kozmidis-Luburić, U. (2013). Monte Carlo simulation of GM probe and NaI detector efficiency for surface activity measurements. Radiation Measurements, 58, 45-51.

Gunoglu, K., & AKKURT, İ. (2012), Investigation Of Gamma-Ray Interaction With Some Travertines In Turkey. available at:- https://avesis.sdu.edu.tr/yayin/47f09768-32dd-441e-9e5f-196c56f03234/investigation-of-gamma-ray-interaction-with-some-travertines-in-turkey

Guvendik, M., 1999. Build up factor formulae for multi-layer shields. Doctorate thesis, university of Missouri-Rolla. Vol. 77.

Hakimabad, H. M., Panjeh, H., & Vejdani-Noghreiyan, A. (2007). Response Function of a 3 x 3 in. NaI Scintillation Detector in the range of 0. 081 to 4. 438 MeV. *Asian Journal of Experimental Sciences*, *21*(2), 233-237.

Harb, S. R. M. (2004). On the human radiation exposure as derived from the analysis of natural and man-made radionuclides in soils (Doctoral dissertation, Hannover: Universität).

Harima, Y., Kurosawa, N., Sakamoto, Y., 2014. Parameter search of geometric-progression formula for gamma-ray isotropic point source buildup factors up to depths of 100 mfp, including contribution of secondary radiations. Progress in Nuclear Science and Technology, Volume 4(2014) pp. 548-552.

Heitler, W., (1954). The Quantum Theory of Radiation, 3rd edn, Clarendon.

Hendriks, P. H. G. M., Maučec, M., & De Meijer, R. J. (2002). MCNP modelling of scintillation-detector γ-ray spectra from natural radionuclides. Applied Radiation and Isotopes, 57(3), 449-457.

Holdsworth, A., F., Eccles, H., Rowbotham, D., Bond, G., Kavi, P., C., & Edge, R., (2019). The Effect of Gamma Irradiation on the Ion Exchange Properties of Cesium-Selective Ammonium Phosphomolybdate-Polyacrylonitrile (AMP-PAN) Composites under Spent Fuel Recycling Conditions. *Separations*, *6*(2), 23.

Hopkins, D., N., 2010. Determination of the linear attenuation coefficients and buildup factor of MCP-96 allow. MSc thesis ball state university – Indiana.

Hubbell, J. H., Veigele, W. J., Briggs, E. A., Brown, R. T., Cromer, D. T., & Howerton, D. R. (1975). Atomic form factors, incoherent scattering functions, and photon scattering cross sections. *Journal of physical and chemical reference data*, *4*(3), 471-538.

Huffert, A. M., Meck, R. A., & Miller, K. M. (1994). Background as a residual radioactivity criterion for decommissioning. US—DOE, Environmental Measurements Laboratory, Report NUREG-1501.

International Agency for Research on Cancer. (2002). *Non-ionizing radiation* (Vol. 80). World Health Organization.

International Atomic Energy Agency, The Safe Use of Radiation Sources, Training Course Series No. 6, IAEA, Vienna (1995).

Ivanova, D., Stadler, K., Steen, Olsen, K., Wood, R., Vita, G., Tukker, A., & Hertwich, E. G. (2016). Environmental impact assessment of household consumption. Journal of Industrial Ecology, 20(3), 526-536.

Jaeger, R., G., Chilton, A. B., Blizard, P., Honig, A., Jaeger, A., Eisenlohr, H., H., 1968. Engineering Compendium on Radiation Shielding, Volume I shielding fundamentals and methods, New York Inc.

Jehouani, A., Ichaoui, R., Boulkneir, M., 2000. Study of the NaI(Tl) efficiency by Monte-Carlo method. Applied Radiation and Isotopes 53 (4e5), 887e891.

Jibiri, N. N., & Abiodun, T. H. (2012). Effects of food diet preparation techniques on radionuclide intake and its implications for individual ingestion effective dose in Abeokuta, Southwestern Nigeria. *World Journal of Nuclear Science and Technology*, *2*(03), 106.

Joel, G. S. C., Maurice, N. M., Jilbert, N. M. E., Ousmanou, M., & David, S. (2018). Monte Carlo method for gamma spectrometry based on GEANT4 toolkit: Efficiency calibration of BE6530 detector. Journal of environmental radioactivity, 189, 109-119.

Jubair, S., I., 2011. Calculation of Buildup factors for Ceramic Materials: Iraqi Journal of Applied, Iraqi Society for Alternative and Renewable energy Sources and Techniques (I.S.A.R.E.S.T.).

Justice, H., 2016. Quality comtrol and dosimetry of a wooden cough top for megavoltage external beam radiotherapy. MSc thesis of medical physics, university of Ghana, college of basic and applied science.

Kalilainen, J. (2015). Fission product transport in the primary circuit and in the containment in severe nuclear accidents.

Kara, Ü., & Akkurt, İ. (2019). Yüksek Enerjili Klinik Lineer Hızlandırıcı Modellemesi ve Radyasyon Sızıntı Ölçümleri. Avrupa Bilim ve Teknoloji Dergisi, (16), 707-712.

Karkosh, H. L. M. H. N. (2016). Searching for Abandoned Radioactive Sources in Scrap Yards at Al-Tuwaitha Nuclear Site. *journal of the college of basic education*, *22*(96/72-63

Kavas, E., Ekinci, N., 2016. Energy absorption and exposure Buildup factors in polymers by nuclear track detectors, Asian journal of chemistry, Vol. 28, No. 8 (2016), 1673-1681. Available at: http://dx.doi.org/10.14233/ajchem.2016.19783.

Kiran, K. U., Ravindraswami, K., Eshwarappa, K. M., & Somashekarappa, H. M. (2015). Experimental and simulated study of detector collimation for a portable 3 ″× 3 ″NaI (Tl) detector system for in-situ measurements. *Journal of Radiation Research and Applied Sciences*, *8*(4), 597-605.

Knoll, G., F., (2000). Radiation Detection and Measurement3rd edition John Wiley and Sons. New York.

Knoll, G., F., (2010). Radiation detection and measurement. John Wiley & Sons.

Knolls Atomic, 2003. Chart of the Nuclides - Sixteenth Edition.iIlL

Kovaltchouk, V., Machrafi, R., 2011. Monte Carlo simulations of response functions for gas filled and scintillator detectors with MCNPX code. Annals of Nuclear Energy 38, 788e793.

Krane, K. S., & Halliday, D. (1987). *Introductory nuclear physics*.

L'Annunziata, M. F. (Ed.). (2012). Handbook of radioactivity analysis. Academic press.

Lipps, F. W., & Tolhoek, H. A. (1954). Polarization phenomena of electrons and photons. II: Results for Compton scattering. *Physica*, *20*(1-6), 395-405.

Mahdi, K., H., Ahmed, Z. S., & Mkhaiber, A., F., (2017). Calculation and Study of Gamma ray Attenuation Coefficients for Different Composites. Ibn AL-Haitham Journal For Pure and Applied Science, 25(3), 133-141.

Mann, K. S., Heer, M. S., & Rani, A. (2016). Gamma-ray double-layered transmission exposure buildup factors of some engineering materials, a comparative study. Radiation Physics and Chemistry, 125, 27-40.

Mann, K., S., Heer, M., S., 2013. Gamma-ray buildup factors study for deep penetration in some silicates, Radiation Physics and Chemistry, journal homepage: www.elsevier.com/locate/radphyschem.

Mann, K., S., Singla, J., Kumar, V., Sidhu, G., S., 2012. Investigations of mass attenuation coefficients and exposure buildup factors of some low-Z building materials: Annals of Energy 43 (2012)157-166, journal homepage :- www.elsevier.com/locate/anucene

Manohara, S., R., Hanagodimath, S., M., Gerward, L., Mittal, K., C., 2011. Exposure Buildup Factors for Heavy Metal Oxide Glass: A Radiation Shield, Journal of the Korean Physical Society, Vol.59, No.2, August 2011, pp.2039~2042.

Martin, A. (2012). An Introduction to Radiation Protection 6E. CRC Press.

Martin, J., E., (2006). Physics for radiation protection: a handbook. John Wiley & Sons.

Masson, O., Baeza, A., Bieringer, J., Brudecki, K., Bucci, S., Cappai, M., ... & Didier, D. (2011). Tracking of airborne radionuclides from the damaged Fukushima Dai-ichi nuclear reactors by European networks. Environmental Science & Technology, 45(18), 7670-7677.

Mayerhöfer, T. G., Pahlow, S., & Popp, J. (2020). The Bouguer-Beer-Lambert law: Shining light on the obscure. *ChemPhysChem*, *21*(18), 2029.

McHaney, R., (2009). Understanding computer simulation. Bookboon.

Milbrath, B. D., Runkle, R. C., Hossbach, T. W., Kaye, W. R., Lepel, E. A., McDonald, B. S., & Smith, L. E. (2005). Characterization of alpha contamination in lanthanum trichloride scintillators using coincidence measurements. Nuclear Instruments and Methods in Physics Research Section A: Accelerators, Spectrometers, Detectors and Associated Equipment, 547(2-3), 504-510.

Moe, H. J., & Vallario, E. J. (1988). *Operational health physics training*. Argonne National Laboratory.

Moe, H., J., 1992. Operation health physics training, Argon National Laboratory, Chicago, available to DOE and DOE Contracts from the office of Science and Technology information, ANL-88-26. Available at:

Mohamed, Y. M. B. (2014). *Monte Carlo Modeling of Effective Shielding Systems for Fast Neutrons* (Doctoral dissertation, Sudan University of Science and Technology).

Moreira, M. C. F., Conti, C. C., & Schirru, R. (2010). A new NaI (Tl) four-detector layout for field contamination assessment using artificial neural networks and the Monte Carlo method for system calibration. Nuclear Instruments and Methods in Physics Research Section A: Accelerators, Spectrometers, Detectors and Associated Equipment, 621(1-3), 302-309.

Mostafa, G., Sing, R., F., McKeown, R., Huynh, T., T., & Heniford, B., T., (2002). The hazard of scattered radiation in a trauma intensive care unit. Critical care medicine, 30(3), 574-576.

Mouhti, I., Elanique, A., & Messous, M. Y. (2017). Monte Carlo modelling of a NaI (Tl) scintillator detectors using MCNP simulation code. Journal of Materials and Environmental Science, 8(12), 4560-4565.

Mouhti, I., Elanique, A., Messous, M. Y., Belhorma, B., & Benahmed, A. (2018). Validation of a NaI (Tl) and LaBr3 (Ce) detector's models via measurements and Monte Carlo simulations. Journal of radiation research and applied sciences, 11(4), 335-339

Nakamura, T., 1983. Monte Carlo calculation of peak efficiencies of Ge(Li) and Pure Ge detectors to volume sources and comparison with environmental radioactivity measurement. Nuclear Instruments and Methods 205, 211e218.

Orion, I., & Wielopolski, L. (2002). Limitations in the PHOTON Monte Carlo gamma transport code. Nuclear Instruments and Methods in Physics Research Section A: Accelerators, Spectrometers, Detectors and Associated Equipment, 480(2-3), 729-733.

Pelowitz, D.B., 2005. MCNP-X TM User's Manual, Version 2.5.0. LA-CP-05e0369. Los Alamos National Laboratory.

Perez-Andujar, A., & Pibida, L. (2004). Performance of CdTe, HPGe and NaI (Tl) detectors for radioactivity measurements. Applied radiation and isotopes, 60(1), 41-47.

Price, B., T., Horton, C., C., & Spinney, K., T. 1957. Radiation Shielding (International Series of Monographs on Nuclear Energy). Available at:- http://ec.europa.eu/energy/nuclear/euratom/euratom_en.htm.

Radiological Control Technician, RCT 1.05-SG, 2013. Sandia National- U.S Depart of energy's / National Security Administration DOE-AC04-94AL85000. SAND.NO.2013-0024P.

Radiological Control Technician, RCT 1.06-SG, 2013. Sandia National- U.S Depart of energy's / National Security Administration DOE-AC04-94AL85000. SAND.NO.2013-0024P.

Radiological Control Technician, RCT 1.07-SG, 2013. Sandia National- U.S Depart of energy's / National Security Administration DOE-AC04-94AL85000. SAND.NO.2013-0024P.

Radiological Control Technician, RCT 1.13-SG, 2013. Sandia National- U.S Depart of energy's / National Security Administration DOE-AC04-94AL85000. SAND.NO.2013-0024P.

Ranft, J. (1972). Estimation of radiation problems around high-energy accelerators using calculations of the hadronic cascade in matter. Part. Accel., 3, 129-161.

Reguigui, N., (2006). Gamma Ray Spectrometry. Practical Information.

Rwashdi, Q., 2017. Investigation of Radiation Shielding Properties of Some steels. MSc thesis Fen Bilimleri Enstitusu- SDU.

Salgado, C. M. (2015). Photopeak efficiency response function of an underwater gamma ray NaI (TI) detector using MCNP X.

Salgado, C. M., Brandão, L. E. B., Schirru, R., Pereira, C. M. D. N. A., & Conti, C. D. C. (2012). Validation of a NaI (Tl) detector's model developed with MCNP-X code. *Progress in Nuclear Energy*, *59*, 19-25.

Salgado, C. M., Brandão, L. E. B., Schirru, R., Pereira, C. M. N. A., Ramos, R., Silva, A. X., 2009. Prediction of volume fractions in three-phase flows using nuclear technique and artificial neural net work. Applied Radiation and Isotope 67,1812e1818.

Samad, O. E., & Baydoun, R. (2018). Implementation of Quality Assurance System in Gamma Spectroscopy Laboratory: Best Practice for Accreditation.

Saraiva, A., Oliveira, C., Reis, M., Portugal, L., Paiva, I., & Cruz, C. (2016). Study of the response of an ORTEC GMX45 HPGe detector with a multi-radionuclide volume source using Monte Carlo simulations. Applied Radiation and Isotopes, 113, 47-52.

Schoenung, S., (2011). Energy storage systems cost update. SAND2011-2730.

Seco, J., & Verhaegen, F. (Eds.). (2013). Monte Carlo techniques in radiation therapy. CRC/Taylor & Francis.

Shah, K., S., Glodo, J., Klugerman, M., Moses, W. W., Derenzo, S., E., & Weber, M., J., 2002. LaBr/sub 3: Ce scintillators for gamma ray spectroscopy. In *Nuclear Science Symposium Conference Record, 2002 IEEE* (Vol. 1, pp. 92-95). IEEE.

Shazly, A., Kany, A. M. I., Osman, A., El Samman, H., & El-Mongy, S. A. (2011). Recent Approach For Uranium Isotopic Ratio Verification of Ores Source Nuclear Material.

Shi, H. X., Chen, B. X., Li, T. Z., & Yun, D. (2002). Precise Monte Carlo simulation of gamma-ray response functions for an NaI (Tl) detector. Applied radiation and isotopes, 57(4), 517-524.

Shimizu, A., Hirayama, H., 2003. Calculation of gamma ray Buildup factor up to depths of 100 mfp by the method of invariant embedding (I). J. Nucl. Sci. Tech., Vol. 40, No.4, pp.192-200.

Shin, K., and Hirayama, H., 2001. Calculation of gamma-ray buildup factors for two-layered shields made of water, concrete and iron and application of approximation formula radiation physics and chemistry 61 (2001) 583.

Shirakawa, Y., 2000. A Build-up treatment for thickness gauging of steel platesbased on gamma-ray transmission: Applied Radiation and Isotopes 53(2000)581-586.

Shirani, A., and Alamatsaz, M., H., 2013. Calculation of exposure buildup factors for point isotropic gamma ray sources in stratified spherical shields of water surrounded by lead and optimization of water-lead combination, Iranian Journal of Science & Technology, A1: 29-34.

Shirmardi, S. P., Shamsaei, M., & Naserpour, M. (2013). Comparison of photon attenuation coefficients of various barite concretes and lead by MCNP code, XCOM and experimental data. Annals of Nuclear Energy, 55, 288-291.

Shleien, B. (1992). The Health Physics and Radiological Health Handbook", Scinta. *Inc., Silver Spring, Md*.

Shleien, B., 1992. The health physics and radiological health handbook. Silver Spring, MD: Scinta. Available at:- https://www.abebooks.com/book-search/title/radiological-health-handbook/.

Sidhu, B., S., Dhaliwal, A., S., Mann, K., S., & Kahlon, K., S. (2012). Study of mass attenuation coefficients, effective atomic numbers and electron densities for some low Z compounds of dosimetry interest at 59.54 keV incident photon energy. *Annals of Nuclear Energy*, *42*, 153-157.

Sidhu, B., S., et al., 2000. Studied experimentally the effect of collimator size and absorber thickness on the gamma ray buildup factor for extended media of soil and water up to 5 mfp using point isotropic 137Cs source.

Sima, O., 1990. Monte Carlo simulation versus semi empirical calculation of auto absorption factors for semiconductor detector calibration in complex geometries. Progress in Nuclear Energy 24, 327e336.

Singh, B., Kumar, V., Devi, M., & Sidhu, G., S. (2013). Chemical composition dependence of exposure buildup factors for some biological materials. Int. J. Latest Res. Sci. Technol., 5, 65-69. Available at: http://www.mnkjournals.com/ijlrst.htm.

Singh, S., Ghumman, S., S., Singh, C., Thind, K., S., Mudahar, G., S., 2010. Buildup factor of gamma ray photons in flyash concretes, Annals of Nuclear Energy:37.681–684.

Smathers, K. L., & Karp, A. H. (2008). *U.S. Patent No. 7,350,070*. Washington, DC: U.S. Patent and Trademark Office.

Smith, B. T. (2010). Introduction to radioactivity and radioactive decay.

Sood, A., & White, M., C., (2004). Doppler energy broadening for incoherent scattering in MCNP5, part II. Los Alamos National Laboratory internal memorandum LA-UR-04-0488, Los Alamos, NM.

Sudarshan, M., & Singh, R., (1991). Effect of fast neutron damage on the performance of a high resolution HPGe coaxial detector. *Measurement Science and Technology*, *2*(12), 1192.

Tait, W. H. (1980). Radiation detection.

Tekin, H. O. (2016). MCNP-X Monte Carlo code application for mass attenuation coefficients of concrete at different energies by modeling 3× 3 inch NaI (Tl) detector and comparison with XCOM and Monte Carlo data. Science and Technology of Nuclear Installations, 2016.

Thilagam, L., Priya, M., R., & Mohapatra, D. K. (2015). Validation of analytical functions to fit detection efficiencies of NaI (Tl) scintillation detector in the energy range of 122–1332 keV. Radiation Protection and Environment, 38(4), 130.

Tsoulfanidis, N. (1995). Measurement and Detection of radiation. In *Fuel and Energy Abstracts* (Vol. 4, No. 36, p. 303).

Tsoulfanidis, N., (1984). Computational Methods in Reactor Shielding.

Tsoulfanidis, N., 'Measurement and detection of radiation', 2nd edition, Taylor & Francis Company, 1995.

Ullah, A., Shah, S. N. M., Ali, A., Naz, R., Mahar, A., & Kalhoro, S. A. (2015). Factors affecting the adoption of organic farming in Peshawar-Pakistan. *Agricultural Sciences*, *6*(06), 587.

United Nations Environment Programme (UNEP), Radiation Effects and Sources, Austria, 2016.

United Nations. Scientific Committee on the Effects of Atomic Radiation. (2000). Sources and effects of ionizing radiation: sources (Vol. 1). United Nations Publications.

Vahabi, S. M., Bahreinipour, M., & Zafarghandi, M. S. (2017). Determining the mass attenuation coefficients for some polymers using MCNP code: A comparison study. Vacuum, 136, 73-76.

Vahlbruch, H., Mehmet, M., Danzmann, K., & Schnabel, R. (2016). Detection of 15 dB squeezed states of light and their application for the absolute calibration of photoelectric quantum efficiency. Physical review letters, 117(11), 110801.

Vitorelli, J. C., Silva, A. X., Crispim, V. R., Da Fonseca, E. S., & Pereira, W. W. (2005). Monte Carlo simulation of response function for a NaI (Tl) detector for gamma rays from 241Am/Be source. Applied radiation and isotopes, 62(4), 619-622.

Vlachoudis, V. (2006). flair for FLUKA.

Waheed, F. Q. W., & Akkurt, İ. (2017). Investigation Of Buildup Factor In Γ–Ray Measurement.

Waheed, F. Q., AL-Kazzaz, H. H., AL-Aubaedy, S. D., & AL-Dulaimi, M. J. (2017). قياس التعرضات الاشعاعية لمنظومة الفحص بالاشعة المؤينة من نوع RapiScan-GaRDS. Journal of Madenat Alelem University College, 9(1), 131-142.

Waheed, F., Q., & Akkurt, I., 2017. Investigation of buildup factor in gamma ray measurement. MSc. Thesis Fen Bilimleri Enstitusu- SDU.

Waheed, F., Q., Akyildirim, H., Günoğlu, K., Akkurt, İ., 2018. The Importance of the Buildup Factor for NaI(Tl) Detector System. 5thinternational Conference on Computational And Experimental Science And Engineering (ICCESEN-5), ISBN:978-605-68728-0-8, 12-16 October 2018, Antalya-Turkey, 298-300.

Waheed, F., Q., Akyildirim, H., Günoğlu, K., Akkurt, İ., 2019. A Monte Carlo simulation: To determination the buildup factor. 5th International Conference on Computational And Experimental Science And Engineering (ICCESEN-6), ISBN:978-605-68728-0-8, 23-27 October 2019, Antalya-Turkey, 298-300.

Waheed, F., Q., Akyildirim, H., Günoğlu, K., Akkurt, İ., 2019. Modeling of 3" x 3" NaI(Tl) Scintilation Detector System by Monte Carlo Code program. 2nd International Conference on Sustainable Sciences and Technology (ICSuSaT-2) ISBN: 978-605-68728-2-2, 05-07 July 2019 Istanbul-TURKEY, 47-49.

Waheed, F., Q., Günoğlu, K., Akyildirim, H., Akkurt, İ., 2018. Variation of Detector Resolution with the Source-Detector Distance. 5thinternational Conference on Computational And Experimental Science And Engineering (ICCESEN-5), ISBN:978-605-68728-0-8, 12-16 October 2018, Antalya-Turkey, 290-297.

Waheed, F., Q., Günoğlu, K., Akyildirim, H., Akkurt, İ., 2018. Variation of Detector Resolution with the Source-Detector Distance. 5thinternational Conference on Computational And Experimental Science And Engineering (ICCESEN-5), ISBN:978-605-68728-0-8, 12-16 October 2018, Antalya-Turkey, 290-297.

Waheed, F., Q., Günoğlu, K., Akyildirim, H., Akkurt, İ., 2019. An Experimental work on the Total efficiency of Cylindrical Scintillation Gamma-Ray Detector. 2nd International Conference on Sustainable Sciences and Technology (ICSuSaT-2), ISBN: 978-605-68728-2-2, 05-07 July 2019 Istanbul-TURKEY, 102-104.

Waheed, F., Q., Günoğlu, K., Akyildirim, H., Akkurt, İ., 2019. Determination of the Gamma Ray Attenuation Coefficient Of Magnetite Aggregate Concretes. 6th International Conference on Computational And Experimental Science And Engineering (ICCESEN-6), ISBN:978-605-68728-0-8, 23-27 October 2019, Antalya-Turkey, 290-297.

Wania, F., Hoff, J. T., Jia, C. Q., & Mackay, D. (1998). The effects of snow and ice on the environmental behaviour of hydrophobic organic chemicals. Environmental Pollution, 102(1), 25-41.

Wright, S. A., Conboy, T. M., & Rochau, G. E. (2011). Supercritical CO2 Power Cycle Development Summary at Sandia National Laboratories (No. SAND2011-6640C). Sandia National Lab.(SNL-NM), Albuquerque, NM (United States).www.orau/documents/ivhp/health-physics/anlhp.pdf.

Young-Yong, J. I., Chung, K. H., Kim, C. J., & Park, S. T. (2015). Application of the dose rate spectroscopy to the dose-to-curie conversion method using a NaI (Tl) detector. Radiation Physics and Chemistry, 106, 320-326.

CURRICULUM VITAE

Name and Surname	: Faez Qahtan Waheed WAHEED
Birth date	: Iraq, Baghdad, 1974
Sex	: male
Marital status	: Married
Languages	: Arabic – English
E-mail	: faez_radiophysics@yahoo.com

Education

High School	: Sallah AL Deen, School AL-shaab, 1992 - Baghdad
Bachelor's degree	: AL Mustansiriyah University College of Science - Baghdad
Department	: Physics Science, 1997
Master's degree	: Süleyman Demirel University/ Graduate School of Natural And Applied Sciences Physics Department: Science, 2017

Professional Experience

Member of Iraqi atomic energy commission staff (IAEC)/ Health physics department From 2002 – 2003.

Member of ministry of science and technology staff (MoST)/ Radiation protection department from 2003 – 2008.

Member of the Iraqi radioactive source regulatory authority staff (IRSRA) from 2008 – till now.

Job Title :- Radiation protection officer in the regulatory body of Iraq.

Training Course

Many training course in the atomic Energy Commission of many countries such as (Iraq, Syria, Jordan, Tunis, Italia, USA, Vienna) held by the international atomic energy commotion (IAEA), the total duration time of training more than 1 Year.

Publications

Waheed, F. Q., AL-Kazzaz, H. H., AL-Aubaedy, S. D., & AL-Dulaimi, M. J. (2017). قياس التعرضات الاشعاعية لمنظومة الفحص بالاشعة المؤينة من نوع RapiScan-GaRDS. *Journal of Madenat Alelem University College*, *9*(1), 131-142.

Waheed, F., Akkurt, İ.,Akyildirim, H., & Gunoglu, K. (2020). Monte Carlo simulation of a NaI (Tl) detector efficiency. *Radiation Physics and Chemistry*, *176*, 109081.

Waheed, F., Akyildirim, H., Günoğlu, K., & Akkurt, İ. (2017). Investigation of Buildup Factor in Gamma-Ray Measurement. *Acta Physica Polonica A*, *132*(3), 1203-1206.

Waheed, F., Q., Akyildirim, H., Günoğlu, K., Akkurt, İ., 2018. The Importance of the Buildup Factor for NaI(Tl) Detector System. 5thinternational Conference on Computational And Experimental Science And Engineering (ICCESEN-5), ISBN:978-605-68728-0-8, 12-16 October 2018, Antalya-Turkey, 298-300.

Waheed, F., Q., Akyildirim, H., Günoğlu, K., Akkurt, İ., 2019. A Monte Carlo simulation: To determination the buildup factor. 5th International Conference on Computational And Experimental Science And Engineering (ICCESEN-6), ISBN:978-605-68728-0-8, 23-27 October 2019, Antalya-Turkey, 298-300.

Waheed, F., Q., Akyildirim, H., Günoğlu, K., Akkurt, İ., 2019. Modeling of 3" x 3" NaI(Tl) Scintilation Detector System by Monte Carlo Code program. 2nd International Conference on Sustainable Sciences and Technology (ICSuSaT-2) ISBN: 978-605-68728-2-2, 05-07 July 2019 Istanbul-TURKEY, 47-49.

Waheed, F., Q., Akyildirim, H., Günoğlu, K., Akkurt, İ., 2020. Estimation the Photon Flux Distribution inside Shielding design. 7thinternational Conference on Computational And Experimental Science And Engineering (ICCESEN-7), ISBN:978-605-68728-0-8, 21-25 October 2020, Antalya-Turkey.

Waheed, F., Q., Akyildirim, H., Günoğlu, K., Akkurt, İ., 2020. Response Function of 3" x 3" NaI(Tl) scintillation for Cobalt (^{60}Co) Isotropic source. 3nd International Conference on Sustainable Sciences and Technology (ICSuSaT-3) ISBN: 978-605-68728-2-2, 25-27 Sebtember 2020 Istanbul-TURKEY.

Waheed, F., Q., Günoğlu, K., Akyildirim, H., Akkurt, İ., 2018. Variation of Detector Resolution with the Source-Detector Distance. 5thinternational Conference on Computational And Experimental Science And Engineering (ICCESEN-5), ISBN:978-605-68728-0-8, 12-16 October 2018, Antalya-Turkey, 290-297.

Waheed, F., Q., Günoğlu, K., Akyildirim, H., Akkurt, İ., 2019. An Experimental work on the Total efficiency of Cylindrical Scintillation Gamma-Ray Detector. 2nd International Conference on Sustainable Sciences and Technology (ICSuSaT-2), ISBN: 978-605-68728-2-2, 05-07 July 2019 Istanbul-TURKEY, 102-104.

Waheed, F., Q., Günoğlu, K., Akyildirim, H., Akkurt, İ., 2019. Determination of the Gamma Ray Attenuation Coefficient Of Magnetite Aggregate Concretes. 6th International Conference on Computational And Experimental Science And Engineering (ICCESEN-6), ISBN:978-605-68728-0-8, 23-27 October 2019, Antalya-Turkey, 290-297.

Waheed, F., Q., Günoğlu, K., Akyildirim, H., Akkurt, İ., 2020. FLUKA Plotting of gamma-Ray Distribution Outside Geometry. 3nd International Conference on Sustainable Sciences and Technology (ICSuSaT-3), ISBN: 978-605-68728-2-2, 25-27 Sebtember 2020 Istanbul-TURKEY.

Waheed, F., Q., Günoğlu, K., Akyildirim, H., Akkurt, İ., 2020. FLUKA modelling of Cesium (^{137}Cs) spectrum. 7thinternational Conference on Computational And Experimental Science And Engineering (ICCESEN-7), ISBN:978-605-68728-0-8, 21-25 October 2018, Antalya-Turkey.

ÖZGEÇMİŞ

Adı	: Faez Qahtan Waheed WAHEED
Doğum yeri – tarihi	: Bağdat/Irak - 1974
Cinsiyeti	: Erkek
Medeni durumu	: Evli
Yabancı dili	: Arapça, İngilizce
E-posta	: faez_radiophysics@yahoo.com

Eğitim Durumu

Yüksekokul	: Sallah AL Deen, School AL-shaab, 1992 - Bağdat
Üniversite	: AL Mustansiriyah Üniversitesi, Bilimler Koleji - Bağdat
Bölüm	: Fizik, 1997
Yüksek lisans	: Süleyman Demirel University
Bölüm	: Fizik, 2017

Mesleki Tecrübe

Irak Atom Enerjisi Komisyonu (Iraqi atomic energy commission (IAEC)) Sağlık Fiziği Bölümünde görevli (2002–2003).

Bilim ve Teknoloji Bakanlığı (Ministry of ScienceandTechnology (MoST)) Radyasyondan Korunma Bölümünde görevli (2003 – 2008).

Irak Radyoaktif Kaynakları Düzenleme Müdürlüğü'nde (Iraqi Radioactive Source RegulatoryAuthority (IRSRA)) araştırmacı (2008'den bu yana).

İş unvanı: Radyasyondan korunma memuru.

Katıldığı Kurslar

Feaz Qahtan Waheed WAHEED Uluslararası Atom Enerjisi Komisyonu (International Atomic Energy Commission (IAEA)) tarafından Irak, Suriye, Ürdün, Tunus, Italya, A.B.D. ve Avusturya gibi ülkelerde düzenlenmiş olan birçok kursa katılmıştır. Toplam katılım süresi 1 yıldan fazladır.

Yayınlar

Waheed, F. Q., AL-Kazzaz, H. H., AL-Aubaedy, S. D., & AL-Dulaimi, M. J. (2017). قياس التعرضات الاشعاعية لمنظومة الفحص بالاشعة المؤينة من نوع RapiScan-GaRDS. *Journal of Madenat Alelem University College*, *9*(1), 131-142.

Waheed, F., Akkurt, İ.,Akyildirim, H., & Gunoglu, K. (2020). Monte Carlo simulation of a NaI (Tl) detector efficiency. *Radiation Physics and Chemistry*, *176*, 109081.

Waheed, F., Akyildirim, H., Günoğlu, K., & Akkurt, İ. (2017). Investigation of Buildup Factor in Gamma-Ray Measurement. *Acta Physica Polonica A*, *132*(3), 1203-1206.

Waheed, F., Q., Akyildirim, H., Günoğlu, K., Akkurt, İ., 2018. The Importance of the Buildup Factor for NaI(Tl) Detector System. 5thinternational Conference on Computational And Experimental Science And Engineering (ICCESEN-5), ISBN:978-605-68728-0-8, 12-16 October 2018, Antalya-Turkey, 298-300.

Waheed, F., Q., Akyildirim, H., Günoğlu, K., Akkurt, İ., 2019. A Monte Carlo simulation: To determination the buildup factor. 5th International Conference on Computational And Experimental Science And Engineering (ICCESEN-6), ISBN:978-605-68728-0-8, 23-27 October 2019, Antalya-Turkey, 298-300.

Waheed, F., Q., Akyildirim, H., Günoğlu, K., Akkurt, İ., 2019. Modeling of 3" x 3" NaI(Tl) Scintilation Detector System by Monte Carlo Code program. 2nd International Conference on Sustainable Sciences and Technology (ICSuSaT-2) ISBN: 978-605-68728-2-2, 05-07 July 2019 Istanbul-TURKEY, 47-49.

Waheed, F., Q., Akyildirim, H., Günoğlu, K., Akkurt, İ., 2020. Estimation the Photon Flux Distribution inside Shielding design. 7thinternational Conference on Computational And Experimental Science And Engineering (ICCESEN-7), ISBN:978-605-68728-0-8, 21-25 October 2020, Antalya-Turkey.

Waheed, F., Q., Akyildirim, H., Günoğlu, K., Akkurt, İ., 2020. Response Function of 3" x 3" NaI(Tl) scintillation for Cobalt (^{60}Co) Isotropic source. 3nd International Conference on Sustainable Sciences and Technology (ICSuSaT-3) ISBN: 978-605-68728-2-2, 25-27 Sebtember 2020 Istanbul-TURKEY.

Waheed, F., Q., Günoğlu, K., Akyildirim, H., Akkurt, İ., 2018. Variation of Detector Resolution with the Source-Detector Distance. 5thinternational Conference on Computational And Experimental Science And Engineering (ICCESEN-5), ISBN:978-605-68728-0-8, 12-16 October 2018, Antalya-Turkey, 290-297.

Waheed, F., Q., Günoğlu, K., Akyildirim, H., Akkurt, İ., 2019. An Experimental work on the Total efficiency of Cylindrical Scintillation Gamma-Ray Detector. 2nd International Conference on Sustainable Sciences and Technology (ICSuSaT-2), ISBN: 978-605-68728-2-2, 05-07 July 2019 Istanbul-TURKEY, 102-104.

Waheed, F., Q., Günoğlu, K., Akyildirim, H., Akkurt, İ., 2019. Determination of the Gamma Ray Attenuation Coefficient Of Magnetite Aggregate Concretes. 6th International Conference on Computational And Experimental Science And Engineering (ICCESEN-6), ISBN:978-605-68728-0-8, 23-27 October 2019, Antalya-Turkey, 290-297.

Waheed, F., Q., Günoğlu, K., Akyildirim, H., Akkurt, İ., 2020. FLUKA Plotting of gamma-Ray Distribution Outside Geometry. 3nd International Conference on Sustainable Sciences and Technology (ICSuSaT-3), ISBN: 978-605-68728-2-2, 25-27 Sebtember 2020 Istanbul-TURKEY.

Waheed, F., Q., Günoğlu, K., Akyildirim, H., Akkurt, İ., 2020. FLUKA modelling of Cesium (^{137}Cs) spectrum. 7thinternational Conference on Computational And Experimental Science And Engineering (ICCESEN-7), ISBN:978-605-68728-0-8, 21-25 October 2018, Antalya-Turkey.